



THE HONG KONG
POLYTECHNIC UNIVERSITY

香港理工大學

Pao Yue-kong Library

包玉剛圖書館

Copyright Undertaking

This thesis is protected by copyright, with all rights reserved.

By reading and using the thesis, the reader understands and agrees to the following terms:

1. The reader will abide by the rules and legal ordinances governing copyright regarding the use of the thesis.
2. The reader will use the thesis for the purpose of research or private study only and not for distribution or further reproduction or any other purpose.
3. The reader agrees to indemnify and hold the University harmless from and against any loss, damage, cost, liability or expenses arising from copyright infringement or unauthorized usage.

IMPORTANT

If you have reasons to believe that any materials in this thesis are deemed not suitable to be distributed in this form, or a copyright owner having difficulty with the material being included in our database, please contact lbsys@polyu.edu.hk providing details. The Library will look into your claim and consider taking remedial action upon receipt of the written requests.

Pao Yue-kong Library, The Hong Kong Polytechnic University, Hung Hom, Kowloon, Hong Kong

<http://www.lib.polyu.edu.hk>

**DEVELOPMENT OF NEW WATER SPRAY
STRATEGIES FOR IMPROVING THE ENERGY
PERFORMANCE OF INDIRECT EVAPORATIVE
COOLING SYSTEMS**

MA XIAOCHEN

PhD

The Hong Kong Polytechnic University

2024

The Hong Kong Polytechnic University
Department of Building Environment and Energy
Engineering

Development of New Water Spray Strategies for
Improving the Energy Performance of Indirect
Evaporative Cooling Systems

MA Xiaochen

A thesis submitted in partial fulfilment of the requirements
for the degree of Doctor of Philosophy

June 2024

CERTIFICATE OF ORIGINALITY

I hereby declare that this thesis is my own work and that, to the best of my knowledge and belief, it reproduces no material previously published or written, nor material that has been accepted for the award of any other degree or diploma, except where due acknowledgement has been made in the text.

_____ (Signed)

MA Xiaochen (Name of student)

ABSTRACT

Along with the increasing energy consumption of space cooling in buildings, the building industry is in urgent need of the environmental-friendly and proven cooling technologies. Indirect evaporative cooling is attracting wider attention as a sustainable technology based on the heat absorption properties of evaporation. It has been demonstrated that the plate surface covered by water membrane in the wet channels has a substantial effect on the operating performance in the practical use of indirect evaporative cooling technology, while the ideal state of the uniform water distribution assumed by existing models is usually difficult to be achieved. Even though several hydrophilic materials have been suggested for indirect evaporative cooler (IEC) to increase surface wettability, the non-uniform water film distribution brought on by improper nozzle settings remains a significant issue that worsens evaporation and leads to the consumption of large amounts of water. In order to enhance the evaporation process, it is crucial to tune the nozzle features in water supply systems and organize the nozzles suitably above the heat exchanger. Therefore, this thesis comprehensively analyzes the impact of the water spray system design on the evaporation efficiency of the IEC wetted channel passage by means of simulations and experiments, taking into account the actual wetting rate in the wetted channel. It also proposes the new water spraying strategies to optimize the evaporation efficiency of the secondary air channel of the IEC system from the perspectives of nozzle selection, installation spacing, air-water configuration, and operating parameters, so as to improve the working performance of the IEC system and to promote the further development of the system in terms

of low energy consumption and high efficiency.

First, a numerical model was developed and validated by experimental results to predict the spray water density distribution of the solid cone nozzles on the impact surface. The actual water spray density obtained from this model could be used to correct the wetting factor in the existing IEC numerical model. Besides, the control variable method was applied to compare the effect of inclined angle and distance between the nozzles, and the arrangement was optimized based on the uniformity coefficient as well as the coverage ratio. The results demonstrated that the optimized nozzle arrangement scheme led to improved air cooling and dehumidification, thereby enhancing the coefficient of performance (COP) of the IEC system.

Second, based on the aforementioned investigations, it was discovered that the distribution of the water film within the wet channel of the IEC has a significant impact on its operational performance. To analyze the motion of the spray droplets and the state of water film coverage on the plate surface, a three-dimensions (3D) Computational Fluid Dynamics (CFD) model was proposed. For experimental validation of the CFD model, a test rig consisting the entire IEC system was constructed, and the simulation results were in good agreement with the experimental results. Using this model, the temperature distribution inside the IEC was demonstrated for variations in spray parameters. In addition, the characteristics of the primary air inlet were parametrically analyzed and the optimal spray design parameters were proposed.

Third, to address the problem that the developed 3D CFD model requires high computer configuration and consumes large computational resources, this thesis developed a prediction

model based on back-propagation artificial neural network (BP-ANN) focused on the influence of the six main operating parameters of the spraying system in order to predict the performance of the IEC system in a simpler way. The model was rigorously validated using relevant experimental data, and the importance of each influential parameter was assessed by gray relational analysis. In addition, the multi-objective optimization method based on Genetic Algorithm (GA) was introduced to efficiently determine the optimal operating parameters of the IEC system.

Last, due to the high applicability of employing IEC as a heat recovery device in data centers (DCs), a 3D simulation model of the diamond-shaped IECs containing the water spray system was developed to compare and analyze the air-water arrangement options in IEC systems currently utilized in DCs, and the corresponding characteristics were explored from the perspective of CFD technology to determine the effects of nozzle configurations on the formation of a water film and evaporation in the wetted channel. Ultimately, it was determined that the top-configured nozzle performed best with the air-water counter-current form of the nozzles, and the effectiveness of the enhanced approaches with hydrophilic and fiber-coated simulations were further analyzed.

The main academic contributions of this thesis are summarized as follows: 1) A spray volume flow distribution model incorporating spray inclination was developed and validated, and the existing IEC model was further modified. 2) A novel 3D CFD model was proposed and validated by the experimental results, which considered the actual coverage factor of the water

film, including the cooling performance of the whole IEC system. 3) Based on the above two models, the nozzle arrangement scheme and setting parameters were optimized, and the improvement of thermodynamic performance as well as energy efficiency of the optimized IEC system was demonstrated in comparison with the original scheme. 4) A ML-based prediction model was developed to accurately estimate the performance of the IEC system, and GA was applied to optimize the IEC-ANN model to achieve efficient performance while maintaining low energy consumption. 5) A CFD model based on the diamond-shaped IEC was developed to explore the air-water flow, heat transfer, and mass transfer capabilities of the IEC as a heat recovery unit, and to identify the optimal nozzle configurations and performances, as well as the enhancement strategies for IEC in DCs. In conclusion, the analyzed and developed new water spray optimization strategies could effectively improve the performance of IEC systems and provide effective guidance for the application and further development of IEC systems.

PUBLICATIONS DURING PHD STUDY

Journal papers:

- [1] **X. Ma**, W. Shi, and H. Yang, “Study on water spraying distribution to improve the energy recovery performance of indirect evaporative coolers with nozzle arrangement optimization,” *Applied Energy*, vol. 318, 2022.
- [2] **X. Ma**, W. Shi, and H. Yang, “Improving the performance of indirect evaporative cooler for energy recovery from the perspective of nozzle configuration: A CFD model analysis,” *Journal of Building Engineering*, vol. 76, p. 107195, 2023/10/01/ 2023.
- [3] **X. Ma**, W. Shi, and H. Yang, “Spray parameter analysis and performance optimization of indirect evaporative cooler considering surface wettability,” *Journal of Building Engineering*, vol. 82, p. 108175, 2024/04/01/ 2024.
- [4] **X. Ma**, W. Shi, Lin Lu and H. Yang, “Performance assessment and optimization of water spray strategy for indirect evaporative cooler based on artificial neural network modeling and genetic algorithm,” *Applied Energy*, vol. 318, 2024.
- [5] **X. Ma**, W. Shi, Lin Lu and H. Yang, “A comprehensive review on the optimization of spray systems and water film distribution in indirect evaporative cooling system: advances in design and materials strategies”. (In preparation)

Conference papers:

- [1] **X. MA**, W. Shi, and H. Yang. Study on water spraying distribution for improvement of indirect evaporative coolers with nozzle arrangement optimization. The 13th International Conference on Applied Energy (ICAE2021), virtual, 29 Nov - 2 Dec, 2021.

- [2] **X. MA**, W. Shi, and H. Yang. Effect of spray nozzle parameters on surface wettability and performance improvement of indirect evaporative cooler. The 2022 MIT "A+B" Applied Energy Symposium (MITAB 2022), virtual, 5-8 July, 2022.

- [3] **X. MA**, W. Shi, and H. Yang. Development of a wettability combined CFD model of indirect evaporative cooler with spray and water film optimization. The 14th International Conference on Applied Energy (ICAE2022), Bochum, Germany, 8-11 Aug, 2022.

ACKNOWLEDGEMENTS

This thesis encapsulates the research I conducted over the course of three years while pursuing my Ph.D. at The Hong Kong Polytechnic University. The journey to this conclusion has been arduous, and upon reflection. It is evident that a considerable distance has been traversed. At this juncture, I wish to extend my heartfelt gratitude to all those who have provided me with assistance and support throughout this endeavor.

First and foremost, I would like to express my deepest gratitude to my chief supervisor, Prof. Yang Hongxing. I am thankful for his decision to take me on as his student three years ago, and for his continuous, clear guidance and encouragement throughout these years. His patience, open-mindedness, and passion for sports have profoundly influenced me both academically and personally, inspiring me to constantly improve and become a better individual.

I wholeheartedly appreciate the invaluable guidance and advice provided by my co-supervisor, Prof. Lu Lin, at every turn. I would also like to extend special thanks to Dr. Cao Sunliang for the significant assistance and support he has offered me. Their professional knowledge, experience, and steadfast support are treasures that I will forever hold dear.

Furthermore, I would like to extend my gratitude to all members of the Renewable Energy Research Group (RERG) for their assistance during my pursuit of a doctoral degree. A special shout-out goes to my companions in the room ZN824 and all the seniors from the IEC. I am also grateful to all the staff and technical personnel for their dependable support in my studies, laboratory work, and daily life.

I would also like to express my gratitude for the funding provided by The Hong Kong Polytechnic University through two General Research Fund (GRF) projects (Project Nos. 15213219 and 15200420). Additionally, the beautiful campus environment and the extensive sports facilities have been immensely helpful in achieving a balance between work and leisure.

Last but certainly not least, I must extend my deepest appreciation to my parents, Mr. Ma Zhaojie and Ms. Li Yanjun. Their unconditional love and support have been the panacea for overcoming all difficulties and pain. Without them, there would not be the healthy, happy, and growing individual that I am today.

TABLE OF CONTENTS

CERTIFICATE OF ORIGINALITY	I
ABSTRACT.....	II
PUBLICATIONS DURING PHD STUDY	VI
ACKNOWLEDGEMENTS.....	VIII
TABLE OF CONTENTS	X
LIST OF FIGURES IN THE THESIS	XVII
LIST OF TABLES IN THE THESIS.....	XXIII
NOMENCLATURE	XXIV
CHAPTER 1 BACKGROUND AND INTRODUCTION	29
1.1 Research background.....	29
1.2 Introduction to basic information about IEC.....	32
1.3 Organization of the thesis	38
CHAPTER 2 LITERATURE REVIEW	41
2.1 Introduction of various types of IEC.....	41
2.1.1 Plate-type IEC.....	42
2.1.2 Tubular IEC	44

2.1.3 Heat pipe IEC	45
2.1.4 Dew-point IEC.....	46
2.2 Experimental research of IEC	48
2.3 Model development of IEC	54
2.3.1 FDM model.....	54
2.3.2 FVM model.....	55
2.3.3 Other models.....	58
2.4 Primary performance influence parameters.....	61
2.4.1 Influence parameters related to water spray system	61
2.4.2 Other parameters.....	70
2.5 Hybrid system of IEC.....	74
2.5.1 IEC+AHU	74
2.5.2 IEC+AHU applied in DC	75
2.6 Summary of research gaps.....	79
CHAPTER 3 PROPOSITION	82
3.1 Project title.....	82
3.2 Aims and objectives.....	82
3.3 Methodologies	84

CHAPTER 4 DEVELOPMENT OF NUMERICAL MODEL FOR NOZZLE OPTIMIZATION OF IEC WITH EXPERIMENTAL VALIDATION.....87

4.1 Introduction of mathematical model 88

 4.1.1 Spray density distribution model..... 88

 4.1.2 Numerical solution..... 92

4.2 Model validation..... 94

 4.2.1 Wettability modification 98

4.3 Results and discussions 102

 4.3.1 Spray distribution of single nozzle 102

 4.3.2 Spray distribution of multi-nozzles 104

 4.3.3 Assessment of wettability performance 107

 4.3.4 Assessment of energy performance 113

4.4 Summary of this chapter..... 114

CHAPTER 5 DEVELOPMENT AND VALIDATION OF CFD MODEL FOR IEC CONSIDERING WATER FILM FORMATION WITH SPRAY PARAMETER ANALYSIS..... 116

5.1 Introduction of CFD model 117

5.1.1 Model geometry.....	118
5.1.2 Control equations.....	120
5.1.3 Boundary conditions.....	123
5.2 Description of experimental system.....	124
5.3 Model validation.....	125
5.3.1 The proof of grid independence.....	125
5.3.2 Water film coverage validation.....	127
5.3.3 IEC system validation.....	129
5.4 Results and discussions.....	132
5.4.1 Influence for single nozzle.....	133
5.4.2 Influence for multi-nozzles.....	138
5.4.3 Influence on IEC performance.....	140
5.5 Summary of this chapter.....	145
CHAPTER 6 PERFORMANCE ASSESSMENT AND OPTIMIZATION OF WATER SPRAY STRATEGY FOR INDIRECT EVAPORATIVE COOLER BASED ON ARTIFICIAL NEURAL NETWORK MODELING AND GENETIC ALGORITHM.....	148
6.1 Concept and model set up.....	149

6.1.1 Data preparation.....	149
6.1.2 IEC-ANN model set up	154
6.1.3 Validation.....	159
6.2 Results and discussions	160
6.2.1 Effect of variations in a single factor.....	160
6.2.2 Combined effect of variations in two factors.....	168
6.2.3 Analysis of the influence of input variables on the output variable	172
6.2.4 Optimization of IEC-ANN model based on genetic algorithm	173
6.3 Summary of this chapter.....	179
CHAPTER 7 PERFORMANCE ANALYSIS AND NOZZLE SETTING OPTIMIZATION OF IEC FOR ENERGY RECOVERY IN DATA CENTERS.....	181
7.1 Description of numerical model	182
7.1.1 Description of the model geometry	182
7.1.2 Mathematical bases of CFD approach.....	183
7.1.3 Simulation settings.....	186
7.1.4 Grid independence verification.....	187
7.1.5 Description of exergy analysis.....	189

7.2 Model validation.....	190
7.2.1 Validation of the water spray system	190
7.2.2 Validation of film thickness	191
7.2.3 Validation of IEC system	192
7.3 Effects of nozzle configuration on cooling characteristics.....	195
7.3.1 Four schemes of nozzle configuration.....	195
7.3.2 Performance evaluation of different nozzle configurations.....	196
7.4 Approaches for cooling performance enhancement	206
7.4.1 Performance enhancement by hydrophilic coating.....	206
7.4.2 Performance enhancement by fiber coating	208
7.4.3 Assessment of the degree of enhancement	210
7.5 Summary of this chapter.....	211
CHAPTER 8 CONCLUSIONS AND RECOMMENDATIONS FOR FUTURE WORK	213
8.1 Summary of the research findings and contributions	214
8.1.1 Development of numerical model for nozzle optimization of IEC with experimental validation	214
8.1.2 Development and validation of CFD model for IEC considering water film	

formation with spray parameter analysis.....	215
8.1.3 Performance assessment and optimization of water spray strategy for IEC based on ANN modeling and GA.....	217
8.1.4 Performance analysis and nozzle setting optimization of IEC for energy recovery in data centers	219
8.2 Recommendations for future work.....	220

LIST OF FIGURES IN THE THESIS

Fig. 1.1 A cross-flow IEC with a water distribution system	30
Fig. 1.2 Basic information about IEC	34
Fig. 2.1 Schematics diagram of plate type IEC.....	43
Fig. 2.2 Schematics diagram of tubular type IEC	45
Fig. 2.3 Schematics diagram of heat pipe type IEC	46
Fig. 2.4 Air flow pattern and psychrometric process of traditional IEC and dew point IEC with M-Cycle.....	47
Fig. 2.5 Six configurations of spray nozzles	49
Fig. 2.6 Five types of nozzles.....	51
Fig. 2.7 Five distributions of different nozzles	51
Fig. 2.8 FDM model developed by Min et al.....	55
Fig. 2.9 Distributions of different nozzles.....	63
Fig. 2.10 Effect of velocity on pressure	66
Fig. 2.11 The spray cone angle of different pressure	69
Fig. 2.12 Schematics diagram of IEC followed by IEC	75
Fig. 2.13 A typical IEC air-conditioning system of DC	77

Fig. 3.1 The flowchart of this thesis.....	86
Fig. 4.1 Sketch employed in the spray volumetric flux distribution model.....	89
Fig. 4.2 Three scenarios of the impact area with/without inclined angle.....	89
Fig. 4.3 Differential element division method adopted in the model.....	92
Fig. 4.4 Flowchart of the spray numerical model calculation process.....	93
Fig. 4.5 Proof of grid independence for the IEC water spray model	94
Fig. 4.6 Schematic diagram of the test rig of the IEC water spray system	95
Fig. 4.7 Photos of the test instruments	96
Fig. 4.8 Validation of the modeling results with the experimental data.....	98
Fig. 4.9 The water density distribution under two different calculation methods.....	99
Fig. 4.10 The element within the wettability factor of the IEC numerical model.....	101
Fig. 4.11 The model validation results of wet-bulb effectiveness based on the published paper.....	102
Fig. 4.12 The effect of the spray cone angle of no-inclined angle on the distribution...	103
Fig. 4.13 The effect of the inclined angle on uniformity coefficient and coverage ratio	104
Fig. 4.14 The proposed multi-nozzle arrangement schemes	105
Fig. 4.15 The effect of the distance of each nozzle on the distribution performance ...	106
Fig. 4.16 The effect of the inclined angle of each nozzle on the distribution performance	

.....	107
Fig. 4.17 Description of the two different nozzle arrangements before and after optimization.....	108
Fig. 4.18 The water distribution results on the aimed sprayed area.....	109
Fig. 4.19 Temperature and humidity distributions of the original and optimal scheme.	111
Fig. 4.20 Comparison of the impact of the spray scheme on IEC performance improvement	112
Fig. 4.21 The energy performance compared by two different spray schemes.....	114
Fig. 5.1 Flowchart for this section.....	117
Fig. 5.2 Configuration of an IEC system with single channel	119
Fig. 5.3 Demonstration model of a single channel pair of a plate crossflow IEC.....	120
Fig. 5.4 Sketches for the division of the numerical model into meshes.....	124
Fig. 5.5 The test bench for the IEC water spray system.....	125
Fig. 5.6 Coverage factor at different accounts of grid.....	126
Fig. 5.7 Demonstration of the division sample	127
Fig. 5.8 Photos of the test instruments	128
Fig. 5.9 Comparison between the tested and simulated data	129
Fig. 5.10 The test bench for the complete IEC system.....	131

Fig. 5.11 The model verification results based on wet bulb efficiency.....	132
Fig. 5.12 Impact of droplet size on the coverage area.....	134
Fig. 5.13 Trend in the effect of droplet size on the coverage area	134
Fig. 5.14 The characteristics of nozzle spray	137
Fig. 5.15 Variation of single nozzle to plate distance.....	139
Fig. 5.16 Impact of distance between two nozzles on coverage factor.....	140
Fig. 5.17 Impact of droplet size on wet-bulb efficiency	141
Fig. 5.18 Description of the two comparison arrangement schemes	141
Fig. 5.19 The coverage area situation of the two schemes.....	142
Fig. 5.20 Temperature distribution of primary air channel	143
Fig. 5.21 Effect of inlet primary air temperature on the energy performance of the two IECs.....	144
Fig. 5.22 Effect of secondary air velocity on the energy performance of the two IECs	145
Fig. 6.1 Schematic diagram of the IEC system	153
Fig. 6.2 Structure of the IEC-ANN model	158
Fig. 6.3 Validation results of the proposed IEC-ANN model	160
Fig. 6.4 The effect of nozzle pressure variations	163
Fig. 6.5 The effect of three other nozzle parameters variations	165

Fig. 6.6 The effect of operation parameters on ϵwb	168
Fig. 6.7 The effect of operation parameters on pressure drop.....	168
Fig. 6.8 The combined effect of two nozzle characteristics factors on ϵwb	171
Fig. 6.9 The combined effect of two nozzle operation factors on ϵwb and pressure drop	172
Fig. 6.10 The importance of different design parameters	173
Fig. 6.11 The flow of GA-ANN optimization.....	175
Fig. 7.1 Two types of IEC models set up in work bench	183
Fig. 7.2 Geometry, mesh and boundary conditions in simulations	187
Fig. 7.3 Coverage ratio and outlet temperature at different accounts of grid.....	189
Fig. 7.4 The schematic diagram of exergy analysis	190
Fig. 7.5 Comparison between the tested and simulated data based on temperature difference.....	191
Fig. 7.6 Validation of film thickness between simulation results and Nusselt empirical formula	192
Fig. 7.7 The model verification results based on the outlet temperature of primary airflow	194
Fig. 7.8 The schematics of the four nozzle configurations	196

Fig. 7.9 The determination of test spray flow rate	197
Fig. 7.10 The water film distribution of the four nozzle configurations	200
Fig. 7.11 The primary temperature distribution of the four nozzle configurations	202
Fig. 7.12 The film formation of two configurations.....	203
Fig. 7.13 The water vapor content distribution of two configurations.....	204
Fig. 7.14 The temperature distribution of two configurations	205
Fig. 7.15 The coverage ratio and outlet temperature of four configurations.....	206
Fig. 7.16 The performance improved by hydrophilic coating.....	208
Fig. 7.17 The performance improved by fiber coating.....	209
Fig. 7.18 The performance comparison among original, hydrophilic coating and fiber coating	211

LIST OF TABLES IN THE THESIS

Table 2.1 Experimental development of IECs.....	53
Table 4.1 The fluid dynamics characteristics of three solid cone nozzles	95
Table 4.2 Specifications of the instrument	96
Table 4.3 Fixed parameters of the simulation process	99
Table 5.1 Specifications of the instrument	128
Table 5.2 Setpoint of the IEC for simulation	130
Table 5.3 Specifications of the test parameters	131
Table 6.1 The primary working range of design parameters.....	150
Table 6.2 Specific values of IEC and experimental conditions.....	154
Table 6.3 Parameter setting of IEC base system	160
Table 6.4 The influence of input variables on the output variable	172
Table 6.5 The range of design parameters.....	176
Table 6.6 The optimization results derived from GA.....	177
Table 7.1 Specifications of the test parameters	193
Table 7.2 The specifications of the nozzle	198

NOMENCLATURE

A	surface area, m ²
C_D	drag coefficient
C_p	specific heat capacity, kJ/(kg· °C)
D	nozzle aperture, mm
d_e	the diameter of the channel, m
e	specific exergy, J/kg
f_{Re}	friction coefficient
g	gravitational acceleration, m/s ²
H	height of the nozzle position, mm
k	thermal conductivity, W/(m·K)
L	height, mm
n	nozzle count
O	output vector of the output layer
P	pressure, Pa
Q	water flow rate, kg/s
r^2	coefficient of determination
Re_s	Reynolds number
t	contact time
u	velocity, m/s
v	kinetic velocity, m/s
W	power, kW

x	original input variable
y	original output variable

Greek letters

ξ	uniformity coefficient
γ	coverage ratio
Γ	water density, kg/(mm·s)
δ_w	the thickness of water film, mm
σ	wettability factor
θ	spray cone angle, °
α	angle of integration in the spray volume flux distribution model, °
β	spray inclined angle, °
ε_{wb}	wet-bulb effectiveness
ε_d	dehumidification rate
Γ	spray density, kg/(s·m ²)
w	the value of the weights
η	effectiveness
γ	air-water ratio
$\bar{\omega}$	longitudinal velocity, m/s

ρ density, kg/m³

μ dynamic viscosity, kg/(m·s)

Subscripts

fan fan

i Neuron number of input layer

j Neuron number of output layer

k Neuron number of hidden layer

l latent

m Count of neurons in input layer

n Count of neurons in output layer

p primary air

s secondary air

w wetted area

wh the whole area of surface

th thermal

me mechanical

ch chemical

in inlet

out outlet

Abbreviations

AC Air conditioning

AHU Air handling unit

ANN Artificial neural network

BP Backpropagation

CFD Computational Fluid Dynamics

COP Coefficient of Performance

DC Data center

DNN deep neural network

DPM Discrete Phase Model

EC Evaporative cooling

EFW Eulerian Wall Film Model

FDM Finite difference method

IEC Indirect evaporative cooler

MVC Mechanical vapor compression

ML Machine learning

NTU Number of transfer unit

RH Relative Humidity

RMSE Root mean square error

RNG Renormalization group

1/2/3-D One/two/three dimensional

CHAPTER 1 BACKGROUND AND INTRODUCTION

1.1 Research background

The demand for electric power for space cooling represents one of the most rapidly expanding sectors of energy consumption within the global construction industry. This surge is primarily driven by rapid urbanization and increasing incomes, projecting a significant potential for growth in the coming years, particularly in Emerging and Developing Economies [1]. Since 2010, air conditioning systems have accounted for more than 10% of the total increase in electricity demand [2]. In regions like Hong Kong, where a persistently hot and humid climate necessitates prolonged use of air conditioning, the annual electricity consumption for cooling has surpassed 50% of the total energy usage in buildings [3]. In response, the Green and High-Efficiency Cooling Action Plan has been introduced, targeting the enhancement of energy efficiency in cooling products and the reduction of HFC emissions. As a sustainable technology that eschews chemical refrigerants and operates at a lower energy cost, indirect evaporative cooling has garnered widespread interest and become the focus of extensive research [4].

Indirect evaporative cooling (IEC) technology is increasingly recognized as a promising alternative for cooling, offering the potential for significant reductions in carbon footprint and substantial energy savings. This innovative approach can lower the dry-bulb temperature of air without resorting to the use of CFCs, capitalizing on the latent heat of water evaporation [5]. The IEC system operates with the aid of a water pump and two fans, featuring an array of dry and wet channels that are separated by heat exchange plates, as depicted in Fig. 1.1 [6]. During

normal operation, secondary air is drawn into the heat exchanger channels from an inlet located near the bottom, ensuring a consistent average wind speed. Water is then sprayed into the wet channels from nozzles positioned at the top of the heat exchanger, flowing in a direction counter to that of the airflow [7]. Consequently, the primary airflow in the dry channel is effectively cooled without the introduction of moisture, thereby mitigating the risk of bacterial proliferation and enhancing thermal comfort [8].

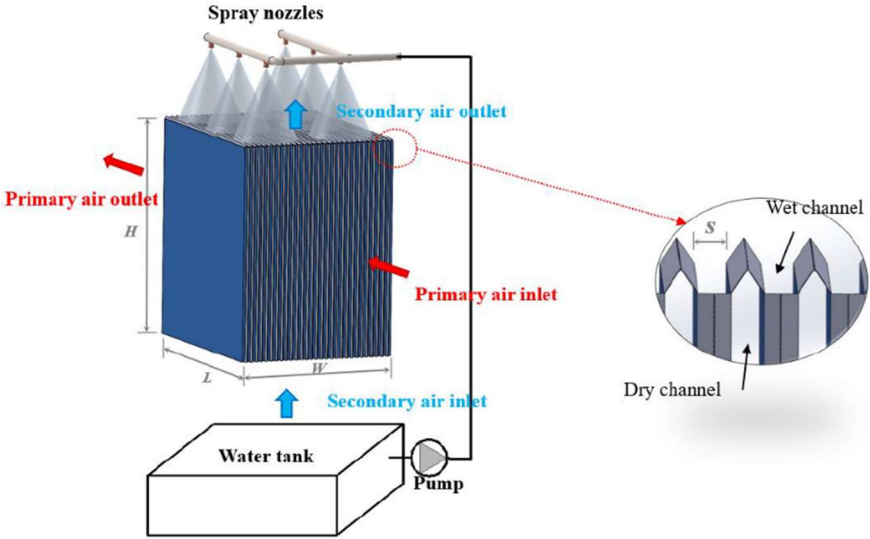


Fig. 1.1 A cross-flow IEC with a water distribution system

As a refrigeration device with significant advantages, the influencing aspects of the operating performance of the IEC system have been gradually clarified in continuous research, mainly including the external airflow properties [8, 9], the structure of the IEC [10, 11], the plate surface material [12, 13], and the addition of dehumidification units [15, 16]. Chen et al. [17] proposed an IEC model with condensation to forecast the yearly performance of a cooling system working in humid and hot environments and carried out the sensitivity analysis [18]. The findings demonstrate that the channel gap as well as the height of cooler are the most

important elements determining an IEC's thermal performance, and that the optimal channel gap varies depending on whether condensation is present. Min et al. [19] proposed and validated a two-dimensional cross-flow model, and the condensation is taken into account in the IEC when contrasting the performance of cross-flow as well as counter-current systems. Results reflected that the condensation rate of the counter-flow IEC was higher than that of the cross-flow IEC for the same conditions, while the wet bulb efficiency was lower. Shi et al. [20] set up a three-dimensional model of the IEC heat exchanger, which improved the simulation accuracy of both outlet temperature as well as moisture content, compared with the two-dimensional model. In the developed mathematical models of IEC, the water sprayed into wet channels is mainly assumed as a stagnant water membrane uniformly distributed on the heat exchange plates [21].

At the same time, surface wettability, as an important influencing factor affecting the evaporative heat absorption process in the IEC system, is almost impossible to achieve the ideal conditions [23, 24]. Therefore, multifaceted studies have been proposed to investigate and optimize the wetting ratio of the working air channels. Regarding the airflow direction, Antonellis et al. [24] concluded that the counterflow of the nozzles is better than the downstream flow through performing a series of experiments in a data center under different working conditions. In terms of the geometry of heat exchanger plates, Cignatta et al. [25] stated that the mesh protrusions can achieve a reasonable compromise among general heat transfers, wetting and plate stiffness compared with the plates with other complex protrusions. Guilizzoni et al. [24] performed a novel hydrophilic lacquer on the heat exchanger plates which could

enhance the wet-bulb effectiveness to more than 10%.

In addition, because of the complexity and high cost of optimizing the surface materials and shapes, researchers gradually set their sights on the installation of water spray systems [26, 27]. The water distribution in an IEC is influenced by many factors, such as water mass flow rate [28], nozzle type [23], nozzles arrangement and air flows [29]. Al-Zubaydi et al. [30] explored the performance of an innovative counter-flow IEC with internally sprayed water by using flexible tube nozzles inserted inside the wet channels, which proved the cooling capacity in force mixing mode was increased by 25%. Antonellis et al. [29] also experimentally examined airflow for IEC systems supported by cross-flow heat exchangers and noted that the best system performance exists when water or working air is supplied from the top and the heat exchanger plates are positioned horizontally and vertically. Huang et al. [23] studied the spray distribution of five types of nozzles experimentally, and the results revealed that the performance of spiral nozzles was optimal.

1.2 Introduction to basic information about IEC

When the IEC system is in operation, water is uniformly sprayed on the surface of the vertical wetting channel (as shown in Fig. 1.2), forming a thin film of water while secondary air (working air) passing over the wet side of the plate and primary air (product air) passing over the dry side. The sensible heat transfer from the plate, along with the latent heat transfer resulting from the evaporation of water from the wet surface, work in conjunction to cool the primary air [31]. Consequently, the primary air is cooled to a temperature that is in close

proximity to the wet bulb temperature of the incoming working air. Simultaneously, the latent heat released during the water evaporation process is transferred to the working air. Due to the disparity in secondary airflow and water content between the water film and the wet channel, the water film undergoes continuous evaporation, resulting in the cooling of the sheet. In contrast, the primary air in the dry channel is cooled isohyetically through convective heat transfer [32]. As the secondary air follows its designated path, it undergoes a gradual saturation process and experiences a temperature rise before being discharged into the atmosphere in a saturated state. To ensure efficient heat transfer, the temperature of the exhaust air should be lower than that of the incoming air. Theoretically, the decrease in enthalpy in the dry channel air should be equal to the increase in enthalpy in the wet channel air [33]. Fig. 1.2 Basic information about IEC exemplifies the enthalpy as well as humidity diagram of the IEC auxiliary air conditioner, where the primary air on the dry channel side undergoes an equal enthalpy cooling process and the secondary air on the wet channel side experiences a both cooling and humidification process. The secondary air completes isoenthalpic cooling from state point 1 to state point 4, which is approximated as an adiabatic process. Meanwhile, the heat from the drying channel is transferred to the secondary channel and the water at state point 4 continues to warm up and evaporate faster, eventually reaching state point 3 [34].

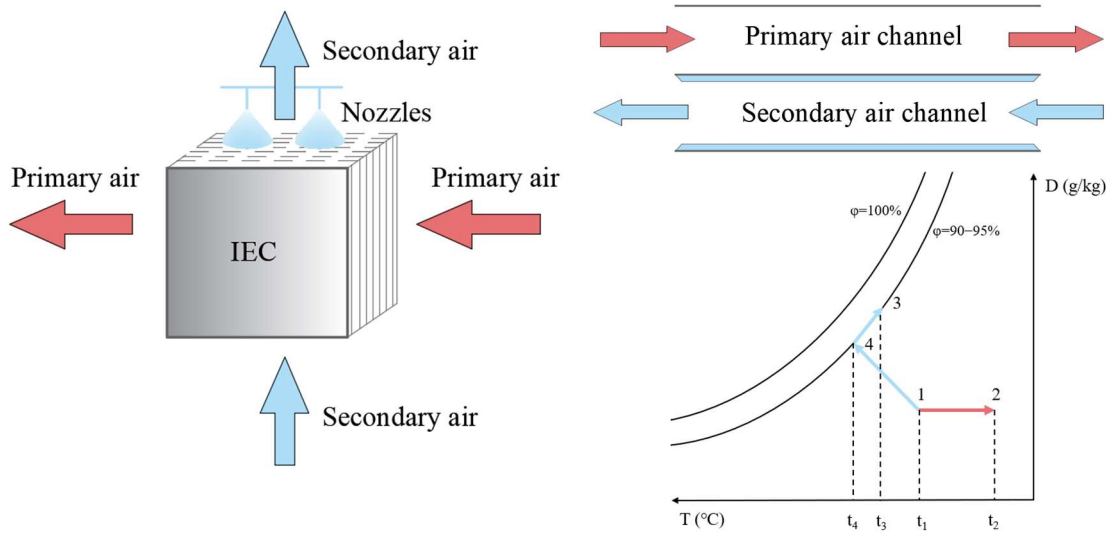


Fig. 1.2 Basic information about IEC

As summarized from studies on the operation of IECs and their water spray systems, the primary performance evaluation parameters could be grouped into the following three categories: uniformity coefficient and coverage ratio, which are used to assess the uniformity of water distribution in the spray system [23] [35]; wetted ratio and wettability [36] [37], which are used to assess the distribution of the water membrane on the walls of the wetted channels; and wet-bulb efficiency, cooling capacity, power consumption, water evaporation rate, pressure drop, and coefficient of performance (COP), which are symbolic of the cooling potential of the IEC [18] [19] [38]. Each evaluation parameter is listed in categorized order as shown below:

(1) Uniformity coefficient

The uniformity coefficient, which is used to assess the uniformity of the spray distribution, is calculated using Eq. (1), where a smaller coefficient of uniformity indicates a higher degree of uniformity in the spray distribution [23].

$$\xi = \frac{1}{\bar{x}} \left(\sqrt{\frac{\sum_i^N x_i - \bar{x}}{N}} \right) \quad (1)$$

where x_i represent the water collected in each specific cell, ml; \bar{x} represents the average amount of water collected by all the water collection units, ml.

(2) Coverage ratio

The coverage ratio, introduced as an evaluation parameter for identifying the coverage region of the water spray, is calculated using Eq. (2). The formula indicates that a higher coverage ratio corresponds to a wider coverage area [23].

$$\gamma = \frac{S_w}{S} \quad (2)$$

S_w is the region where spray water is distributed, mm²; and the entire region affected by the water collection units is denoted by S , mm².

(3) Wetted ratio

Since the presence or absence of a water membrane on the plate surface of the wetted channel can lead to differences in heat and mass transfer within the IEC, a wetting ratio is introduced, defined as the proportion of the wetted channel wall surface that is covered by a water film as a percentage of the entire wall surface area [36].

$$\varphi = \frac{A_w}{A_{pl}} \quad (3)$$

A_w is the region where covered by water membrane, mm²; and the entire area of the plate surface is denoted by A_{pl} , mm².

(4) Wettability

Furthermore, in the context of a vertical surface with a stable and fully developed laminar flow, the following parameters can be expressed to describe the modified conditions: Reynolds number, film velocity, water film thickness, and spray density. These parameters are relevant for characterizing the flow dynamics and properties of the modified system [37]:

$$\sigma = \dot{m}_w \frac{h}{2\delta_w v_w \rho_w} \quad (4)$$

$$Re_w = \frac{4\Gamma_i}{\rho_w \mu_w} \quad (5)$$

$$v_w = 1.5 \times \left(\frac{\mu_w g}{48} \right)^{\frac{1}{3}} (Re_w)^{\frac{2}{3}} \quad (6)$$

$$\Gamma_i = \frac{\dot{Q}_i}{L_f} \quad (7)$$

$$\delta_w = \left(\frac{3\mu_w^2}{4g} Re_w \right)^{\frac{1}{3}} \quad (8)$$

whereas σ represents the wettability of the wet channel; v_w represents the average velocity of water film, m/s; δ_w represents the thickness of the water film above the wet channel, mm.

(5) Wet-bulb efficiency

Wet-bulb efficiency is a measure of how effectively an IEC system cools the air, and it is determined by comparing the outlet temperature of the primary air to the wet-bulb temperature of the secondary air. Eq. (3) is a commonly used expression to calculate wet-bulb efficiency and a higher wet-bulb efficiency indicates more effective cooling [39].

$$\varepsilon_{wb} = \frac{t_{p,in} - t_{p,out}}{t_{p,in} - t_{wb,s}} \quad (9)$$

(6) Pressure drop

The hydraulic computation process can be used to compute the pressure drop [40]:

$$f_{Re} = 96 * (1 - 1.3553\left(\frac{L}{S}\right) + 1.9467\left(\frac{L}{S}\right)^2 - 1.7012\left(\frac{L}{S}\right)^3 + 0.9564\left(\frac{L}{S}\right)^4 - 0.2537\left(\frac{L}{S}\right)^5) \quad (10)$$

$$d_e = \frac{2sL}{s + L} \quad (11)$$

$$\Delta P = \frac{f_{Re}L\rho u^2}{2Red_e} \quad (12)$$

(7) Power consumption

Energy consumption is a crucial metric for evaluating the performance of an IEC system. This environmentally friendly technology has a lower energy consumption compared to mechanical air-conditioning systems, as it only considers that the power required to operate the water pumps and fans. The energy consumption of an IEC system could be calculated using empirical methods, definitions of words, and coefficient values found in Chen's reference [18]. By using these formulas, the energy consumption of an IEC system could be calculated using the following equation.

$$W_{fan} = \frac{Q \Delta P}{3600 \times 1000 \times \eta_0 \times \eta_1} \times K \quad (13)$$

$$W_{pump} = m_w g (h_{gravity} + h_{nozzles} + h_{val}) \times K \quad (14)$$

where fan efficiency and motor capacity coefficient, denoted by η_0 , η_1 and K , respectively, are 0.75, 0.9, and 1.1.

(8) COP

Cooling capacity of the IEC divided by system power consumption is called energy efficiency, or COP [41]. A mathematical expression for this definition would be:

$$Q_p = m_p c_{pg} (t_{p,in} - t_{p,out}) \quad (15)$$

$$COP = \frac{Q_p}{W_{fan} + W_{pump}} \quad (16)$$

(9) Water evaporation rate

A number of operational factors, including as the inlet air temperature and humidity, air velocity, treated cooling load, and system cooling efficiency, affect the rate at which water evaporates in an IEC system. In theory, the water evaporation rate indicates how much moisture is introduced to the secondary air during the indirect cooling procedure [38]. It can be determined as the amount of moisture that increases in the working air when the machine is operating.

$$\dot{E}_w = \frac{\dot{E}_{s,out} \rho_s}{\rho_w} (\omega_{s,out} - \omega_{s,in}) \quad (17)$$

1.3 Organization of the thesis

This thesis presents a thorough analysis and optimization of the water spraying strategies for cross-flow plate-type IEC, meticulously documenting the research methodology and findings. The structure of this thesis is outlined in the following sections:

Chapter 2 offers an exhaustive review of the latest research developments IEC technology. It critically examines various types of IECs and offers an extensive examination of water spray systems within IEC, through the lens of both model simulations and experimental research. The chapter also explores the current state and potential optimization strategies for the design of secondary airflow channels, with a particular focus on the role and improvement of wetting

factors. Stemming from this thorough overview, the chapter discerns the research gaps and clearly defines the objectives that this thesis aims to address. Then, Chapter 3 outlines the aims and objectives of this thesis as well as the main research methodologies.

In Chapter 4, a numerical model for water spray using commonly employed full-cone nozzles in the IEC system was developed. This model was validated through the construction of an experimental platform designed specifically for the IEC spray system. The actual water spray density obtained from the model was subsequently used to refine the existing model. The impacts of tilt angle and nozzle spacing were assessed using the model, and the analysis results were utilized to optimize the layout scheme for multiple nozzles.

Chapter 5 presents a 3D CFD model to analyze the motion of spray droplets and the state of water film coverage on plate surfaces. For experimental validation, a test rig comprising the entire IEC system was constructed, and the simulation results exhibited strong agreement with the experimental data. This model was used to demonstrate the temperature distribution inside the IEC under varying spray parameters. Additionally, a parametric analysis of the primary air inlet characteristics was conducted, leading to the proposal of optimal spray design parameters.

Chapter 6 addresses the high computational resource demands of the developed 3D CFD model by introducing a predictive model based on back-propagation artificial neural networks (BP-ANN). This model focuses on the influence of the six main operating parameters of the spraying system to predict IEC system performance more efficiently. The model was rigorously validated using relevant experimental data, and grey relational analysis was employed to assess

the importance of each influential parameter. Additionally, a multi-objective optimization method based on Genetic Algorithms (GA) was introduced to efficiently determine the optimal operating parameters of the IEC system.

In Chapter 7, the development of a 3D simulation model for a diamond-shaped IEC system with a water spray system is discussed. From the perspective of CFD techniques, the chapter compares and analyzes air-water arrangement schemes used in IEC systems in data centers (DCs) to determine the influence of nozzle configuration on the formation and evaporation of water film in the wetted channel. The chapter further explores the effectiveness of methods for enhancing hydrophilicity and fiber coating simulation. Finally, Chapter 8 summarizes the main findings of this thesis and outlines plans for future work.

CHAPTER 2 LITERATURE REVIEW

This chapter provides a comprehensive literature review of recent research advances in the field of indirect evaporative cooling (IEC). The review is organized into three main sections in order to provide a comprehensive view of the current state of existing research. The first part concentrates on the different types of IEC, as well as their main characteristics and applications. The second part focuses on IEC water spray systems as well as wet-channel performance to provide an overview of the current state of IEC research from experimental and model simulation perspectives, respectively. The factors affecting evaporation and heat transfer are then summarized, taking into account the characteristics of the spray system itself, the environmental conditions and the configuration of the IEC system. This section emphasizes the critical role of the attached spray system in ensuring the effective operation of the IEC system. In addition, the thesis evaluates the performance and utilization of IEC hybrid air conditioning systems to demonstrate the superiority of IEC as a heat recovery unit. By demonstrating these categories, this chapter identifies research gaps in the field of IEC and lays the foundation for this dissertation to analyze and optimize novel water spray strategies for IEC.

2.1 Introduction of various types of IEC

As a refrigeration device with significant advantages, the influencing aspects of the operating performance of the IEC system have been gradually clarified in continuous research, mainly including the external airflow properties [12, 13], the structure of the IEC [14, 15], the plate surface material [16, 17], and the addition of dehumidification units [18, 19]. There are

several types of IECs, including plate, tube, pipe and dew heat exchanger IECs, which transfer heat from the incoming air stream to the wet channel in different forms but on the same principle. Each type of IEC has its own characteristics and is suitable for different applications, which are classified and summarized in this section based on previous studies.

2.1.1 Plate-type IEC

The plate-type IEC is the most common form including cross flow and counter flow structures, as illustrated in Fig. 2.1 (a) and (b), respectively. The plate IEC usually consists of multiple parallel drying channels and wetting channels, where water is uniformly sprayed on the inner surface of the wetting channels through nozzles or drip tips to form a thin film. When the air in the drying channel flows through the plate IEC, they come into contact with the water film and absorb the latent heat of water evaporation, thus reducing the temperature of the air. The structure of a plate IEC is usually composed of a series of parallel metal plates, and the distance and angle between the plates can be adjusted as needed to achieve the best results.

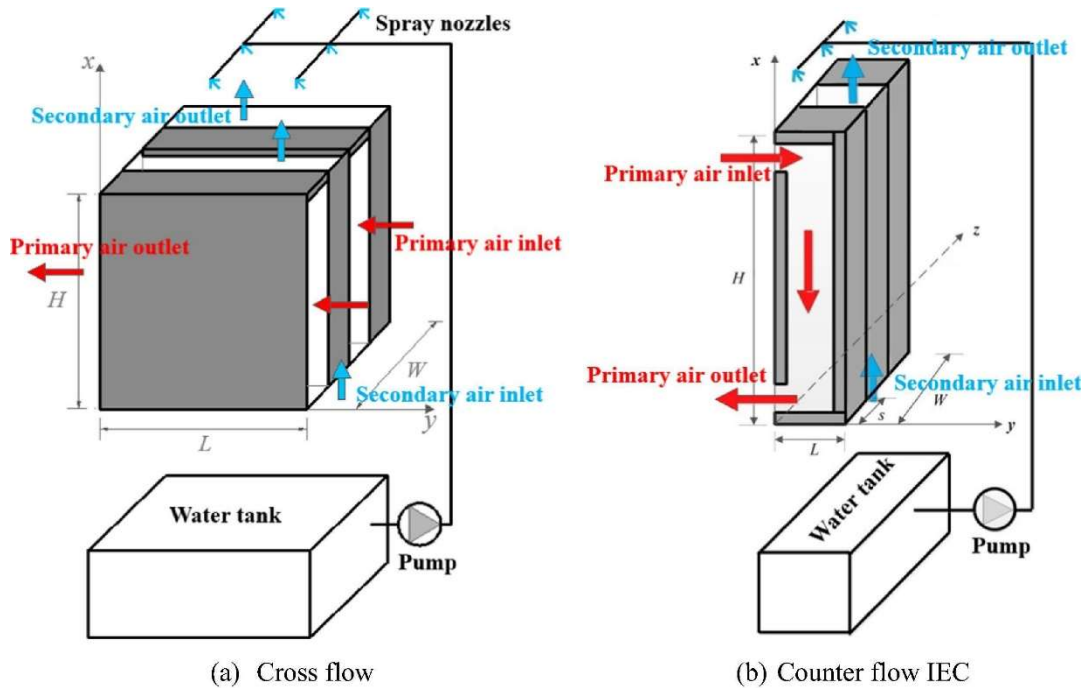


Fig. 2.1 Schematics diagram of plate type IEC

Chen et al. [20] proposed an IEC model with condensation to forecast the yearly performance of a cooling system working in humid and hot environments and carried out the sensitivity analysis. The findings demonstrate that the channel gap as well as the height of cooler are the most important elements determining an IEC's thermal performance [18], and that the optimal channel gap varies depending on whether condensation is present. Min et al. [19] proposed and validated a two-dimensional cross-flow model, and the condensation is taken into account in the IEC when contrasting the performance of cross-flow as well as counter-current systems. Results reflected that the condensation rate of the counter-flow IEC was higher than that of the cross-flow IEC for the same conditions, while the wet bulb efficiency was lower. Shi et al. [20] set up a three-dimensional model of the IEC heat exchanger, which improved the simulation accuracy of both outlet temperature as well as moisture content, compared with the two-dimensional model.

The IEC plate design boasts a compact and streamlined structure, however, the narrow channels through which the fluid flows can be susceptible to blockages, making maintenance a challenging task. Additionally, ensuring a tight seal between the wet and dry channels in the plate IEC can prove to be a tricky feat, often resulting in unwanted leaks. These issues can be mitigated with proper attention and care.

2.1.2 Tubular IEC

After years of research and application, significant progress has been made in the development of tubular IEC technology. In Fig. 2.2, a photo of the porous ceramic tube is displayed, which is a crucial component of the tubular IEC. These ceramic tubes are put together in a steel casing to create the IEC product, as depicted in Fig. 2.2. Both the working air inlet and outlet as well as the product air outlet are flanged for simple connection to air ducts. The secondary air flows vertically, while the primary air flows horizontally through the IEC, as depicted in the figure. Yu et al. [42] conducted experiments and derived the relationship equation between the Reynolds number and Sherwood number of air and water film flow in tubular indirect evaporative coolers. Braun et al. [43] obtained the equation for the mass transfer coefficient of water injection and air versus the decrease in air-side resistance for different circulating water flow and inlet air flow conditions after a study. Additionally, Camagor et al. [44] used engineering test data to validate the numerical simulation methods and results.

Tubular IEC has emerged as a promising solution to address the limitations of plate IEC. One of the major advantages of tubular IEC is its ability to form a stable water film outside the

tube, which enhances the efficiency of the evaporation process compared to plate IEC. Additionally, the lower manufacturing cost of tubular IEC makes it a more competitive option in the market. Considering the economic level and water quality, tubular IEC is a better-suited choice for applications in the northwest region of China.



Fig. 2.2 Schematics diagram of tubular type IEC

2.1.3 Heat pipe IEC

The heat pipe indirect evaporative cooler (HPIEC) is an innovative heat exchanger that boasts a compact structure, high efficiency, and a flow path that is not easily blocked, as depicted in Fig. 2.3 [45]. The process inside the tube involves a phase change that absorbs heat and evaporates the working fluid. Since the saturation pressure difference between the evaporation and condensation sections, the vapor flows into the condensation part, where it releases heat and turns into liquid. This liquid then flows back to the evaporating part under the capillary action of the absorbing core in the heat pipe, evaporates again, and repeats this cycle [46]. The main advantage of HPIEC is its excellent thermal conductivity and high heat transfer coefficient, which is hundreds or even thousands of times higher than general metals.

HPIEC is typically used in evaporative cooling centralized air conditioning systems where it recovers energy from the exhaust air throughout the year, reducing the energy consuming of the AC system. A heat pipe is a sealed tube filled with a small amount of working fluid, such as water. When heat is utilized to one end of the tube (the evaporator), the liquid working fluid evaporates and the resulting vapor condenses at the cooler end (the condenser or ceramic vessel), releasing energy. After that, an internal wick, such as a stainless-steel mesh, returns the liquid working fluid to the evaporator. As the heat transfer process involves a phase change, a significant amount of heat can be transferred using HPIEC [47].

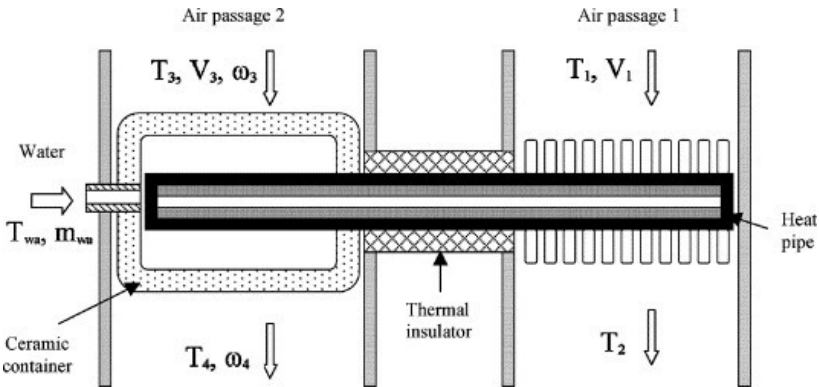


Fig. 2.3 Schematics diagram of heat pipe type IEC

2.1.4 Dew-point IEC

Due to its superior cooling performance and potential for energy savings, a novel kind of heat and mass exchanger (HMX) using the Maisotsenko cycle (M-Cycle) has increased a lot of interest recently. The dew point counter-flow HMX of IEC is designed based on the M-Cycle principle, as depicted in Fig. 2.4 (b) [48]. The HMX is normally made up of a number of fibrous sheets supported by parallel studs. Each sheet has a waterproof covering applied to one side,

creating a dry and a wet surface for the HMX channels. In contrast to how adjacent sheets' dry surfaces face one another and form a number of dry channels, wet surfaces of adjacent sheets likewise face one another and produce many wet channels that are separated by air guides.

The conventional IEC has a limit temperature equal to the wet-bulb temperature of the working air. However, in practical engineering applications, the efficiency of IEC is typically around 70%, which makes it difficult to meet the requirements of the supply air state point when the supply air temperature is too high, hindering the achievement of air conditioning in indoor buildings [49]. On the other hand, dew point IEC technology, which incorporates a pre-cooling process into the original IEC, can achieve a limit temperature equal to the dew point temperature of outdoor air. This technology has significant energy-saving potential, and as a result, it has garnered extensive attention from scholars both domestically and internationally.

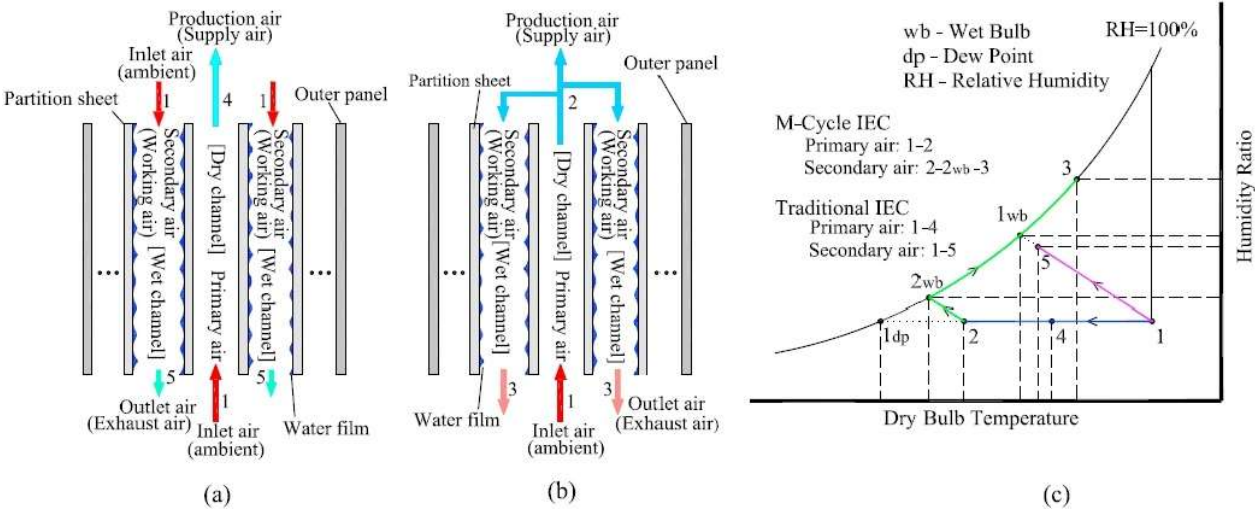


Fig. 2.4 Air flow pattern and psychrometric process of traditional IEC and dew point IEC with M-Cycle: (a) traditional IEC (b) M-Cycle IEC (c) psychrometric process [50]

2.2 Experimental research of IEC

The efficiency of evaporative heat and mass transfer in the wet channel plays a crucial role in determining the performance of the IEC system, and the wetting factor is a key parameter that affects the wet channel. Numerous experiments have been conducted to investigate the operating characteristics of IEC systems under various spray conditions.

De Antonellis et al. [51] conducted the first comprehensive experimental study of cross-flow IEC systems in a data center environment. They found that water flow rate has a significant effect on IEC performance and that nozzle counterflow configurations perform better than parallel designs, so system performance could be improved by optimizing nozzle layout and controlling water flow rate. However, this study did not explore different heat exchanger geometries and materials, and control factors were relatively limited. In a subsequent study, he [52] experimentally analyzed the impact of heat exchanger plate geometry on the performance of the IEC system and concluded that the plate geometry affects the heat transfer rate and surface wettability, and that the mesh plate cast improves the system efficiency. Furthermore, they discovered that, in contrast to counter flow configurations, parallel water flow and secondary airflow patterns resulted in higher wet bulb efficiency and lower pressure drop. He [29] also further explored the effect of water nozzle and airflow arrangement on the system performance based on experiments as shown in Fig. 2.5, and found that optimizing the water nozzle and heat exchanger plate arrangement can effectively improve the wet-bulb efficiency of the AC IEC, which leads to improved energy efficiency and reduced energy consumption.

However, the experiment only covers a limited range of operating conditions, which may limit its applicability in practical application scenarios.

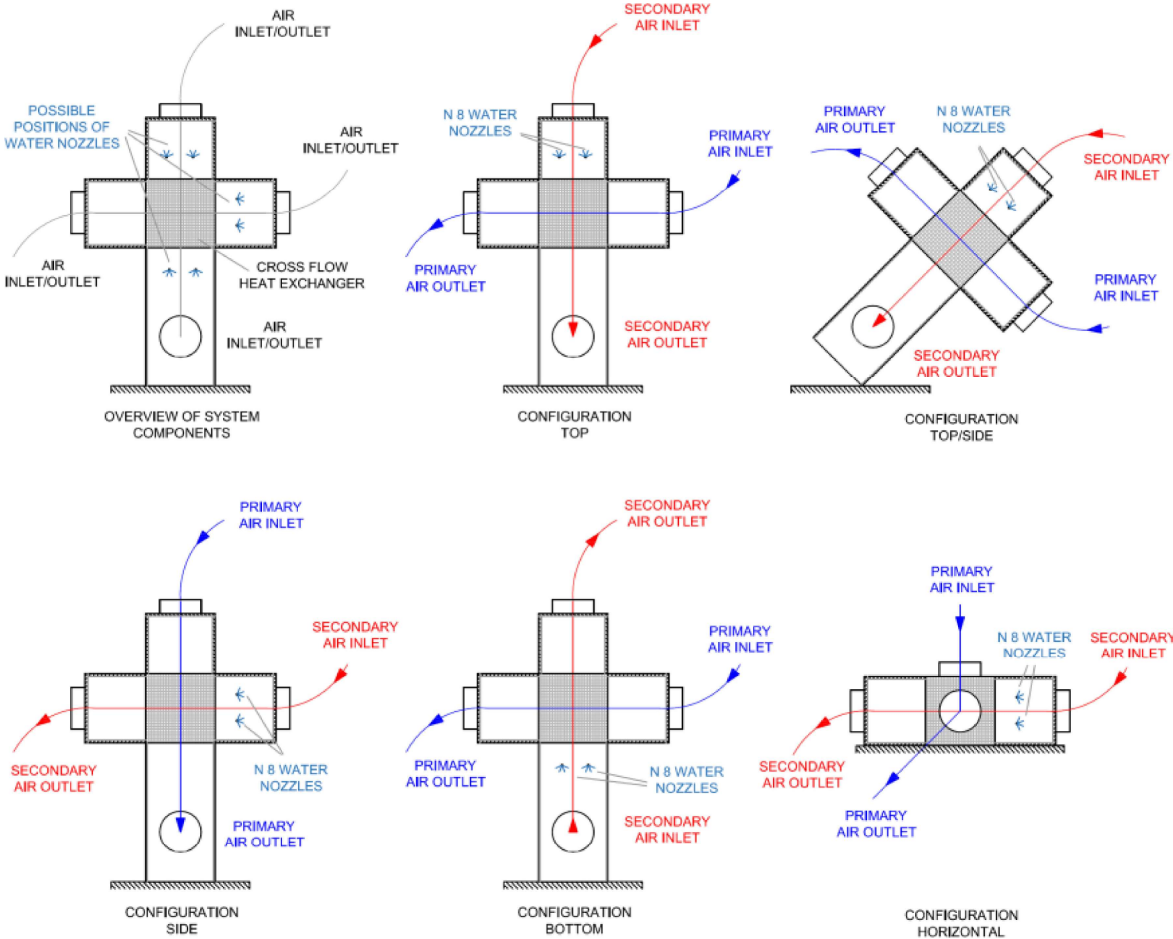


Fig. 2.5 Six configurations of spray nozzles

From the standpoint of water spray, Sun et al. [23] conducted experimental studies on IEC systems. The study aimed to quantitatively assess the water distribution capacity of five frequently used nozzles across various water volumes (Fig. 2.6). Three key metrics, namely coverage, uniformity coefficient, and water volume of the impact area, were utilized for evaluation. The results demonstrated that the spiral nozzle is the optimal choice for IEC applications due to its high coverage, excellent uniformity, and reasonable water volume for the impact area (Fig. 2.7). Zhou et al. [53] verified the effect of water distributor on the uniform

distribution of water film in IEC air conditioning and the effect of water distributor on the heat and mass transfer effect of IEC section through theoretical calculations and engineering practice, and proposed a new water distributing method and a model of water distributing that can be learned from. Al-Zubaydi et al. [54] conducted an experimental study comparing three water spray modes in IEC systems: external, internal, and hybrid internal and external. The results of the study indicated that the internal water spray mode exhibited superior performance compared to the external water spray mode. Moreover, the hybrid mode, combining both internal and external water spray, demonstrated the best performance in terms of wet-bulb efficiency, cooling capacity, and COP of the IEC system. Qi et al. [55] carried out an experimental study to evaluate the impact of various system characteristics on the cooling performance of IEC systems. The results indicated that, depending on the operating conditions, the cooling performance could be enhanced by 20% to 80% when maintaining a spray area percentage of 45%. Furthermore, in addition to plate-based IEC systems, tubular IECs have gained popularity due to their unique structural and performance characteristics. Zhou et al. [56] analyzed the effect of tubular IEC retrofitted with secondary make-up grids by experimental comparison and found that due to the segmentation effect and surrounding uniformity of the wire mesh, the water droplets are uniformly distributed into fine water particles of similar sizes, which improves the heat and mass transfer effect, and the efficiency of the larger-sized IEC is increased even more.

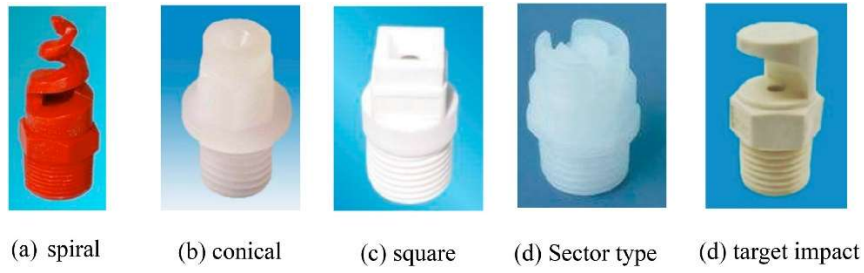


Fig. 2.6 Five types of nozzles

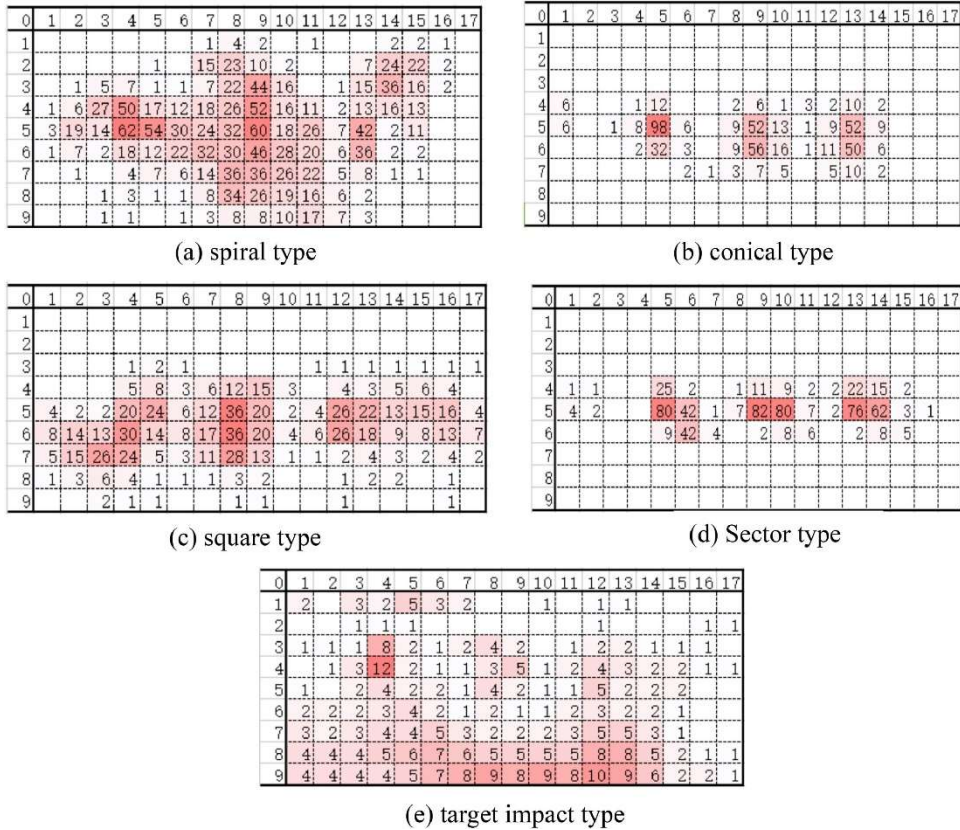


Fig. 2.7 Five distributions of different nozzles

The wetting characteristics of the wetted channel play a significant role in the cooling performance of the IEC, and in order to optimize its wettability, porous ceramics are often applied as a new material for the IEC in addition to fiber fabrics [57]. The porous structure of an IEC system possesses water storage capacity and hydrophilicity, leading to improved wetting properties of the wetted channel. Additionally, the porous structure increases the specific

surface area, enhancing the wet bulb efficiency of the IEC system. Wang et al. [58] pioneered the development and assessment of porous ceramic tubular IECs. These IECs exhibited high hydrophilicity, which significantly enhanced their efficiency by expanding the heat and mass transfer area. Moreover, the water storage capabilities of these IECs enabled intermittent water delivery, resulting in reduced energy consumption of the pumps. Experimental findings demonstrated that the new IEC design could achieve energy savings of up to 95% compared to conventional pumps, with a maximum COP reaching 34.9. Through an experimental study on porous ceramic IEC, Sun et al. [59] carried out optimizations of the secondary air/primary air flow rate ratio. The findings revealed that the porous ceramic IEC prototype exhibited optimal performance at a primary air velocity of 3.4 m/s, a secondary air velocity of 4.0 m/s, and a secondary air/primary air volume ratio of 0.9. Furthermore, to propose effective combinations of spray cycles and intermittent cycles for improved wet-bulb efficiencies and reduced water consumption, Sun et al. [60] also evaluated various intermittent spraying tactics on tubular porous ceramic IECs. The results indicated that the recommended intermittent spraying strategy consisted of a 10 s to 12 s spray period followed by a 1D intermittent period. Shi et al. [13] developed and constructed a plate cross-flow IEC known as PIEC, which incorporated sintered porous layers on the surface of each secondary air passage. The PIEC system was extensively tested and evaluated using an experimental setup. The results demonstrated that the PIEC system was capable of maintaining the supply air temperature within a narrow fluctuation range of 0.5°C for a duration of 2105 s, even without the need for water injection. This led to a significant reduction in the operational time of the water system, amounting to a 94.6% decrease.

Furthermore, the COP of the PIEC system increased by an average of 117.5% compared to conventional continuous spray patterns.

Table 2.1 Experimental development of IECs

Study	Research objectives	Type of IEC	Primary findings
[51]	Nozzles orientation, characteristics, number, water flow rate, secondary air inlet conditions	Cross-flow plate IEC	The performance of IEC is marginally affected by the number and dimensions of nozzles but is significantly influenced by the water flow rate.
[52]	Outlet conditions and the performance of IEC with/without secondary air humidification.	Cross-flow plate IEC	For cross-flow plate IECs, increasing the water flow rate enhances the humidity of the secondary air stream, thereby resulting in a larger temperature decrease (ΔT_p) of the primary air.
[29]	Water flow rate, Secondary air inlet conditions	Cross-flow plate IEC	The optimum configurations for spray systems are TOP and HORIZONTAL. The performance relies on the operating air conditions and water flow rate.
[23]	Five different types of nozzles, intermittent spray strategy	Tubular PIEC	Spiral nozzles are the best choice for IEC applications. The proposed intermittent spray strategy for porous ceramics IEC is a combination of a 10 s to 12 s spray cycle with a 1 min intermittent cycle.
[54]	The impact of the three water spray patterns on IEC performance for different inlet temperatures and primary airflow rates.	Hexagonal quasi-counter-flow IEC	Internal spraying is an effective way to improve the IEC of a hexagonal plate heat exchanger, mainly by increasing the wetted surface area
[55]	Discuss the impact of different spraying	Plate-fin IEC	The heat transfer enhancement showed a similar trend as the spray ratio was changed,

	parameters on spray cooling performance and study the effect of spray ratio on heat transfer improvement and temperature fluctuation.		with the shorter the spray interval, the better the heat transfer enhancement. Spray cooling systems are suitable for hot weather conditions.
[60]	Effect of secondary air to primary air ratio and water spray flow rate, intermittent water spraying.	Tube-type IEC	Optimal primary air/secondary air volume ratio of 0.9, using intermittent spraying, pump energy consumption of only 5% of the traditional IEC.
[13]	Studying the cooling potential of its cross-flow PIEC prototype and evaluating its performance.	PIEC	The PIEC prototype has a wet bulb efficiency of up to 0.642 and a COP of 7.2. The porous layer proved to have a reliable water retention capacity, enabling an intermittent spray strategy.

2.3 Model development of IEC

2.3.1 FDM model

Min et al. [19] formulated a 2D steady-state mathematical model to simulate a cross-flow IEC system (Fig. 2.8). The equations were discretized using the finite difference method (FDM) with a second-order central scheme. Notably, the model accounted for condensation on the dry side of the plate and aimed to compare the performance of crossflow and counter-flow IEC systems under fully condensing conditions. Guo et al. [61] proposed a 2D numerical model to analyze heat and mass transfer in a cross-flow IEC system. The model assumed to include a unit wetting factor and the equations were solved using FDM and MATLAB to investigate the

impact of condensing area ratio on heat exchanger performance. Validation based on experimental data showed differences as high as 8.6%. Riangvilaikul et al. [62] developed a numerical model to predict the outlet air conditions and system effects of a dew point evaporative cooling system. The model utilized numerical methods and was validated using experimental data and relevant literature. By utilizing the model, the researchers were able to optimize system parameters and investigate the impact of different inlet air conditions.

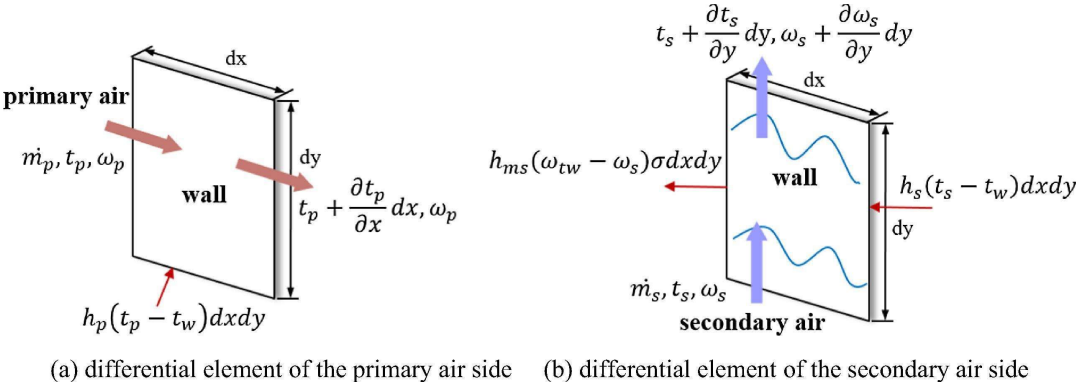


Fig. 2.8 FDM model developed by Min et al.

2.3.2 FVM model

In the realm of spray simulation, discrete phase model (DPM) of ANSYS Fluent harnesses the power of the Eulerian-Lagrangian method [63]. This sophisticated approach captures the fluid's behavior through a set of modified Navier-Stokes equations, while simultaneously charting the course of individual entities like particles, bubbles, or droplets. These elements, which make up the dispersed phase, are meticulously tracked as they navigate the established fluid flow, engaging in the transfer of momentum, mass, and energy with the liquid or gas they move through [64]. For the sake of computational efficiency, the model typically overlooks the

potential interactions between these dispersed entities, a reasonable simplification when their collective volume is minimal. Despite this, the model can still accommodate a substantial mass load. The trajectories of these discrete phase elements are determined at strategic points throughout the ongoing fluid phase analysis, ensuring a harmonized and accurate depiction of the spray dynamics [65].

In the conducted simulation, a solid-cone injection model was adeptly chosen to mimic the behavior of the water spray nozzle, with the entire system presumed to operate in a steady state for simplicity [66]. To capture the nuances of turbulence, the realizable k- ϵ model was employed, noted for its enhanced capability in accurately forecasting the expansion patterns of both planar and cylindrical jets, marking a notable improvement over the conventional k- ϵ model [67]. Although the discrete element model (DEM) stands as a favored technique for the study of multiphase flows, its broader adoption in simulating complex, large-scale industrial multiphase flow scenarios are often hampered by the substantial computational demands it imposes [68] [69].

Wan et al. [70] developed a 2D steady-state computational fluid dynamics (CFD) model for an IEC system in a counter-flow configuration. The model employed the finite volume method (FVM) and Ansys Fluent 6.3 software for solving the heat and mass transfer equations. The numerical results of this model were used as input to the 1D analytical model of Ren and Yang [21] for the analysis of the mean Nusselt and Sherwood numbers. By comparing the obtained results with the available numerical data for the counterflow wet surface heat

exchanger, a high level of agreement was observed, with the dimensionless temperature difference falling within the range of 0.75-1.94%. However, the model relies on assumptions such as constant air density and a single surface wetting factor. You et al. [71] proposed a 3D CFD model to analyze a cross-flow IEC system. The model assumes incompressible fluid, laminar flow, ignores water film thickness and drag, and considers condensation on the dry side of the IEC system plate. The evaporation-condensation coefficients were identified by numerical-experimental matching. The equations were solved using Ansys Fluent software and validated with experimental data displaying a maximum difference of 5% in outlet primary air temperature and humidity. Packel et al. [72] applied CFD to analyze the energy efficiency of an IEC with the aim of determining the pressure loss and air distribution characteristics in an indirect heat exchanger. The numerical and empirical calculations were compared with certified data obtained following the EN 308:1997 standard. The validation results demonstrated that the model uncertainties aligned well with the experimental results. These findings hold significant value for the implementation of IEC in air conditioning systems, particularly in mild and humid climatic conditions. Zhao et al. [73] carried out numerical simulations using a FVM model to optimize the geometry and operating conditions of an exchanger so as to enhance its cooling effectiveness and maximize the energy efficiency of a DPEC. The simulation results revealed that the cooling effectiveness and energy efficiency are significantly influenced by factors such as the size of the airflow passages, airflow velocity, and working air ratio. In contrast, the inlet water temperature had a lesser impact on these performance metrics. The research conducted by Cui [74] and colleagues utilized a Euler-Lagrange CFD approach to assess the efficiency of

the cooling system under a range of operating scenarios. Validation of the model was achieved through a comparison with empirical data. Findings from the simulations indicated that the innovative dew-point evaporative air cooler excelled in reaching superior wet bulb and dew-point temperatures, particularly when operating with reduced airflow speeds, diminished channel heights, increased length-to-height ratios, and decreased ratios of primary to secondary airflow. Zhan et al. [75] executed a FVM numerical simulation to model a dew point countercurrent indirect evaporative cooler. This model diverged from traditional approaches by incorporating more authentic boundary conditions at the partition wall, enhancing precision of the model through the concurrent resolution of intertwined momentum, energy, and mass transfer equations. The outcomes of the simulation revealed that the supply air temperature's maximum discrepancy fell within a narrow margin of $\pm 3.53\%$. Additionally, the refined model facilitated a thorough examination of operational responsiveness of the system.

2.3.3 Other models

Wan et al. [76] crafted a two-dimensional numerical framework designed to scrutinize the heat and mass exchange processes within countercurrent IEC setups. This innovative model operates under the presumption of a uniform air density and a singular wetting factor, while also accommodating the phenomenon of condensation on the plate's dry side and considering a non-unitary Lewis number. Leveraging CFD, the model was adeptly applied to both singular and composite factor analyses, aiming to refine the correlation between average heat and mass transfer coefficients. For the resolution of the equations, the finite element method (FEM) was

employed, utilizing the advanced capabilities of COMSOL Multiphysics software. Adam et al. [22] introduced a steady-state numerical representation for a cross-flow IEC system, incorporating an empirical approach to the wetting factor with an emphasis on evaluating efficiency alongside the wetting factor itself of the heat exchanger. The solution to the equations was meticulously achieved through the application of the fourth-order Runge-Kutta method (RK4). Validation efforts, grounded in experimental data, highlighted a minimal temperature discrepancy of 0.44°C , underscoring the model's accuracy. The RK4 method played a crucial role in the successful validation of this model.

Zhan et al. [75] developed a mathematical model that intricately maps the intertwined dynamics of heat and mass transfer between primary and secondary air, employing the FEM for the resolution of these equations. Their findings illuminate that reductions in channel air velocities, decreases in inlet air relative humidity, and increases in the ratio of secondary to primary air significantly enhance cooling performance of the system. Optimal channel configurations were identified, recommending a channel height of 4 mm and advocating for a dimensionless ratio of channel length to height falling between 100 and 300. Anisimov et al. [77] [78] conducted an extensive analysis of the Maisotsenko cycle heat and mass exchanger using a numerical model that enhances the effectiveness-Number of Transfer Units (e-NTU) method. The precision of the proposed mathematical framework is substantiated through rigorous validation against empirical data. The outcomes of the study reveal that the exchanger boasts a significant efficiency enhancement and possesses the capability to pinpoint the most favorable operating parameters across a spectrum of inlet conditions. Liu et al. [79] devised an

advanced 2D numerical model for the heat-mass exchanger within a DPEC. This model intricately fuses momentum and mass transfer equations with the energy equation, utilizing a variety of heat-mass transfer models for a comprehensive approach. The investigation delves into the impact of wettability of the wet channel surface, the overall design of the system, the geometry of the heat mass exchanger, operational parameters, and the conditions of the incoming air. Furthermore, the research includes optimizing the design and operational tactics of the DPEC, along with evaluating its effectiveness in various climate settings. Francisco et al. [80] embarked on an empirical exploration of the energy efficiency of a dew-point indirect evaporative cooler (DIEC) under varying intake scenarios. They crafted and corroborated a comprehensive DIEC model grounded in the ϵ -NTU method, which served as a tool for dissecting and enhancing the DIEC system. Their findings indicate that the ideal geometric configuration and operational parameters are contingent upon the specific environmental space and its ventilation requirements. Furthermore, it was observed that the most favorable COP values are consistently achieved when the air flow volume is maintained at lower levels. Zhu et al. [81] crafted a sophisticated 3D numerical model to assess the efficacy of a countercurrent dew-point evaporative cooler, with a particular emphasis on how uneven water distribution impacts performance of the cooler. The findings indicate that the discrepancy between the experimental trials and the 3D numerical simulations remains below 3.77% across various inlet scenarios. Notably, the 3D model enhances the accuracy of simulations by 5.46% when contrasted with conventional two-dimensional models, offering valuable insights for the cooler's design and optimization proces. Zheng et al. [82] formulated a 2D analytical model

tailored for cross-flow setups in IEC systems, with a particular emphasis on condensation phenomena. The fidelity of model was confirmed through experimental validation. The research delves into the operational performance of IEC units under varying conditions, closely examining condensation dynamics and assessing the water usage of IEC systems. Such insights are crucial for comprehending the functionality and condensation patterns of IEC in regions characterized by high heat and humidity.

2.4 Primary performance influence parameters

2.4.1 Influence parameters related to water spray system

2.4.1.1 Nozzle type selection

In the realm of IEC, various spray types can be classified into several categories, including drip, slit or hollow, rotary, jet, universal piping, and internal depth methods [83]. The drip method involves creating uniform channels in a collector pipe that is evenly distributed, a technique often employed in co-cooling applications [84]. Slit or hollow spray methods are achieved by making cuts or perforations directly in the pipe, with the precision of these openings being crucial for optimal performance [85]. Rotary spraying, on the other hand, utilizes different nozzle designs that either spin the pipe or the nozzle itself to disperse water, enhancing the inward flow of water and providing a large, even distribution area, albeit with higher maintenance and initial costs [86]. The universal piping approach involves mounting multiple pipes atop the heat exchanger, ensuring direct contact between the water flow and the

heat exchanger, with the resulting spray coverage being influenced by the height of jet [86]. To determine the most effective wetting performance with minimal water usage, five distinct nozzle and flow configurations within IEC systems were examined. Despite this, the study did not include an analysis of a device to measure a constant water parameter. Factors such as nozzle layout, size, water flow rate, and volume were considered, with findings indicating that water volume, along with nozzle range and size, significantly impacts the efficiency of the operation of cooling system [87]. Moreover, the strategic arrangement of nozzles leads to the intersection of spray zones, creating a pattern of regular intervals where only the overlapping regions receive water (Fig. 2.9). This effect can be minimized by selecting an appropriate spray strategy. However, if the spacing of water rings results in excessive overlap, it can inaccurately reflect cooling performance, necessitating frequent maintenance and replacement of tower packing due to the inundation of the targeted area with water [88].

An evaluation of various nozzle designs reveals distinct features that influence droplet dispersion and the efficacy of IEC systems. Spiral-type nozzles are characterized by their compact design and helical internal flow, which facilitates the dispersal of water across a broad area. In contrast, solid cone nozzles produce a more localized and intense spray pattern, with a circular distribution that is denser at the center. Square nozzles offer a balanced performance with a moderate spray volume and a distinctly square coverage area, while fan nozzles deliver a narrow, linear pattern, making them ideal for placement in corners or areas lacking coverage. Target-impact nozzles, recognized for their wide-angle spray, generate fine droplets by propelling water at high velocities against a target plate, resulting in a wide dispersal. When

assessing the uniformity of droplet distribution, target impingement nozzles lead the pack, with spiral, square, solid cone, and fan nozzles following in descending order. A lower uniformity coefficient indicates a more even distribution of droplets. In terms of IEC system performance, spiral nozzles stand out with a coverage efficiency of 78.4%, making them well-suited for IEC applications. Although target impingement nozzles excel in uniformity, spiral nozzles offer a superior compromise between coverage and uniformity, potentially making them a more optimal choice for IEC systems. Regarding the distribution of water volume, target impingement nozzles may fall short in fulfilling IEC requirements due to their limited spread within the collector grid. Other nozzle types exhibit varying water volume distributions based on their design, yet spiral nozzles generally provide a more favorable distribution across the spray area.

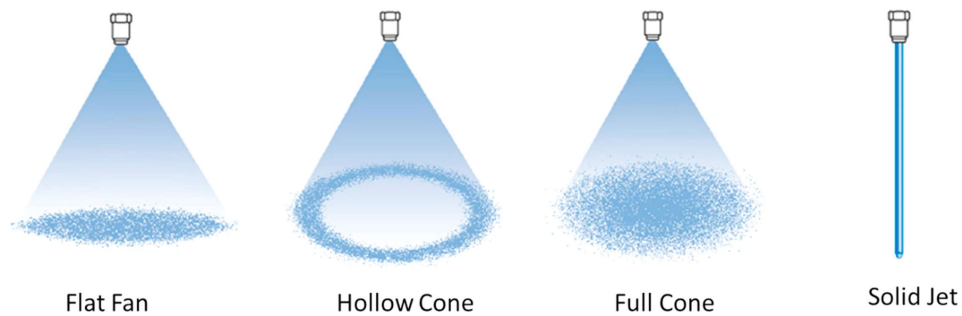


Fig. 2.9 Distributions of different nozzles

2.4.1.2 Nozzle characteristics

When evaluating the performance of a nozzle used in industrial settings, it is essential to take into account a set of parameters that define the nature of the spray. These parameters encompass the rate of fluid flow, the size of the droplets produced, the breadth of the spray's angle, and the force of impact upon the target. The rate at which fluid is dispensed is influenced

by factors such as the cross-sectional area of the nozzle, its design, and the physical characteristics of the fluid. Moreover, the flow rate is critically dependent on the pressure differential, which is the variance in pressure between the fluid inside the pipeline prior to the nozzle and the ambient pressure in the receiving environment.

The fundamental characteristics of spray nozzles are crucial for evaluating their practical impact. Research and design documentation have established relationships between key parameters such as spray cone angle, droplet diameter, pressure, and flow rate. These parameters are encapsulated in various equations that describe the main features of nozzle performance. Lefebvre and McDonnell have demonstrated that the theoretical mass flow rate from a nozzle can be calculated using a specific equation, often referred to in their work. This equation takes into account the fluid properties, nozzle design, and operating conditions to provide an estimate of the mass flow rate that can be expected from the nozzle under given circumstances. Understanding these relationships is essential for optimizing spray processes in a wide range of applications, from agricultural spraying to fuel injection in combustion engines. By adjusting the nozzle design and operating conditions, one can control the spray characteristics to achieve the desired outcome, whether it be efficient coverage in crop spraying or optimal fuel atomization in an engine [89].

$$\dot{m}_{th} = \rho A_o \left(\frac{2\Delta P}{\rho} \right)^{0.5} \quad (18)$$

The average droplet diameter could be determined using the following equation [89]:

$$d = 9.5d_j / (\Delta P_1 \sin(\alpha/2)) \quad (19)$$

Moreover, the correlation for the spray cone angle, formulated as Eq. (20), is based on the inviscid theory, which serves as the foundation for this relationship [90].

$$2\alpha = 334.32K^{-0.165} \left(\frac{D_s}{D_o}\right)^{-0.484} W_e^{0.043} Re_p^{-0.065} \quad (20)$$

The interplay between flow rate, pressure, droplet diameter, and spray cone angle in nozzles is a complex one, requiring careful adjustment to achieve optimal nozzle performance. Equations (18) and (19) illustrate that an increase in nozzle spray pressure leads to a higher flow rate and a reduction in droplet diameter. Additionally, the spray cone angle typically exhibits an initial increase followed by a decrease with rising nozzle pressure and flow rate, in line with specific design criteria. It is clear that jet pressure at the nozzle exerts the most significant influence on spray droplet size, with droplet dimensions remaining relatively stable under constant pressure conditions [91]. Wang et al. [92] delved into the cooling characteristics of multi-nozzle spray systems using computational fluid dynamics, revealing that the Sauter mean diameter of droplets decreases with increasing inlet pressure. In a related study, Han et al. [93] investigated the effects of varying pressures on the rate of droplet decay. The trajectory of droplet velocity reduction along the nozzle axis, as depicted in Fig. 2.10, shows that lower pressures are associated with more gradual slopes on the velocity decay curve. This suggests a slower decrease in droplet velocity as it moves away from the nozzle, underscoring the importance of selecting the appropriate water pressure to enhance spray efficiency.

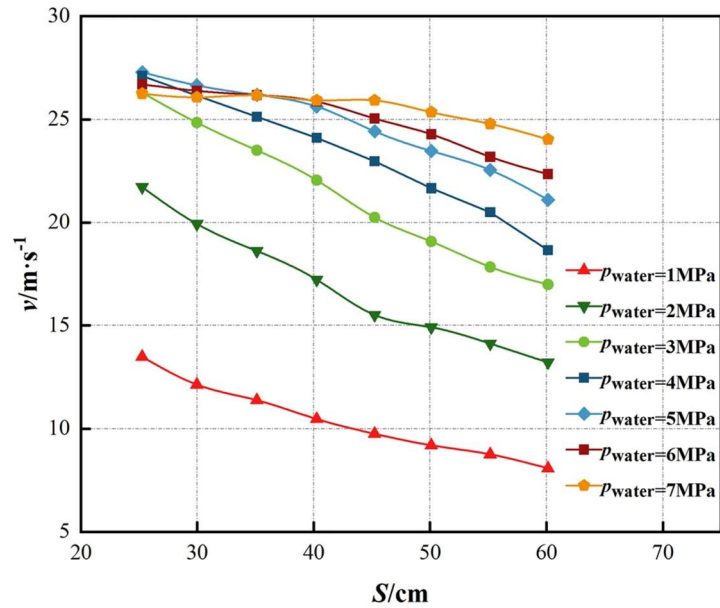


Fig. 2.10 Effect of velocity on pressure

Higher flow rates provide more liquid supply, increasing opportunities for evaporation and heat transfer, thus enhancing cooling effectiveness. By increasing the flow rate, a thin layer of liquid can be formed on the evaporative surface, creating more contact area for liquid droplets and vapor, thus increasing heat absorption and evaporation rate [94]. However, excessively high flow rates may result in excessive liquid waste and inefficient droplet atomization, so it is necessary to select an appropriate flow rate that balances cooling performance and resource conservation [95].

The size of the droplets in a spray is a crucial characteristic that impacts the spray's cooling effectiveness. For example, a droplet's mass, which depends on its diameter, determines its kinetic energy. Quantifying droplet size is crucial because the average resistance that the atmosphere poses to a droplet's forward motion is related to its diameter. Droplet size in a spray nozzle case is determined by a number of parameters, including fluid properties and nozzle type. The three main determining elements are specific gravity, viscosity, and pressure [96].

Smaller droplet diameters in IEC systems can provide a larger surface area, facilitating water evaporation. When small droplets come into contact with the surrounding air, the water on the droplet surface evaporates rapidly, absorbing heat from the air and achieving the cooling effect. Therefore, smaller droplet diameters could enhance the cooling efficiency of the system. However, smaller droplet diameters also increase the energy consumption and water consumption of the system. Generating small droplets requires higher energy input, such as using higher pressure to atomize the liquid [97]. Additionally, small droplets evaporate more quickly, necessitating a larger water supply to maintain droplet availability, leading to increased water consumption. Furthermore, when droplets are too small, their surface area is relatively small, making them more susceptible to disturbance and impact from airflow. This makes the droplets more likely to be carried away by the air, preventing the formation of a stable water film. When droplets are quickly carried away, their evaporation efficiency diminishes, thereby reducing the cooling effect of the system. Therefore, when designing IEC systems, it is crucial to ensure an appropriate droplet size that allows for the formation of a stable water film within the heat exchanger. Both excessively large and excessively small droplet sizes can affect system performance. By optimizing parameters of the spray system, such as nozzle design and spray flow control, an appropriate droplet size can be achieved to promote water film formation and facilitate effective evaporative heat transfer.

The properties of the fluid and the feed pressure dictate the nozzle's spray angle. Larger spray angles are typically associated with higher feed pressures. The area that a spray covers is greatly influenced by the proper spray angle of nozzle. The term "spray impact" describes how

a spray hits its intended target. Droplet size, gas velocity, feed pressure, and flow rate are among the many variables that affect it [98]. Typically, the following formula is used to calculate the impact of spray (Fig. 2.11):

From the equations discussed earlier, it is evident that an increase in flow rate and pressure amplifies the spray's impact and momentum. As fluid pressure escalates, so does its total internal energy. Nonetheless, the design of the nozzle plays a crucial role in dictating the proportion of this heightened energy dedicated to atomizing the spray versus that allocated to boosting velocity and impact. As a general rule, the best nozzles for converting energy into momentum are solid stream, followed by flat fans, hollow cones, and full cone nozzles. It should be mentioned that although ineffective at transferring energy, energy-efficient nozzles are highly effective at utilizing the inherent energy of fluid to atomise the material. Therefore, in some nozzles, boosting pressure to achieve a greater impact occasionally proves to be less successful. For example, the higher pressure will produce finer droplets if the nozzle is effective in atomizing the spray. Since these smaller droplets have less momentum by nature, the spray's overall effect and projection won't really increase.

A smaller spray cone angle helps concentrate the spray into a narrower cone, resulting in a more focused distribution of droplets in a specific area. This increases the contact area between the droplets and air, promoting faster evaporation and cooling effects. However, a smaller spray cone angle may require higher spray pressure to ensure that the droplets disperse within the desired range in the air. This can lead to increased energy consumption. Additionally,

a smaller spray cone angle may result in a more concentrated distribution of droplets, requiring a greater number of droplets to cover the entire surface of the heat exchanger, thereby increasing water consumption. On the other hand, a larger spray cone angle allows the droplets to disperse and scatter more quickly in the air, reducing mutual interference between droplets [99]. This helps minimize the impact of airflow on the droplets and the likelihood of them being carried away, facilitating the formation of a stable water film. In contrast, a smaller spray cone angle may make the droplets more susceptible to airflow interference, making it difficult to establish a stable water film. Therefore, when designing an IEC system, the choice of spray cone angle needs to strike a balance between these factors. It is important to find an optimal spray cone angle that maximizes the contact area between droplets and air, ensures efficient evaporation, minimizes energy consumption, and maintains a stable water film.

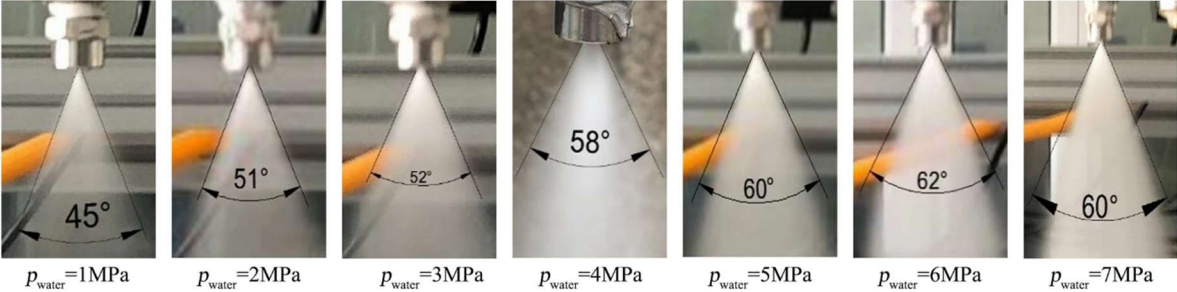


Fig. 2.11 The spray cone angle of different pressure

Furthermore, another direction worth focusing on is the arrangement parameter of spray nozzles. Through studies, Sun et al. [23] experimentally tested five different types of commonly used nozzles and found that spiral nozzles provided the highest coverage and the best uniformity. However, the cooling capacity of the IEC system only increased in a specific range with increasing water spray flow. Antonellis et al. [24] studied the five different configurations of

water nozzles over IEC and determined that the TOP configuration consumed the least amount of water while maintaining the highest wet bulb efficiency. It was found that a better spray configuration resulted in more surface contact region and reduced the heat transfer resistance between the two air flows. Sotelo-Salas et al. used CFD simulations to optimize the nozzle characteristics of a double-layer façade (DSF) for dry thermal conditions with evaporative cooling. The study determined that the optimal DSF configuration comprises an air cavity width of 0.4 m, a droplet of 25 μm , and a nozzle spacing of 0.6 m [20]. Besides, a comprehensive study of the performance of optimized nozzle arrangements on IEC using a mathematical model developed by Ma et al. [25] found that optimized arrangements could lead to a 16 % increase in wet-bulb efficiency.

2.4.2 Other parameters

2.4.2.1 Temperature and relative humidity

The efficacy of IEC technology is notably influenced by the prevailing outdoor temperature and humidity conditions. In general, IEC systems perform best at higher outdoor temperatures and lower humidity conditions [100]. In environments with high outdoor temperatures, IEC systems outperform conventional air conditioning systems in terms of efficiency. While conventional systems consume more energy to cool the air in hot environments, IEC technology effectively reduces air temperature through water evaporation without introducing additional humidity. As a result, higher outdoor temperatures create a greater temperature differential, which enhances the cooling effect of IEC systems. In lower

humidity environments, the rate of evaporation of water from the air increases, enhancing the evaporative effect within the IEC system. This allows the air on the moist side to absorb heat from the dry side more quickly, thus increasing the overall cooling efficiency of the system [101] [102]. It is crucial to acknowledge that the potential for temperature decrease using IEC technology is inherently bounded by the outdoor air's wet-bulb temperature. This particular temperature is a hybrid metric that encapsulates both thermal and moisture aspects, representing the air's maximum moisture saturation point. Consequently, the IEC system's ability to cool is confined by this wet-bulb threshold. Although IEC systems are adept at lowering the primary air stream's temperature to levels nearing the wet-bulb limit, surpassing this boundary to achieve further cooling proves challenging. The underlying reason is that as the system nears the wet-bulb temperature, the evaporation rate of water diminishes, leading to a deceleration in both heat absorption and the subsequent reduction of air temperature.

2.4.2.2 Air velocity

Wet channel sprinkler systems are a key component of IEC technology and involve spraying water in wet channels to increase humidity and promote evaporative cooling. Air flow rate directly affects the effectiveness of wet channel sprinkler systems. Lower air flow rates increase the residence time of moisture in the wet channel, providing more time for evaporation. This enhances the opportunity for moisture evaporation and improves cooling. However, low air flow rates can lead to excessive build-up of moisture in the wetted channel, resulting in oversaturation and potential performance degradation or condensation problems. Higher air

flow rates, on the other hand, accelerate the rate at which air passes through the wetted channel, reducing the residence time of moisture and limiting the evaporation process. This may reduce cooling effectiveness. However, higher air flow rates can help disperse moisture evenly in the wetted channel and reduce droplet build-up, thereby reducing the risk of condensation. When designing and operating an IEC system, air flow rates need to be balanced with the operational requirements of the wet channel sprinkler system to achieve optimum cooling performance [103].

Airflow velocity plays a pivotal role in the thermal exchange efficacy within IEC systems. Elevated airflow velocities augment the interface between the airstream and the moistened channel, fostering a more potent heat transfer mechanism. This dynamic facilitates a swifter conveyance of thermal energy from the air to moisture of the channel, thereby amplifying the cooling effect. Nonetheless, excessively high airflow velocities may induce a pronounced pressure drop and escalate the energy demands of the system. Optimal airflow velocities contribute to a diminution of the thermal boundary layer's thickness, which in turn bolsters heat transfer efficiency. A slimmer thermal boundary layer enhances the ease with which thermal energy is imparted to the moisture in the wetted channel, expediting the evaporation process. In essence, airflow velocity exerts a profound influence on the performance of indirect evaporative cooling technologies and wet-channel sprinkler systems. Judiciously regulated airflow velocity not only boosts water evaporation and thermal exchange efficiency in the wet channel but also elevates the IEC system's overall cooling prowess. However, to attain peak system performance, it is crucial to balance considerations such as cooling effectiveness, energy

expenditure, and system pressure differentials when determining the appropriate airflow velocity [104] [105].

2.4.2.3 Contact conditions

The properties of the wet channel wall surface, such as droplet contact angle and wettability, have a significant impact on IEC technology. The droplet contact angle on the wet channel wall surface is the angle between the droplet and the wall surface. The magnitude of the droplet contact angle affects the spreading and morphology of the droplet on the wall. Walls with lower contact angles allow droplets to unfold more easily, resulting in a larger liquid film area. This helps to increase the contact area between water and air, promoting more efficient evaporation and improving the cooling effect of the IEC system. Therefore, walls with lower droplet contact angles help improve the performance of IEC systems. Wettability of wetted channel walls, on the other hand, refers to the ability of the wall material to absorb and retain moisture. Walls with good wettability absorb and retain more moisture, allowing the moisture to remain on the surface for a longer period of time. This facilitates a larger evaporation area and sufficient time for moisture to evaporate, thereby enhancing the cooling effect of the IEC system. Therefore, good wettability of the wall material is critical to improving the efficiency of the IEC system [106] [107].

Selection of the appropriate wetted channel wall material is critical to ensure proper operation and efficient cooling of IEC technology. Wall materials with low droplet contact angles and good wettability aid in the diffusion and evaporation of moisture, increasing the

contact area with air and improving heat transfer efficiency. Together, these factors improve the overall performance of the IEC system. It is critical to note that factors such as material durability, resistance to contamination and maintenance costs should also be considered when selecting wetted channel wall properties to ensure the long-term reliability and economy of the system.

2.5 Hybrid system of IEC

Traditional single-stage IEC systems often face limitations in cooling effectiveness due to specific climatic conditions, which initially hindered their widespread adoption. To meet the higher cooling load demands of contemporary buildings, designers and engineers have investigated hybrid systems that integrate IEC with other air conditioning technologies. Recently, several innovative concepts have emerged, garnering attention in the cooling technology sector. This section will review these hybrid systems, emphasizing their potential to enhance cooling efficiency and reduce energy consumption. By integrating IEC with additional technologies, designers can develop more versatile and effective cooling systems tailored to the requirements of modern buildings.

2.5.1 IEC+AHU

IEC technology is an energy-efficient cooling technology that has gained popularity since its low energy consumption and effective cooling capacity. In buildings with high cooling loads, IEC has been integrated as a pre-cooling unit prior to mechanical air conditioning systems to

expand its application in temperate or humid regions. Fig. 2.12 illustrates the workflow of an IEC AHU combination system, where the IEC is accountable for air pre-cooling while the RH of the fresh incoming air is low [62]. To improve the cooling efficiency of the IEC, the discharged air from the AC space is utilized as secondary air for energy recovery. In the case of hot and humid outdoor air, condensation occurs, which means that the IEC is not only a pre-cooling device but also a pre-dehumidifier. This integration of IEC with other cooling technologies shows great potential for increasing cooling efficiency in a variety of building types and climates. By utilizing the benefits of each technology in a hybrid system, designers and engineers can create more efficient and sustainable cooling solutions for modern buildings.

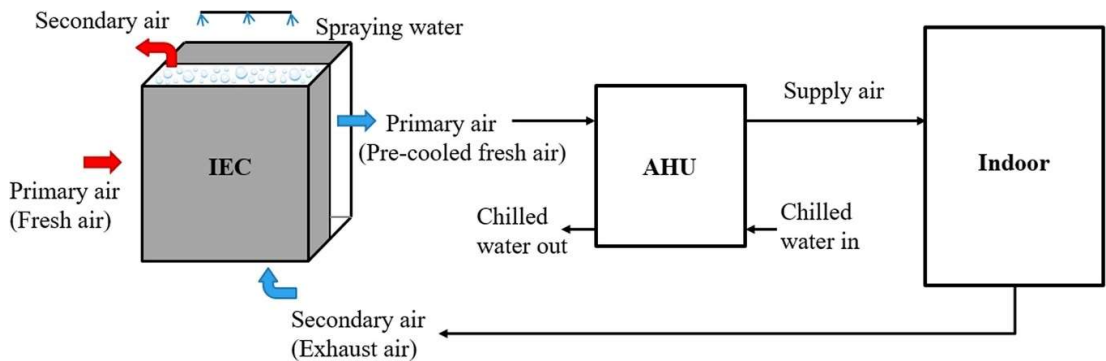


Fig. 2.12 Schematics diagram of IEC followed by IEC

2.5.2 IEC+AHU applied in DC

The growth in information demand driven by the Covid-19 pandemic involving global regions and the rapid development of emerging 5G network technologies have led to a surge in demand for cloud-based storage, data transfer and processing services across all industries. Today, data centers (DCs), the places where centralized electronic information equipment is

built to operate, have been scaled up at an unprecedented rate. Despite having a lower average power use effectiveness (PUE) value for DC than the global average, Southeast Asia is experiencing the fastest increase in the size of the DC market [108]. In Hong Kong, the electricity consumption of the DC sector increased by 10.3% in 2019, taking up 4483 TJ and 750 kilotons of carbon dioxide emission [81]. The average PUE of the DC industry in Hong Kong is as high as 2.2 [110], which intensifies the power supply and environmental issues. According to statistics [111], the DC consumes 30-50% of its total energy usage towards cooling to maintain the reliable operations of high-density servers. The cooling solution for DCs in Hong Kong mainly relies on active cooling systems such as Mechanical Vapor Compression Refrigeration (MVCR) which is challenging the climate pledges [112]. Improving the PUE of DCs and reducing carbon emissions with more energy-efficient cooling technologies is therefore essential, especially for areas with limited free cooling resources located in hot and humid climates.

Owing to the high-power consumption of air conditioning (AC) caused by the uninterrupted operation and year-round cooling of DCs, the use of natural cooling resources can help to reduce the burden of DC frequency power supply, achieve long-term business sustainability and improve competitiveness. Indirect evaporative cooling as a widely developed natural cooling technology can transfer heat through the evaporation of water without a compressor thereby reducing the temperature of the medium being cooled [85]. By absorbing the latent heat of vaporization, the secondary air is brought into direct contact with water to complete the isoenthalpy and cool the treated air on the other side of the plate to a lower

temperature than itself [113]. Fig. 2.13 shows the system diagram of a typical IEC for air-conditioning of DC. The water is sprayed into fresh air which is utilized as the secondary air, and the humidity of supply air can be maintained without adding any moisture. The separated channels of fresh air and indoor return air can avoid the cross-contamination to ensure the high levels of cleanness required by DCs. Driven by only a circulation pump and two fans, the IEC provides a promising and sustainable way to extend DC's free cooling hours.

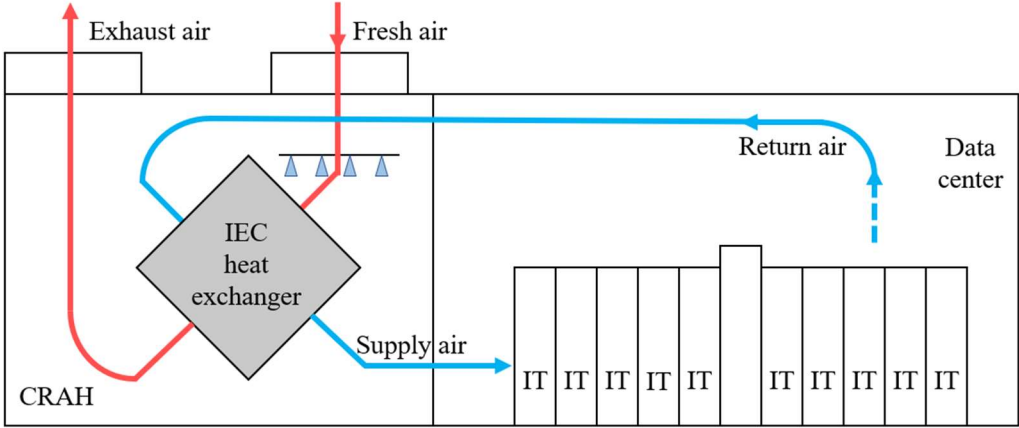


Fig. 2.13 A typical IEC air-conditioning system of DC [114]

With the unique advantages in lowering PUE and cutting down the carbon footprint, the application of IEC for DCs cooling solution has received worldwide recognition. DigiPlex air-to-air indirect evaporative cooling technology takes advantage of Nordic atmospheric conditions and uses low ambient air temperatures combined with the water spray system to maintain a comfortable thermal environment in the DC. It enables a 30% saving in total power consumption in the DC compared to the industry average, without loss of quality [87]. This solution can save as much as one-third of the total power consumption by moving from an ordinary DC (PUE of 1.67) to a more energy efficient center (PUE of 1.2) [116]. The German

company DencoHappel has developed a unit with a double plate-fin heat exchanger core in series to extend the flow time of the return air within the core and the contact area with the core walls, increasing the heat transfer effectiveness of indirect evaporative cooling. The reason why the fresh air does not pass through the condenser after heat exchange is that the cooling capacity carried by the fresh air is already fully utilized inside the core [117]. This plate type double heat exchanger sprayed indirect evaporative natural cooling AC unit is also used in T-block laboratory of Tencent in China, where the PUE tested is less than 1.1, confirming the excellent system energy efficiency [118]. Huawei Linyi, a cloud computing big DC radiating the economic group of southern Shandong and northern Jiangsu, has led the market for cooling solutions for DCs by introducing a new generation of technology that integrates IEC, heat recovery and mechanical cooling in an all-in-one system with an optimized structure. Its application in Linyi Big DC shows an average PUE of 1.25 [119], which is 14% higher than the average value in the same region.

With the widespread adoption of IEC technology in DC, a range of advanced IEC designs have emerged that are more energy efficient. The dew point IEC developed by Maisotenko [120] in 2003 enables the pre-cooling of the secondary air and further reduces the output air temperature around the dew point, and is also called M-cycle. The close proximity to the dew point, the small footprint and the flexibility of the installation form, which can provide output air after wet cooling, are the main research directions for evaporative cooling technology. The M-cycle IEC was adopted at the National Snow and Ice DC (NSIDC) in Colorado [19]. Compare to the traditional refrigeration system, the new system saved the cooling energy

significantly by reducing the PUE from 2.03 to 1.27. Excool [121], a British company, has developed a high-pressure spray plate type indirect evaporative natural cooling AC unit, in the operation process after various physical filtration and chemical purification treatment of water through high-pressure atomization to form a large number of fine droplets, greatly increasing the contact area of water and outdoor fresh air, enhance the effect of water evaporation cooling outdoor fresh air. Besides, for an existing DC in Xinjiang, Guo et al. [18] presented a hybrid system made up of DEC, IEC, and glycol free cooling technology. This system could realize free cooling around the year and a peak yearly energy conservation rate of 73%.

2.6 Summary of research gaps

While it is possible to improve the cooling performance of an IEC by optimizing its construction, doing so often introduces additional complexities and limitations. IEC systems can only operate with the highest cooling efficiency if the height and length of the channels meet certain criteria [74]. Through extensive research on IEC, it has been found that wet passages rely mainly on latent heat exchange, emphasizing the importance of the thermal mass transfer of water for the cooling effectiveness of IEC. Therefore, the focus has been on ensuring rapid penetration and evaporation of water on wet surfaces [122]. Currently, with the growing emphasis on low energy consumption and carbon neutral concepts, natural cooling technologies, particularly those utilizing water evaporation, are being studied more comprehensively. However, existing studies have mainly focused on direct evaporative cooling through spray systems or structural optimization of IEC systems [123]. On the other hand, focusing on the

study and optimization of spray systems in IECs, with particular attention to the impact of spray droplets on the walls of wet channels, represents a simpler and more effective approach to enhancing the cooling performance of IECs. Based on the comprehensive review in the previous sections, several research gaps still can be recognized and summarized as follows.

- 1) Most of the existing analyses of the IEC water spray state are based on experimental data, and few mathematical models can quantitatively simulate the various parameters of the water spray distribution of the solid cone nozzle.
- 2) Besides, the existing heat and mass transfer model of IEC has not been fully discussed on the wetting ratio, and the ideal assumed value of the same interval in the model needs to be corrected by specific calculations.
- 3) In the actual operation of the IEC system, inappropriate nozzle parameter settings can lead to an undesirable water film coverage area on the plate surface, thus weakening the evaporation phenomenon within the channel. The current 2D model is not enough to accurately simulate the state of the water film distribution within the IEC channel, and to deal with 3D problems, to deal with more complex hydraulic and thermal properties.
- 4) The optimal nozzle arrangement scheme to maintain the best wetted situation of the IEC wet channel is not clear, and the nozzle parameters required for maximum coverage of the water film on the plate surface of wet channel have not been identified.
- 5) Additionally, the developed 3D model is capable of accurately predicting the

performance of IEC and optimizing the spray scheme. However, this model has high computational requirements and a long computation time. Therefore, in large-scale practical engineering applications, there is a need for faster methods to predict IEC performance and optimize spray design parameters within a reasonable range.

- 6) Last but not least, the IEC units used as heat recovery units combined with AHU for DCs cooling in conjunction with their special diamond-shaped design structure require targeted water injection system settings.

CHAPTER 3 PROPOSITION

3.1 Project title

This thesis focuses on the modeling and experimental research work of IECs, with an emphasis on enhancing IEC performance by optimizing the spray strategy during IEC operation. The proposed research work to be reported in this thesis is therefore entitled ‘Development of New Water Spray Strategies for Improving the Energy Performance of Indirect Evaporative Cooling Systems’.

3.2 Aims and objectives

The research aims of this thesis could be provided with the intention of filling the knowledge gaps mentioned in this section.

- 1) A numerical model is proposed and validated to predict the spray water density distribution of the solid cone nozzles on the impact surface with uniformly divided square grids. The actual water spray density obtained from this model could then be used to correct the wetting factor in the existing IEC numerical model.
- 2) To identify the movement of the spray droplets as well as the formation and flow state of the water membrane covering the plate surface, a 3D CFD model is therefore developed. The water coverage area of the plate surface is reflected in the simulation model to predict the performance of the IEC under normal operation more accurately.
- 3) An experimental setup was established to study the distribution of spray water, along

with a visualizable wet channel equipped with a complete IEC system to validate the proposed model. The experimental results confirmed the accuracy of the developed numerical model, demonstrating its suitability for further parameter analysis and performance optimization of IEC systems.

- 4) Then, based on the two developed model to compare the effects of the original and optimized nozzle arrangement scheme and nozzle setting parameters on the thermodynamic performance as well as the energy performance of the IEC system, the superiority of the nozzle optimization scheme is demonstrated, which also provides a reference for further performance optimization of the IEC system.
- 5) Moreover, a high-efficiency prediction model based on ML (IEC-ANN model) is developed to accurately estimate the performance of the IEC system by considering six influencing factors related to spray operation. The genetic algorithm (GA) is employed to optimize the operational parameters of the system, achieving improved performance while reducing energy consumption.
- 6) Finally, a coupled model of the water spray system and water film distribution of a diamond-shaped IEC was established for the characteristics of the IEC as a heat recovery device in DCs to study the comprehensive effects of nozzle settings and airflow configuration on the surface wettability of the IEC, and to determine the optimal nozzle arrangement scheme.

3.3 Methodologies

The research methodology is projected and demonstrated in this chapter after the gaps and IEC objectives have been determined. It primarily consists of the four elements listed below:

1) Numerical modeling of the IEC:

Firstly, the MATLAB software was used to build a mathematical model to simulate the distribution and uniformity of spray droplets in the upper part of IEC, followed by ANSYS FLUENT software to set up a CFD model of the whole IEC system to perform the simulation of dynamic process of water droplets produced from the nozzles and entrained in water film along the surface. Furthermore, an IEC-ANN model is established using MATLAB software programming, and GA is applied to optimize the water spray system strategy.

2) Experiment:

The different types of nozzles used in the experiments were acquired by the authors from the same nozzle manufacturer, which provided the parameters and specifications of the nozzles, and the IEC was assembled from special thin aluminum plates. Then, the IEC prototype was tested on an established test rig in ZB204 (Zone Z) with controlled temperature and consistent humidity. The ability of test stand to accommodate various temperatures and humidity levels, which can mimic genuine environmental conditions, is made possible by the heater and humidifier that it uses as its equipment.

In addition, a field test of the IEC as a heat recovery unit operating in combination with an AHU for cooling was set up at a printing room in Chai Wan, Hong Kong.

3) Data analysis

The results collected from the modeling and experimental research are recorded and analyzed based on Excel and MATLAB.

4) Figure formation

The structure and diagrams are based on PowerPoint and SOLIDWORKS, while the data analysis and comparison charts are described by Origin 2021 in this report.

Last, the research flowchart of the thesis is presented in Fig. 3.1 The flowchart of this thesis to show the process and connection among each component.

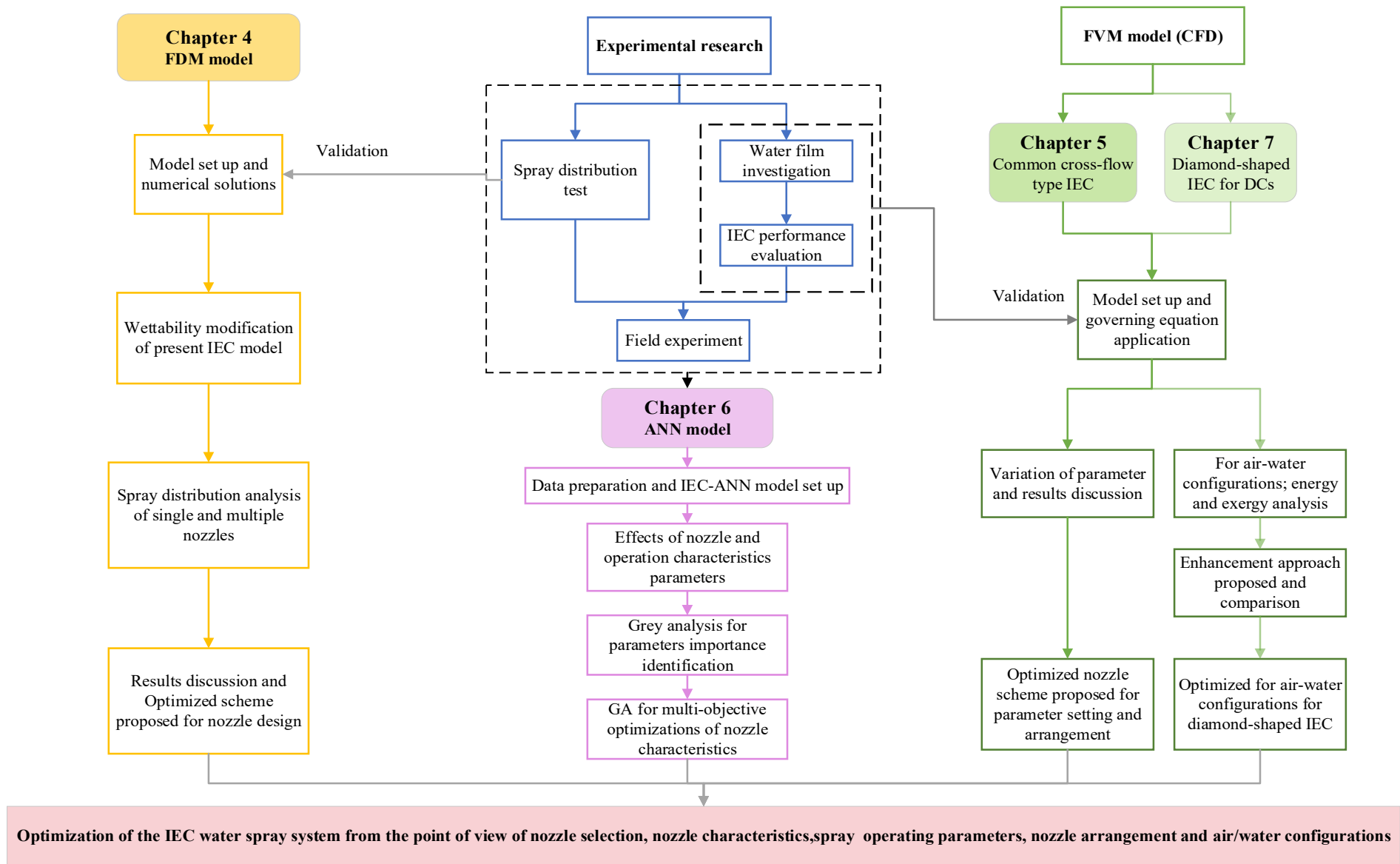


Fig. 3.1 The flowchart of this thesis

CHAPTER 4 DEVELOPMENT OF NUMERICAL MODEL FOR NOZZLE OPTIMIZATION OF IEC WITH EXPERIMENTAL VALIDATION

In Chapter 4, a numerical model of water spray from a full cone nozzle commonly used in IEC systems is developed and experimentally validated, which is carried out on a test rig built in the laboratory of PolyU. The structure of this chapter is as follows: First, the numerical model is developed, described, and validated, from which the actual water spray density obtained can be used to correct the wetting factor in the existing IEC numerical model. Secondly, the effects of tilt angle and nozzle spacing are compared using the control variable method. Then, the optimal arrangement scheme was determined based on the uniformity factor and coverage of the water spray. Finally, the results were analyzed.

The objectives of this analytical study can be summarized as follows: 1) to establish a mathematical model to quantitatively simulate the spray distribution of solid conical nozzles with different parameters and arrangements; 2) to comprehensively analyze the wetting rate of the wetted channel and to correct the ideal assumed values in the existing model of heat and mass transfer within the IEC; and 3) to propose the optimal nozzle arrangement scheme to maintain good wettability of the IEC surface.

This chapter is written based on a published paper of this thesis' author. The paper is titled "*Study on water spraying distribution to improve the energy recovery performance of indirect evaporative coolers with nozzle arrangement optimization*" in *Applied Energy*.

4.1 Introduction of mathematical model

The whole water system in an IEC usually consists of four elements, a certain number of solid cone nozzles, water pipes, water pumps and water tanks. The spray distribution above the heat exchanger, whose sprayed water will later fall into the secondary airflow channel, is regarded as the key research object. Therefore, this thesis first focused on the modeling of the solid cone nozzle spray system in the IECs.

4.1.1 Spray density distribution model

Because of the uneven distribution of water spray across the affected area, a numerical model should be proposed to predict the density distribution of solid cone nozzle spray at a certain height [124]. Based on the ordinary spray volume flux distribution model developed by Mudawar et al. [125], a numerical model for predicting the spray density distribution at various locations above the heat exchanger is established. Instead of describing the spray distribution range accepted by the circle with R as the radius, the new model with the differential element method could obtain the spray volume distribution value at different locations by integrating dx and dy in an infinitely small area at different locations. In addition, the presence of inclination angle factors in spraying is also included in this model, which facilitates a more comprehensive comparison and analysis of spray density distribution. As shown in Fig. 4.1, for a solid cone single nozzle, the overall shape of the spray is conical. The profile of the cut surface is triangular, and the bottom surface connected to the heat exchanger is circular. The connection between these geometric shapes and their characteristics follows the basic principle that governs

the modeling process. Other additional assumptions are as follows:

- Spray droplets have no mass exchange with the surroundings.
- The entire spray flow volume is evenly distributed on any spherical surface centered on the spray orifice with the limitation of the spray solid cone angle (θ).
- The effects of air resistance are ignored due to the short drop distance and fast drop rate of the spray droplets.

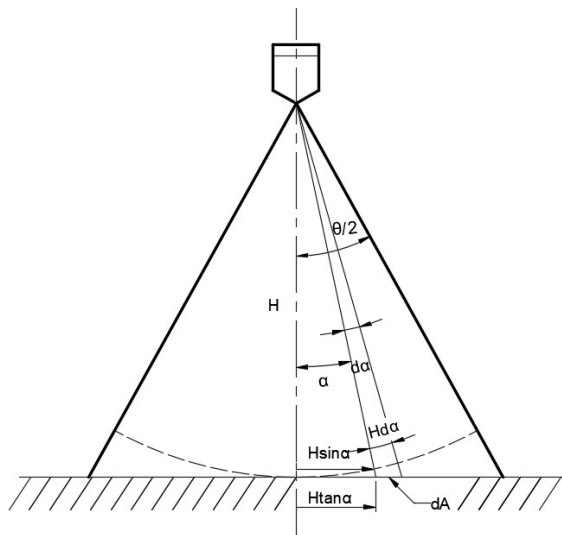


Fig. 4.1 Sketch employed in the spray volumetric flux distribution model

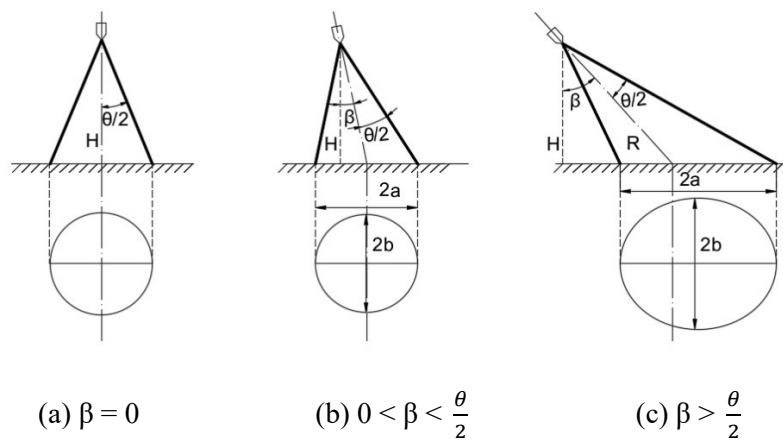


Fig. 4.2 Three scenarios of the impact area with/without inclined angle

The proposed spray distribution model was divided into three scenarios shown in Fig. 4.2, namely no inclination angle, the inclination angle less than half of the spray solid cone angle and the inclination angle greater than half of the spray solid cone angle. Due to the different relative positions and geometries of the nozzle and spray projection, the calculations were conducted for the three states. The curve equations for the boundary of the spray area without or with the inclined angle are shown as:

$$x^2 + y^2 = \left(H \times \tan \frac{\theta}{2}\right)^2 \quad (21)$$

$$\frac{(x - x_0)^2}{a^2} + \frac{(y - y_0)^2}{b^2} = 1 \quad (22)$$

For the geometric relationship of the imaginary spherical surface of the spray zone,

$$R = \sqrt{x^2 + y^2 + H^2} \quad (23)$$

$$\cos \alpha = \frac{H}{R} \quad (24)$$

$$dA = 2\pi R^2 \times \frac{\sin \alpha}{\cos \beta} d\alpha \quad (25)$$

$$A = 2\pi R^2 \times \frac{\left[1 - \cos\left(\frac{\theta}{2}\right)\right]}{\cos \beta} \quad (26)$$

For the volume flux of spray surface area A ,

$$Q'' = \frac{Q}{2\pi R^2 \times \left[1 - \cos\left(\frac{\theta}{2}\right)\right]} \times \cos \beta \quad (27)$$

For the flow rate per infinitesimal element,

$$dQ = Q'' r d\phi dr = Q'' dx dy \quad (28)$$

$$dQ = Q'' dx dy = \frac{Q \times H}{2\pi R^3 \times \left[1 - \cos\left(\frac{\theta}{2}\right)\right]} dx dy \quad (29)$$

where θ is the spray solid cone angle, °; α is the spray integral angle introduced for calculation, °; β is the tilt angle of the spray installation, °.

According to Fig. 4.2, the boundary conditions of each element x_i were written as follows:

for $\beta = 0$,

$$y = \pm \sqrt{R^2 - x_i^2} \quad (30)$$

for $\beta \neq 0$,

$$b = a \times \cos\beta \times \sqrt{1 - \tan^2\beta \times \tan^2\left(\frac{\theta}{2}\right)} \quad (31)$$

$$y = \pm b \times \sqrt{1 - \frac{(j - x_0)^2}{a^2}} \quad (32)$$

for $0 < \beta < \frac{\theta}{2}$,

$$a = \frac{H}{2} \times \left[\tan\left(\frac{\theta}{2} - \beta\right) + \tan\left(\frac{\theta}{2} + \beta\right) \right] \quad (33)$$

$$j = x_0 - a + i \quad (34)$$

and for $\beta > \frac{\theta}{2}$,

$$a = \frac{H}{2} \times \left[\tan\left(\frac{\theta}{2} + \beta\right) - \tan\left(\frac{\theta}{2} - \beta\right) \right] \quad (35)$$

$$j = i + H \times \tan\left(\beta - \frac{\theta}{2}\right) \quad (36)$$

4.1.2 Numerical solution

The upper plane of the heat exchanger was divided into infinitesimal elements as shown in Fig. 4.3, which were integrated to give the volume flow distributed within each square grid in Eq. (37). Since the wet and dry channels inside the IEC are separated by the upper and lower edges of the interconnected aluminum plates, while the shape of the closed ends of the dry channels can be seen as sharp corners, so the thickness of the aluminum plates here is negligible. At the same time, we default to spray droplets hitting the top corner and sliding towards the inclined surface, then falling into the wet channels on both sides, so the total length of the water-receiving part of each wet channel can be equivalent to $2s$ ($0.5s + s + 0.5s$).

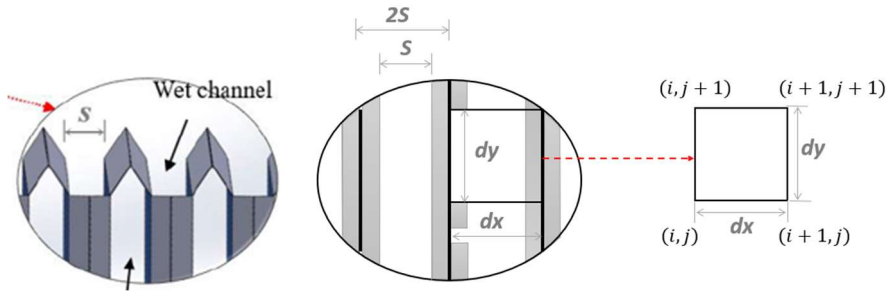


Fig. 4.3 Differential element division method adopted in the model

$$Q_{(i,j)} = \int_{x_i}^{x_{i+1}} \int_{y_i}^{y_{i+1}} \frac{Q \times H}{2\pi(\sqrt{x^2 + y^2 + H^2})^3 \times \left[1 - \cos\left(\frac{\theta}{2}\right)\right]} dx dy \quad (37)$$

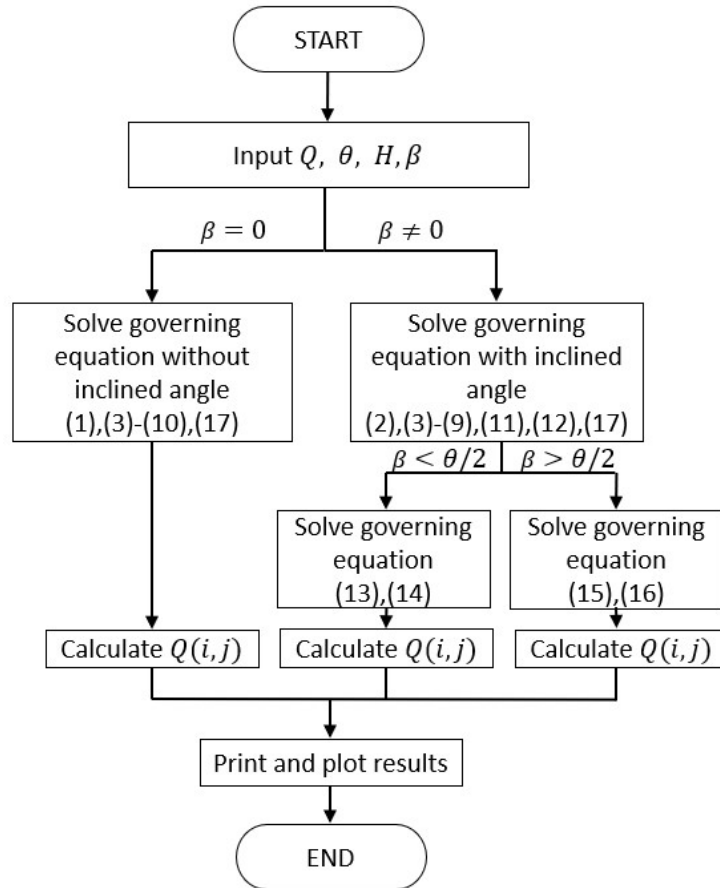


Fig. 4.4 Flowchart of the spray numerical model calculation process

Combined with the boundary conditions, the flow rate obtained per unit was solved by the differential element method with MATLAB. The model solving process was summarized in Fig. 4.4. To reduce the calculation work and simplify the experimental device on the premise of ensuring the accuracy of the numerical model simulation results, the fixed spray coverage area was set at 400 mm × 400 mm and divided into different sizes to detect the optimal grid division area. Throughout the simulation process, the grid size ranges from 10 mm × 10 mm to 50 mm × 50 mm at intervals of 10 mm, while the nozzle flow rate, height and spray cone angle are fixed. To avoid the influence of spray flow rate and thus analyze the most suitable grid size in a targeted manner, 220 L/s is selected as the test spray flow rate.

As shown in Fig. 4.5, the optimal grid size is 40 mm × 40 mm under the limit of allowable accuracy.

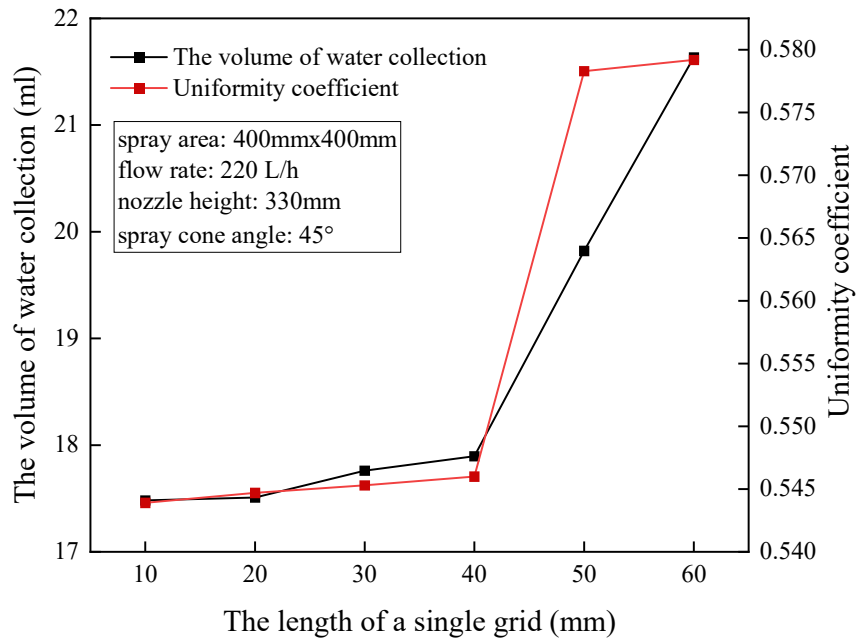


Fig. 4.5 Proof of grid independence for the IEC water spray model

4.2 Model validation

The proposed model was validated by experimental data. Fig. 4.6 illustrates the schematic diagram of the experimental apparatus for the nozzle water distribution model. The components included water distribution pipes, nozzles ($H = 330$ mm), circulating water pumps, water tanks and water collection grids. Since the immersion length of a single nozzle is 330 mm [102], the specification of the water collection grid is designed to be 400 mm × 400 mm, which includes 40 mm × 40 mm independent cells.

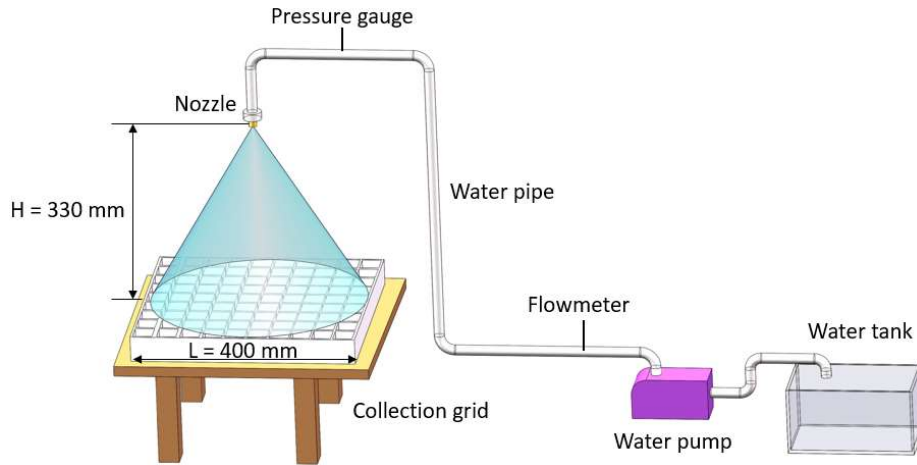


Fig. 4.6 Schematic diagram of the test rig of the IEC water spray system

Regarding the nozzles, three types of full cone nozzles, which are commonly used and easily available, were investigated in this study. Table 4.1 lists the typical fluid dynamics characteristics of these nozzles. In the preparing stage, the nozzle height through the telescopic device was adjusted to determine the nozzle position to obtain the spray state required for the experiment.

Table 4.1 The fluid dynamics characteristics of three solid cone nozzles

Nozzle	Orifice diameter (mm)	Volumetric flow Rate (L/min)	Pressure (bar)	Spray angle (°)
1	2.4	1.9-8.4	0.4-10	45-50
2	3.0	2.9-13	0.4-10	60-70
3	3.2	6.7-16.2	0.4-10	70-75

Besides, this study mainly used a submersible pump in the water tank to drive the water

circulation. The flow meter and pressure gauge are installed on the pipeline from the pump to the nozzle as a measuring device. The nozzle is placed at the end of the water pipe, and the projection position is at the midpoint of the test bench. The spray height is fixed to 330 mm by the bracket. The flow of water in the pipe is controlled by the frequency conversion pump and valve. The measuring instruments are seen in Fig. 4.7, and Table 4.2 lists the specifications of the instruments.

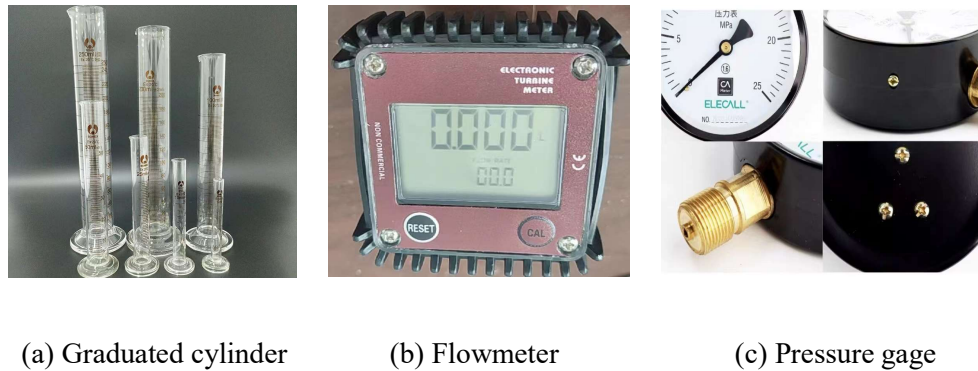


Fig. 4.7 Photos of the test instruments

Table 4.2 Specifications of the instrument

Instrument	Parameter	Range	Accuracy
Graduated cylinder	Water volume	0-10 mL	0.1 mL
		0-100 mL	2 mL
Flowmeter	Water flow rate	1-40 L/min	$\pm 1\%$
Pressure gage	Water pressure	0-1 MPa	$\pm 1\%$

Due to the error caused by the accuracy of the measurement device in the experimental process, it is essential to analyze the data uncertainty of the experimental results [99]. Equations

(38) and (39) illustrate the calculation of the measurement model and uncertainty of the experimental parameters, respectively.

$$U = f(x_1, x_2, x_3, \dots, x_n) \quad (38)$$

$$\delta U = \sqrt{\left(\frac{\delta U}{\delta x_1} \delta x_1\right)^2 + \left(\frac{\delta U}{\delta x_2} \delta x_2\right)^2 + \left(\frac{\delta U}{\delta x_3} \delta x_3\right)^2 + \dots + \left(\frac{\delta U}{\delta x_n} \delta x_n\right)^2} \quad (39)$$

where δU is the overall uncertainty of the required parameter, and δx_n represents the uncertainty of each measurement x_n . According to the accuracy data of each measuring device listed in Table 4.2, it can be calculated that the uncertainty of the uniformity coefficient and coverage ratio of the experimental evaluation indicators are both 2.91%.

The same initial parameters from the experimental model were input into the numerical model. The tests were conducted based on the conditions of: $Q = 220$ L/h, spray cone angle $\alpha = 45^\circ$, nozzle height $H = 330$ mm without inclined angle. The simulation results of the uniformity coefficient and coverage ratio were compared with those from the experiments. As depicted in Fig. 4.8, the maximum discrepancy was 14%, which is acceptable for further analysis.

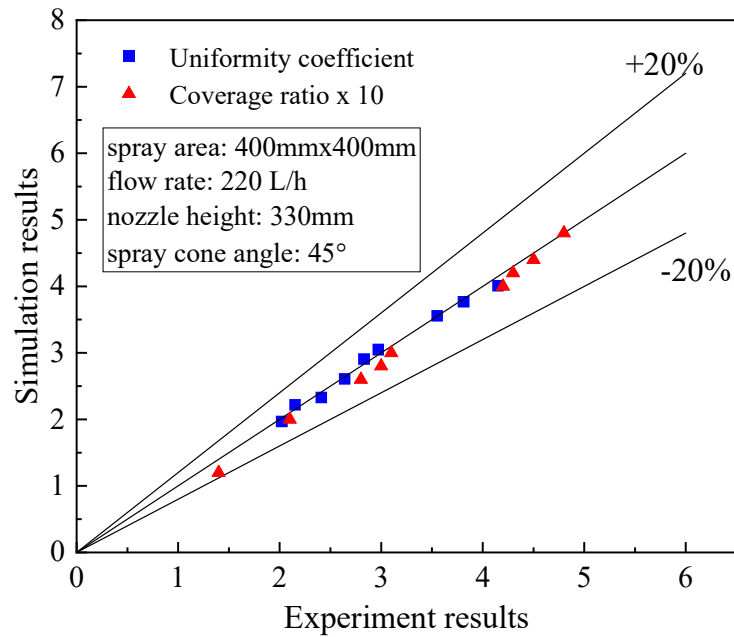


Fig. 4.8 Validation of the modeling results with the experimental data

4.2.1 Wettability modification

Based on the spray volumetric flux distribution model proposed above, the leaching density and unit water flow within each wet channel of the IEC could be revised. The IEC and nozzle parameter settings used here are listed in Table 4.3. Fig. 4.9 (a) presents the sprinkler density calculated by Eq. (40) [100], which is often used as an average value and is considered an important factor for deriving the wettability. However, in the actual spraying process of the nozzle, the water density of each channel length is bound to be impossible to obtain the desired exactly equal result. Therefore, it is reasonable to further apply the spray model developed in this thesis to calculate the actual water density of each channel of the IEC. As seen from Fig. 4.9 (b), the spray density obtained from this developed model is closer to the real spraying situation under the same water flow rate supplied because the result is based on the

accumulation of each infinitesimally small grid rather than a broad mean value.

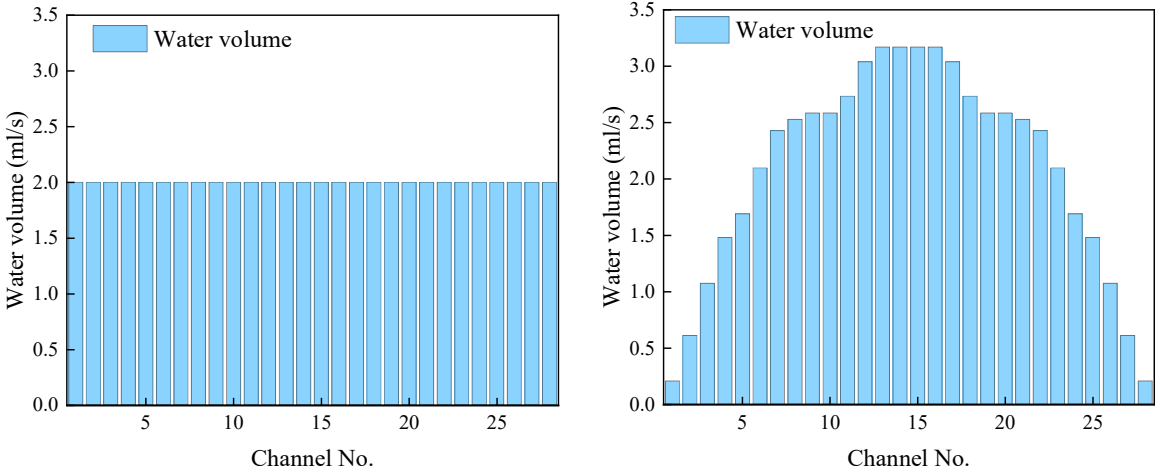
Table 4.3 Fixed parameters of the simulation process

Parameter	Value	Units
Channel pairs	28	-
Channel gap	5	mm
Channel achieved width	10	mm
Heat exchanger length	280	mm
Water flow rate	56	ml/s
Number of nozzles	4	-

The average value of the total flow rate over a unit length plate could be calculated as:

$$\Gamma = \frac{m_w}{(n + 1)L_f} \tag{40}$$

where m_w is the total water mass flow rate, kg/s; n is the total number of secondary air channels; L_f is the length of the plate, mm.



(a) Calculated by the average value of the total flow rate; (b) Calculated by the proposed spray model

Fig. 4.9 The water density distribution under two different calculation methods

In addition, for a vertical surface with a steady and fully developed laminar flow, the Reynolds number, membrane velocity, water membrane thickness and spray density per length after modification could be expressed as [128]:

$$\sigma = \dot{m}_w \frac{h}{2\delta_w v_w \rho_w} \quad (41)$$

$$Re_w = \frac{4\Gamma_i}{\rho_w \mu_w} \quad (42)$$

$$v_w = 1.5 \times \left(\frac{\mu_w g}{48} \right)^{\frac{1}{3}} (Re_w)^{\frac{2}{3}} \quad (43)$$

$$\Gamma_i = \frac{\dot{Q}_i}{L_f} \quad (44)$$

$$\delta_w = \left(\frac{3\mu_w^2}{4g} Re_w \right)^{\frac{1}{3}} \quad (45)$$

where σ is the wettability of the secondary air channel surface; v_w is the mean velocity of water membrane, m/s; δ_w is the thickness of the water membrane above the secondary air channel surface, mm.

Wetting factors have an influence on both heat and mass transfer in the IEC channels. From the perspective of principle, the wetting factor on the surface of the IEC channels is a comprehensive representative parameter of the thickness, flow rate and coverage area of the wet channels water film. When IEC is running stably, the wetting coefficient in the wet channels of the IEC is a key influencing parameter in the evaporation process, and the evaporation process determines the heat as well as mass transfer of IEC to a certain extent. Based on the developed water spray model, the wettability factor (σ) of the original IEC numerical model

(Fig. 4.10) proposed by Min et al. [19] could be corrected by the equations (41)-(45). Furthermore, to validate the modified model the experimental study of Anisimov et al. will be cited, the developed nozzle numerical model was set to the same parameters and arrangement as the experiment, i.e., the nozzle type was a solid cone nozzle with a water spray flow of 3.52 L/h at 10 bar, and a total of eight nozzles were separated on two branch pipes, which were 180 mm apart, while the nozzles on a single pipe were 30 mm apart [51]. Finally, the study calculated of wet bulb effectiveness was compared and validated with the study of Anisimov et al., and the maximum inconsistency was found to be 2.57% according to Fig. 4.11. Therefore, this modified model with corrections of the wettability factor can be used to furtherly analyze the IEC performance.

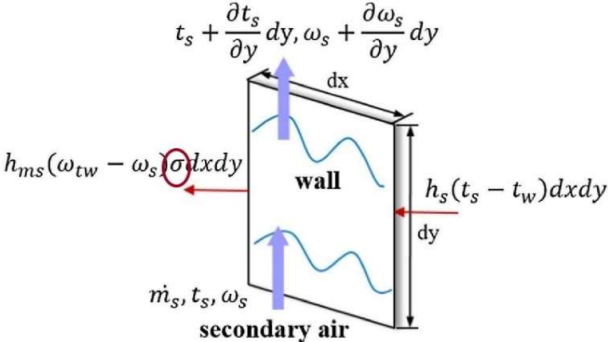


Fig. 4.10 The element within the wettability factor of the IEC numerical model [19]

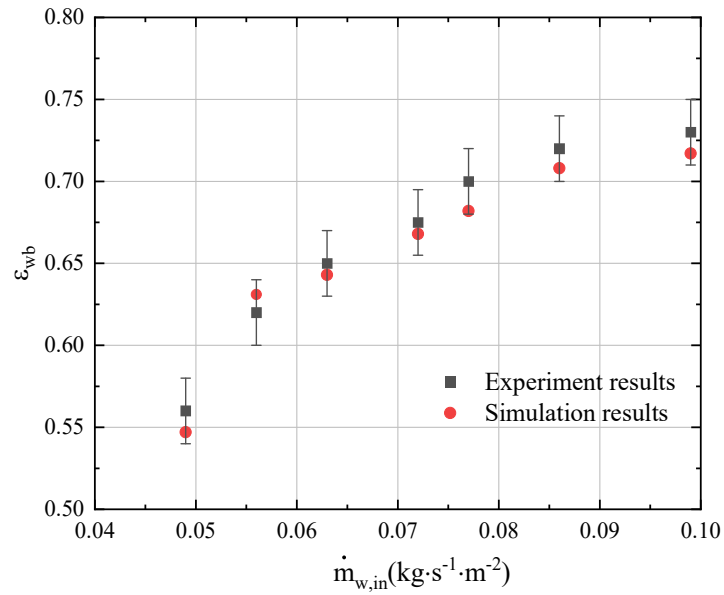


Fig. 4.11 The model validation results of wet-bulb effectiveness based on the published paper [51]

4.3 Results and discussions

4.3.1 Spray distribution of single nozzle

To make a comprehensive comparison to determine the nozzle design that achieves optimal spray uniformity and surface coverage, this section started with a single nozzle by setting the initial conditions for uniformity as follows:

$$H = 330 \text{ mm}, L = 400 \text{ mm}, e = 40 \text{ mm}.$$

4.3.1.1 Nozzles with non-inclined angle

As shown in Fig. 4.12, the spray coverage area is the same when the solid cone angles are 45° and 47° , and then it increases with the larger cone angle of 50° . In respect to the spray distribution, the most uniform value was achieved at the 45° spray cone angle, and the

uniformity coefficient is 2.66, while the unevenness increases by 10% more to 2.9 when the spray angle reached 50°. Therefore, for a 45° angle with a minimum spray uniformity factor but a lower coverage ratio, it is suggested to arrange a multi-nozzle layout to achieve a higher coverage ratio with the optimal uniformity rather than the single nozzle.

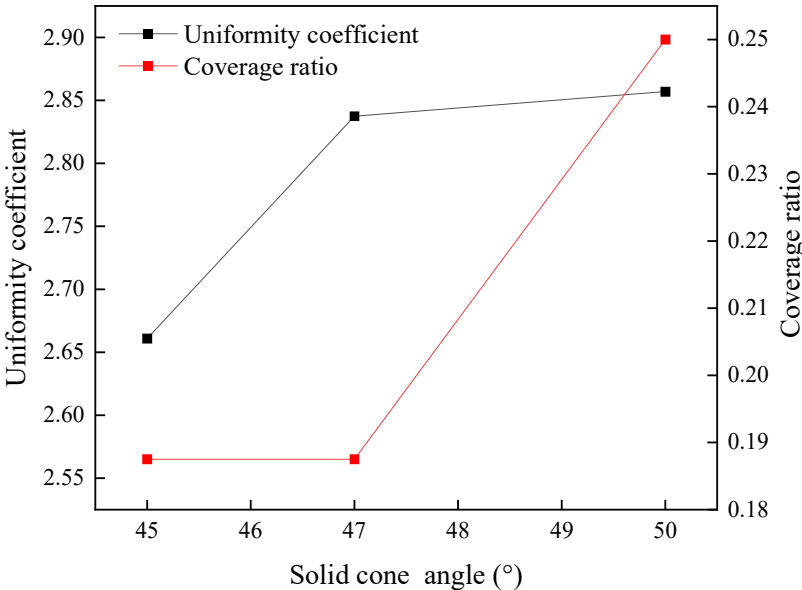


Fig. 4.12 The effect of the spray cone angle of no-inclined angle on the distribution

4.3.1.2 Nozzles with inclined angle

As depicted in Fig. 4.13, with the increase of the inclined angle, the uniformity coefficient of spray distribution increases slowly to 3.38 in the initial stage. However, it decreases sharply after 15° with the growing inclined angle, which ends up by 1.49 at 45°. The spray coverage ratio firstly decreases with the increase of the inclination angle, reaching 0.15 at 15°, and then the coverage area increased significantly after that value to achieve 0.47 at 45°.

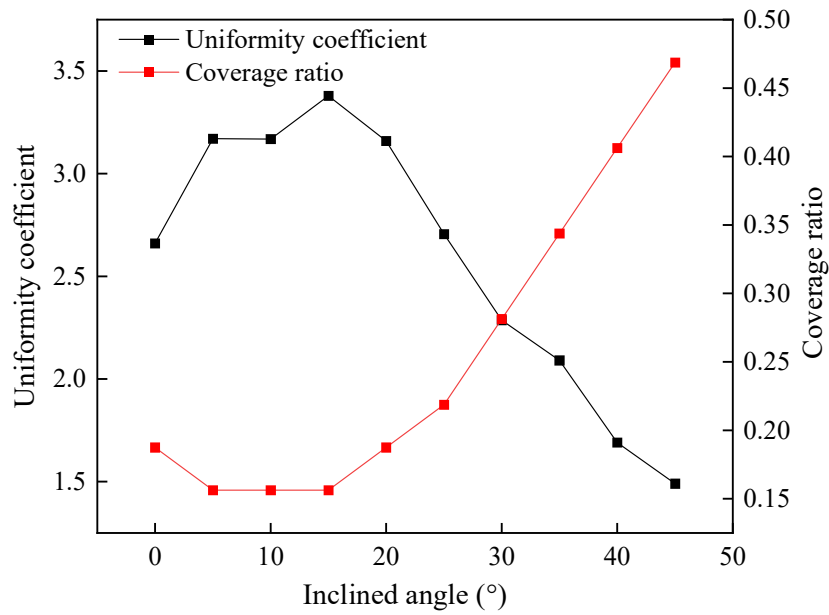
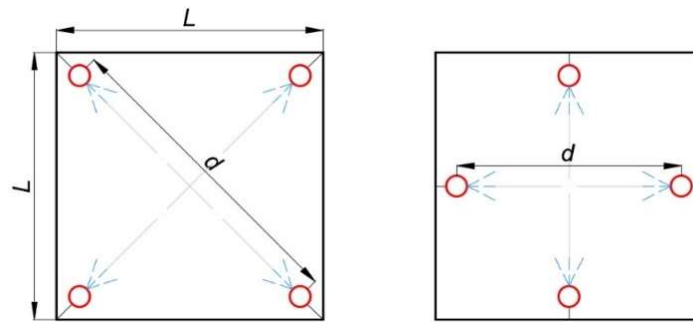


Fig. 4.13 The effect of the inclined angle on uniformity coefficient and coverage ratio

For a single nozzle, when the inclined angle is larger than half of the spray cone angle, greater uniformity and coverage of the spray distribution can be dramatically improved. The optimal value of the uniformity coefficient can reach 1.5, which is 42% lower than that when the nozzle sprays vertically.

4.3.2 Spray distribution of multi-nozzles

Fig. 4.15 Before arranging the layout of nozzles, the length and width of an actual IEC are determined first. The dimension of the heat exchanger is designed as 400 mm × 400 mm, the height of the nozzle is uniformly set to be 330 mm, and the grid size of the heat exchange plate is still 40 mm × 40 mm. By designing multiple nozzles in different arrangements, the best combination of nozzle distance and inclined angle arrangement is obtained. In Fig. 4.14, the two main schemes, namely, diagonal and centerline arrangement of nozzles, are proposed.



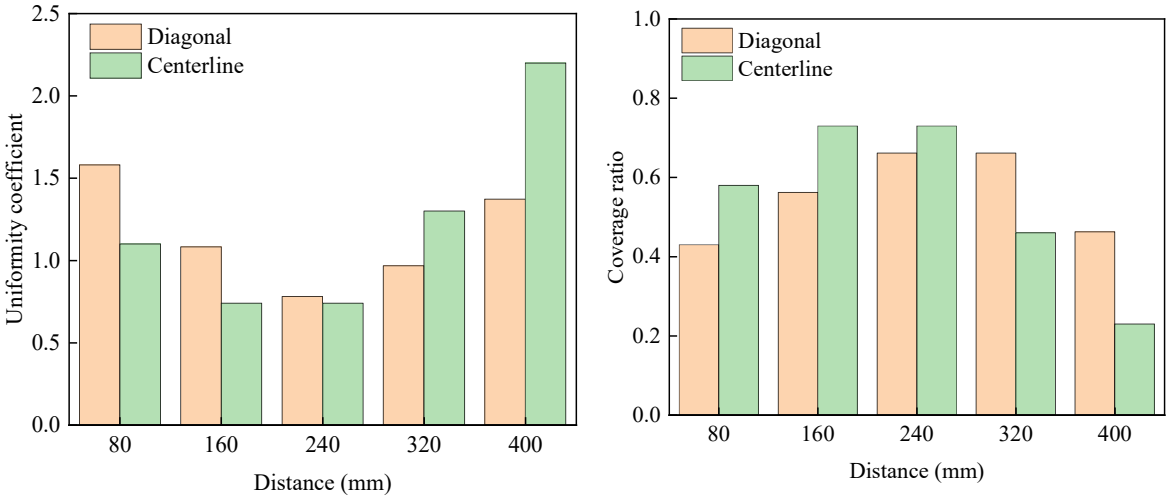
(a) Diagonal arrangement (b) Centerline arrangement

Fig. 4.14 The proposed multi-nozzle arrangement schemes

4.3.2.1 Nozzles with no-inclined angle

Fig. 4.15 (a) and (b) reflect the spray performance variations of the four standard solid cone nozzles mounted vertically at the four top corners as well as the midpoint of the four sides. The trend is presented in a 40 mm interval (the length of each single grid unit). It is noticed that the uniformity coefficients of both diagonal and centerline nozzle arrangements have the same trend of change as the distance decreases, which decreases first and then increases. The coverage ratio grows up with the longer distance in the early stage until 160 mm apart, but suffers from reduction when the distance becomes larger. In summary, considering the two indexes of spray distribution performance evaluation, the best distribution state of the spray is achieved when the nozzle is arranged along the centerline with a distance of 160 mm. At this time, the uniform coefficient is as low as 0.74, which is lower than the minimum value of 0.9 that can be achieved by the previous experimental study of spiral nozzle research [23]. Meanwhile, the coverage ratio of the spray increased to 0.73, much higher than 0.3 when the

same nozzle was randomly arranged.



(a) The uniformity coefficient variation

(b) The coverage ratio variation

Fig. 4.15 The effect of the distance of each nozzle on the distribution performance

4.3.2.2 Nozzles with inclined angle

On the basis of the optimal nozzle distance of 160 mm obtained by section 5.2.2.1, Fig. 4.16 (a) and (b) show the effect of the inclination angle on the water distribution performance. With a single nozzle, the uniformity coefficient of spray in the 0-40° interval showed a tendency to increase first and then decrease later, while the coverage ratio showed the opposite performance. For the diagonal arrangement, the optimal distribution of spray is obtained at 30°, at which point the uniform distribution coefficient and the coverage ratio are 0.78 and 0.62, respectively. For the centerline arrangement, the best values are 1.08 and 0.56, respectively, with a 20° inclined angle. However, the optimal distribution for both cases is far less than the result of the 0 inclined angles, mostly since the spray coverage becomes long and narrow for the case of oblique spray.

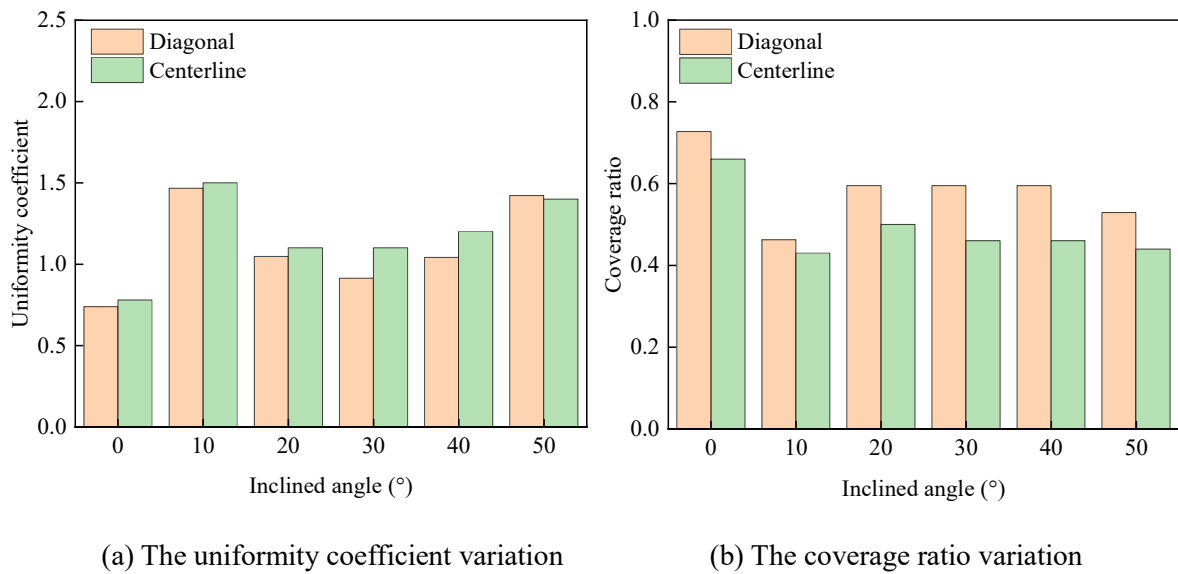


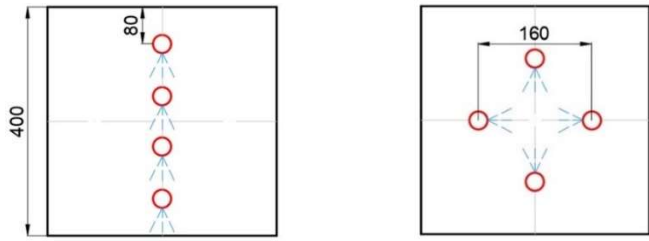
Fig. 4.16 The effect of the inclined angle of each nozzle on the distribution performance

4.3.3 Assessment of wettability performance

4.3.3.1 Wettability comparison

The optimum water distribution of the spray in an IEC system can be achieved by the nozzle arrangement of a size of 400 mm × 400 mm for 160 mm along the centerline with four nozzles. To establish the confidence of the optimized nozzle arrangement, the optimized wettability of wet channels needs to be compared to the original nozzle arrangement scheme. Referring to the common manufacturing instructions and experimental designs of IECs, Zhang et al. explain that the single distribution pipe is usually used as the water distributors in the IECs with small size and small design air volume, and the solid nozzles are arranged equidistant along the length of the pipe [104]. Therefore, considering that the size of IEC studied in this thesis is 400 × 400 × 400 mm³, and the design air volume is 1000 m³/h, the single water distribution pipe scheme arranged by the equidistant nozzles is selected as the original scheme.

For such a specific spray area, Fig. 4.17 (a) and (b) specifically illustrate the two different arrangements of the original single-line scheme and the optimized centerline scheme, and the different water density distribution phenomena obtained were shown in Fig. 4.18, respectively. The coverage area of water is narrow and long in the original nozzle single-line arrangement, and almost half of the area is not involved. From a uniformity point of view, a large amount of water is distributed around the midline, while almost no water droplets fall on both sides, resulting in an extremely uneven overall spray distribution, as shown in Fig. 4.18 (a). Correspondingly, Fig. 4.18 (b) shows the significantly improved coverage area of the optimized nozzle arrangement and the clear reduction of the gap in spray volume distribution at different locations. The comprehensive comparison reflects the superiority of the optimized nozzle scheme for improving the spray performance which is further beneficial to optimizing the wetting factor in the channels. Equations (36)-(40) are applied to calculate the corresponding wetting coefficient values of 0.48 and 0.89, respectively.



(a) Original single-line arrangement (b) Optimized centerline arrangement

Fig. 4.17 Description of the two different nozzle arrangements before and after op

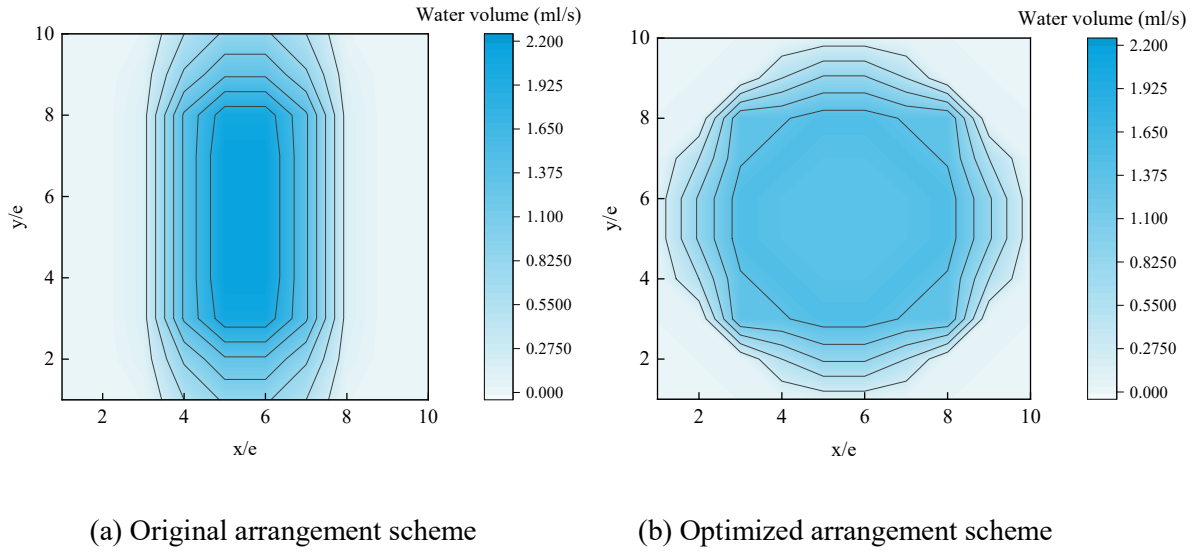


Fig. 4.18 The water distribution results on the aimed sprayed area

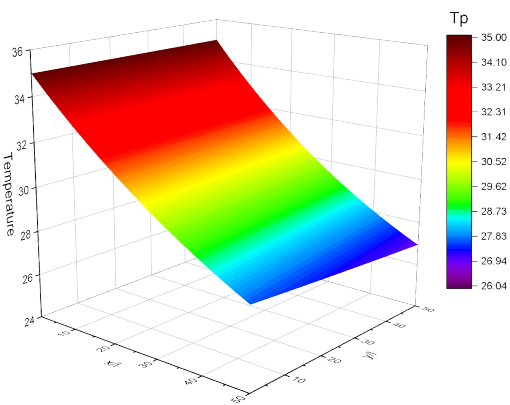
4.3.3.2 Comparison of thermal performance

The following intake characteristics and IEC specifications were studied as examples to compare the air temperature as well as humidity distribution of a cross-flow IEC with different nozzle arrangements. Details of the basic numerical IEC model could be found in the published works by Min et al. [19], and the grid size is $8 \text{ mm} \times 8 \text{ mm}$.

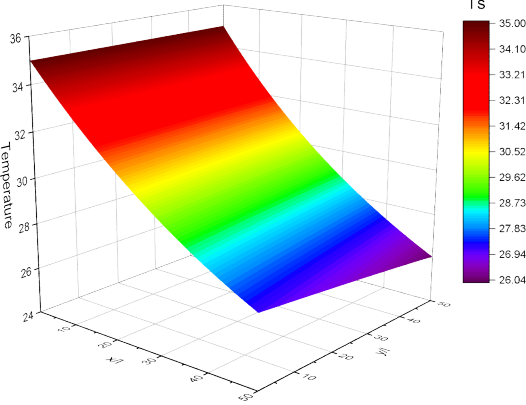
$$t_p = 35 \text{ }^\circ\text{C}, \quad RH_p = 50\%, \quad u_p = 2 \text{ m/s}, \quad t_s = 24 \text{ }^\circ\text{C}, \quad RH_s = 60\%, \quad u_s = 2 \text{ m/s}, \quad s = 5 \text{ mm}, \quad H = 0.4 \text{ m}, \quad L = 0.4 \text{ m}.$$

By combining the observations of Fig. 4.19 (a) and (b), it is found that the optimized nozzle arrangement scheme allows the primary airflow to obtain a greater degree of temperature drop after flowing through the dry channel, which can be reduced to 26.1°C compared to the original scheme at the minimum temperature of 27.4°C at the outlet which is due to the more uniform distribution of the water membrane in the wet channels. A more thorough evaporative

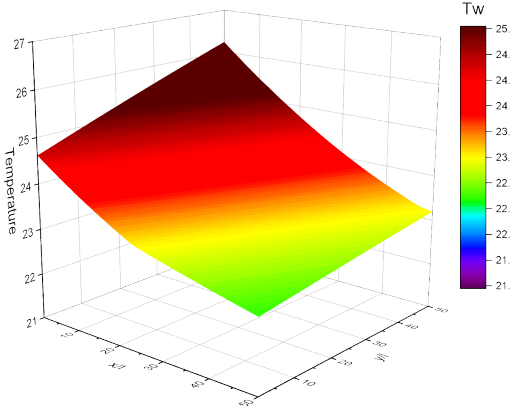
endothermic process can thus be achieved. The further analysis combined with Fig. 4.19 (c, d) and (e, f) could prove that when the surface temperature of the plate is lower than 23.2°C, regardless of the wetting rate is 0.48 or 0.89, condensation begins to appear in the channels, and the humidity on the surface of the plates also begins to decrease at this time. However, when a higher wetting rate is obtained through an improved nozzle arrangement, its rapid temperature drop will also lead to an early occurrence of condensation phenomena, and the final dehumidification rate can reach 0.0170 less than the original 0.0178.



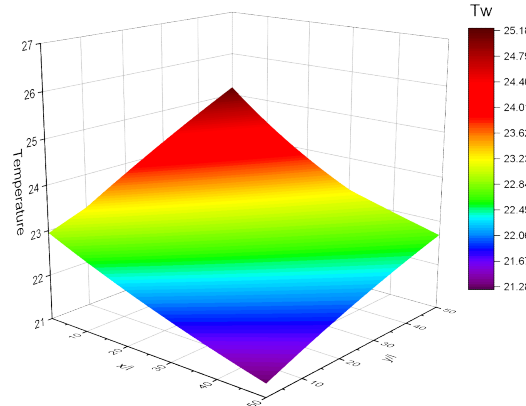
(a) Temperature of primary air by original scheme



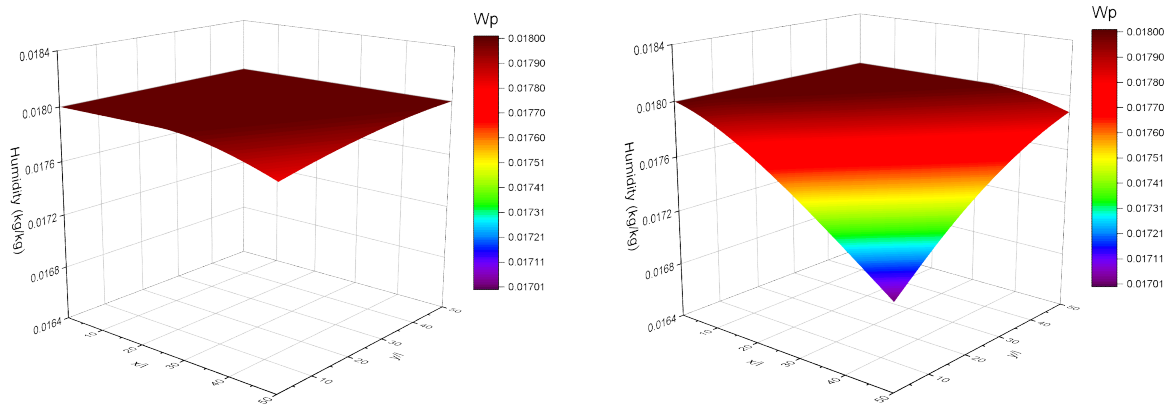
(b) Temperature of primary air by optimized scheme



(c) Temperature of water film by original scheme



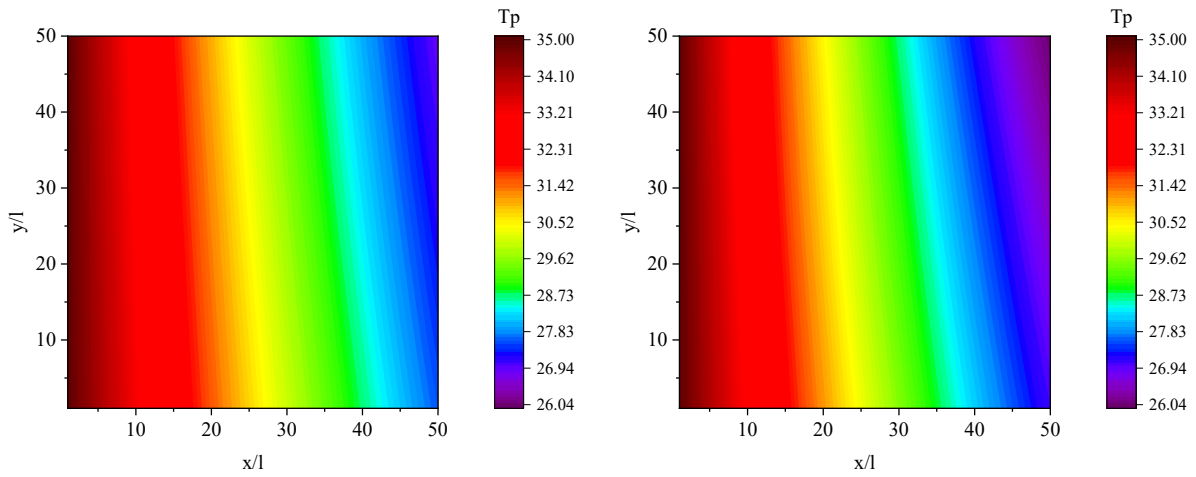
(d) Temperature of water film by optimized scheme



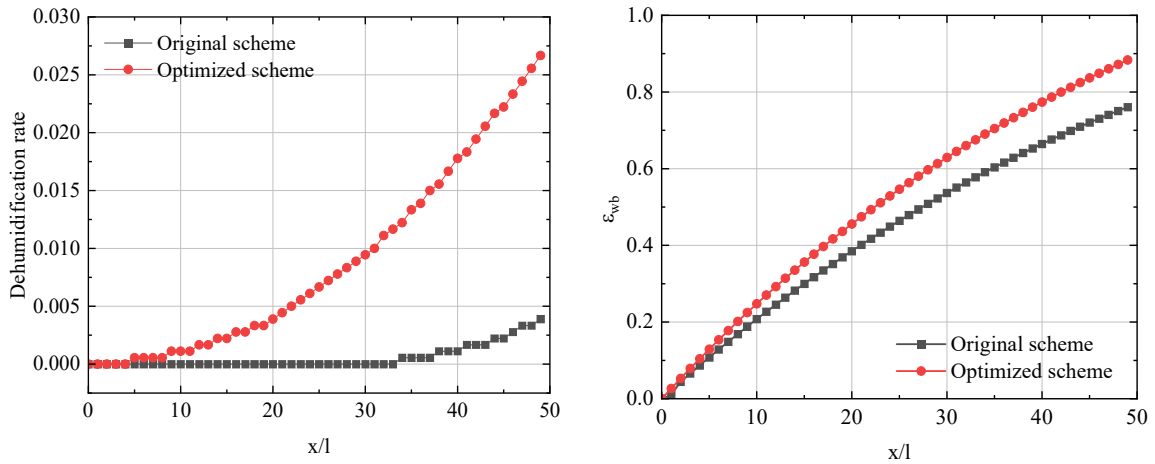
(e) Humidity of primary air by original scheme; (f) Humidity of primary air by optimized scheme

Fig. 4.19 Temperature and humidity distributions of the original and optimal scheme

As described in Fig. 4.19 discussed in the previous section, due to the direction of flow, the temperature distribution on the layout is uneven, and Fig. 4.20 (a) and (b) are given here to more intuitively compare the temperature drop of the primary air in the channel under different nozzle arrangements. The results can clearly state that the closer the temperature drop is to the outlet, the greater the intensity, and as the nozzle distribution improves, the temperature drop of the product airflow is faster and the temperature drop is greater. Besides, the specific average temperature value of the primary air flow outlet is clarified, indicating that the minimum temperature of the product outlet before and after the improvement of the nozzle distribution is 26.61°C and 27.77°C , respectively. Therefore, the optimized nozzle arrangement results in lower outlet temperatures by increasing the wetting rate.



(a) Temperature of primary air by original scheme; (b) Temperature of primary air by optimized scheme



(c) Average value of the dehumidification rate

(d) Average value of wet-bulb effectiveness

Fig. 4.20 Comparison of the impact of the spray scheme on IEC performance improvement

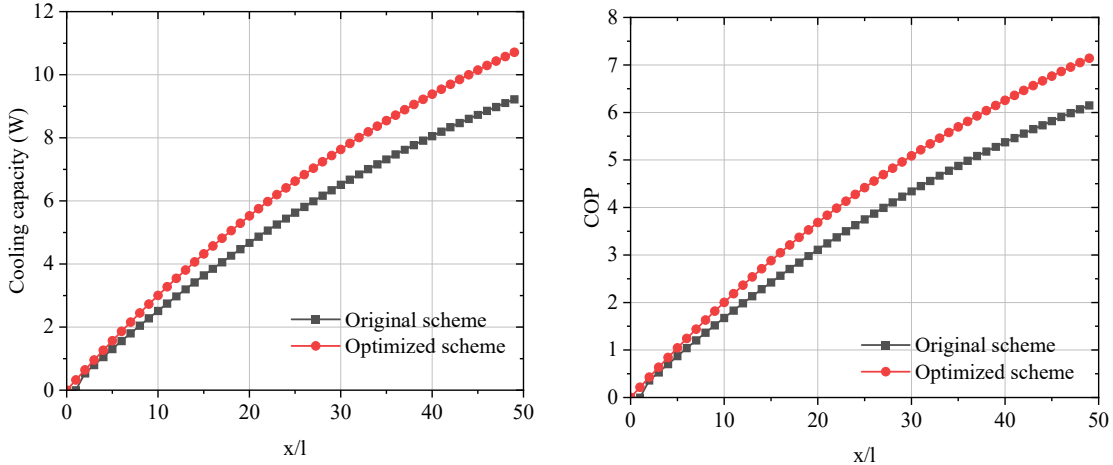
Fig. 4.20 (c) compares in detail the dehumidification rate of the IEC before and after the optimized nozzle arrangement, and the results show that the average outlet dehumidification rate is 0.0039 and 0.0267, respectively, that is, the optimized dehumidification rate is increased by 5.85%. Fig. 4.20 (d) depicts the cooling performance of the original arrangement scheme of the nozzle and the optimization scheme, indicating that its wet-bulb effectiveness is trending upward along the direction of the product airflow and reaches a maximum value at the outlet.

In addition, compared with 76% of the original plan, the optimized solution has improved the IEC's performance by 16%, up to 88%. The results show that since a more uniform spray distribution could achieve higher wettability, the wet surface ratio inside the wet channel is larger with a suitable water membrane thickness, the evaporation rate on the plate will be higher, and the temperature of the plate will be further decreased, which will promote the heat transfer rate. Therefore, the effect of increasing the wettability on the improvement of dehumidification rate and wet-bulb effectiveness is considerable.

4.3.4 Assessment of energy performance

As shown in Fig. 4.21 (a) and (b), the cooling capacity of the IEC system continues to increase with the direction of primary airflow and reaches a maximum value at the airflow outlet. However, when the IEC plate surface wetting rate is 0.89, the cooling capacity can finally reach 10.71, which is 16% higher than 9.22 at a 0.48 wetting rate. Meanwhile, the total water flow provided for the two nozzle distribution schemes is the same, thus the energy consumption of the pump and the fans is the same. The COP value shows the same trend as the refrigeration capacity with the direction of product airflow, which is constantly increasing, and the maximum value is obtained at the outlet. At this time, compared with the original arrangement scheme when the highest COP value of 6 was obtained, the COP value of the improved water distribution scheme increased by 16%, i.e., 7.14. It is noted that the improved water distribution scheme could effectively optimize the uniformity of the water distribution in the IEC heat exchanger plate surface under the same water supply amount, thereby improving the wetting

rate of the plate surface, so that the thermodynamic performance and energy performance of the IEC system are improved. Correspondingly, when achieving the same cooling effect, the energy consumption of the IEC with the original nozzle distribution scheme will be significantly higher than that of the optimization scheme, resulting in a decrease in COP value.



(a) Average value of primary air cooling capacity

(b) Average value of COP

Fig. 4.21 The energy performance compared by two different spray schemes

4.4 Summary of this chapter

In this chapter, in response to the lack of existing research on the numerical study of IEC nozzle arrangements, a numerical model is developed to predict the water spray density distribution of a solid conical nozzle on a uniformly divided square grid impact surface and an experimental rig is constructed to validate the model. The actual water spray density obtained in the model was then used to correct the wetting factor in the existing IEC numerical model, and the optimal nozzle arrangement was determined by comparing the effects of different nozzle tilt angles and distances between nozzles. The main findings from this chapter are

summarized as follows.

- 1) The optimal spray distribution for a single cone spray nozzle scheme has the largest coverage ratio at a spray cone angle of 45° and an inclination angle of 30° , where the uniformity and coverage ratio are 1.49 and 0.47, respectively.
- 2) Based on the uniformity coefficient and coverage of water spray, the optimal arrangement scheme was determined, i.e., the nozzles were installed along the centerline with a spacing of 160 mm. The optimum distribution of fully conical nozzles resulted in a uniformity coefficient of 0.74 compared to the original single-line nozzle arrangement.
- 3) The optimized nozzle arrangement achieved greater air cooling and dehumidification by increasing the wetting factor from 0.48 to 0.89, which resulted in an increase of 6% and 5%, respectively.
- 4) Under the same operating conditions, the coefficient of performance (COP) of the IEC system increased by 16% with the optimized nozzle arrangement, demonstrating the benefits and importance of optimizing the IEC nozzle arrangement.

CHAPTER 5 DEVELOPMENT AND VALIDATION OF CFD MODEL FOR IEC CONSIDERING WATER FILM FORMATION WITH SPRAY PARAMETER ANALYSIS

In this chapter, a spray model based on CFD was established for indirect evaporative cooler, enabling the simulation of dynamic process of water droplets produced from the nozzles and entrained in water film along the surface. A test bench with a complete IEC system was set up to investigate the practical wetted sections on the surface of one channel pair for model verification. Validated by the experimental results, the developed numerical model could be applied to further parametric analysis and optimization on IEC performance. The optimal design on influencing parameters could be obtained by a series of simulation work. To further understand this chapter, a flow chart is shown in Fig. 5.1.

This chapter is written based on a published paper of this thesis' author. The paper is titled "*Spray parameter analysis and performance optimization of indirect evaporative cooler considering surface wettability*" in *Journal of building engineering*.

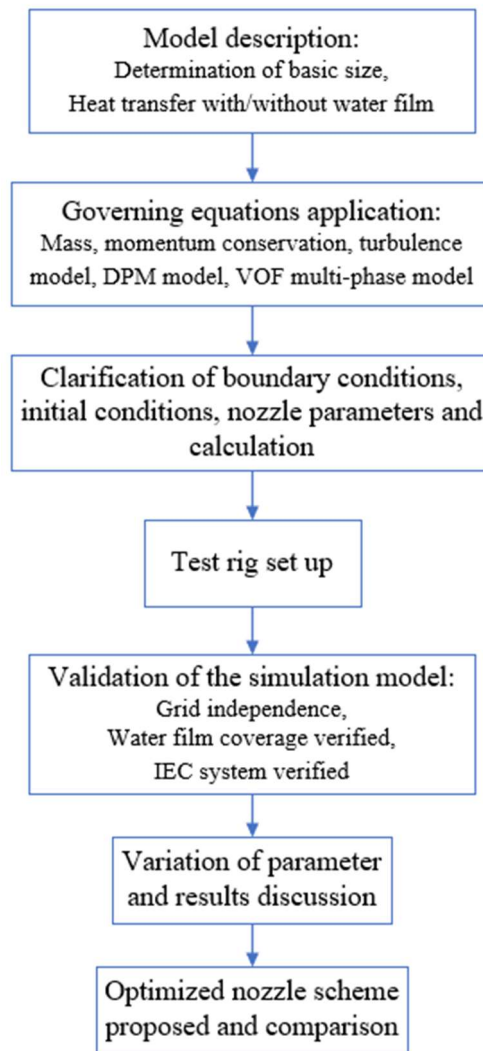


Fig. 5.1 Flowchart for this section

5.1 Introduction of CFD model

The whole water system in an IEC usually consists of four elements, a certain number of solid cone nozzles, water pipes, water pumps and water tanks. The spray distribution above the heat exchanger, whose sprayed water will later fall into the secondary airflow channel, is regarded as the key research object. Therefore, this section focused on the modeling of the solid cone nozzle spray system in the IECs.

5.1.1 Model geometry

The baseline model will be presented through Space claim in ANSYS workbench, where the water film coverage coefficient of the wet channel plate surface is specifically set up and used as a key research factor in this study. A set of hypotheses are presented below for in-depth study.

- The characteristics of water and air are constant, and the entire fluid is incompressible.
- The plate of the heat exchanger is adiabatic, so radiation heat transfer is ignored.
- The water film covering the wet channel is not uniform and completely covered, but its thickness is thin due to the fluidity of the film and the amount of water.

A complete IEC system usually consists of three parts: 1) heat exchanger with alternative dry and wet channels, 2) water spray system, and 3) two separate air loops. Due to the similarity of heat and mass transfer generated within the same type of channel, the two-channel (dry and wet channel) heat exchanger model will be considered here as a representative object of study, as depicted in Fig. 5.2. A solid conical nozzle is provided at a height of above the heat exchanger keeps the water flow in the wet channel and the secondary airflow in a reverse direction. The water system works by releasing a series of water droplets from the nozzles, some of which get into touch with the flat plate and produce a water film that runs down the plane. At the same time, secondary airflow flows from the bottom to the top of the wet channel, where it comes into contact with the downward flowing liquid film.

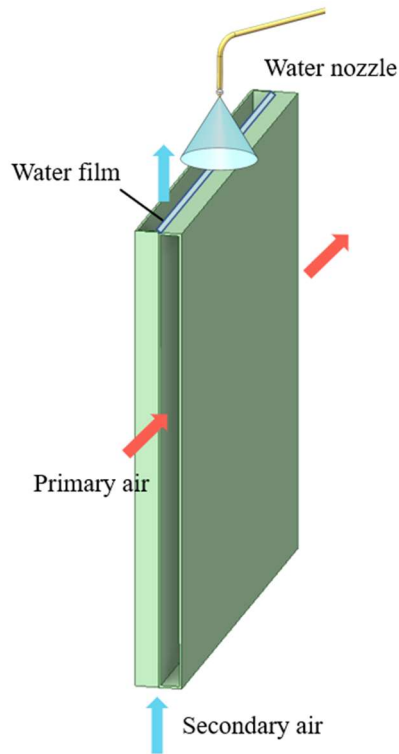


Fig. 5.2 Configuration of an IEC system with single channel

By virtue of the spread features of water, the water film formed by spraying often does not allow the plate surface of the wet channel to be completely wet, and the study conducted in Yang et al [105], confirmed that there is a clear difference in heat and mass transfer at the wet and dry sections of the wet channel as identified Fig. 5.3.

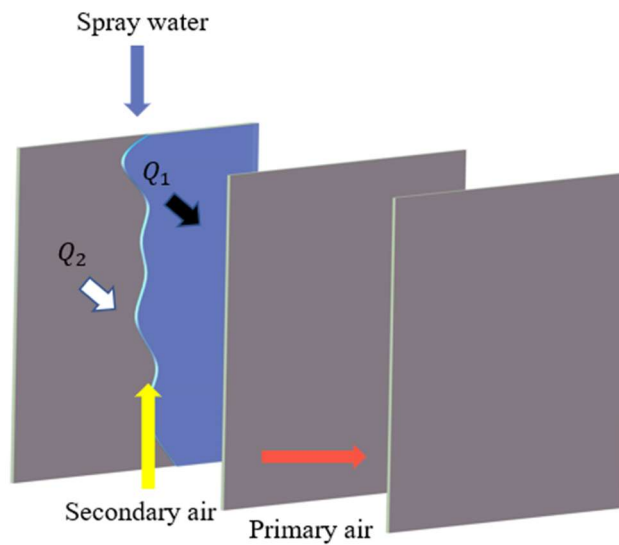


Fig. 5.3 Demonstration model of a single channel pair of a plate crossflow IEC

Therefore, a coverage factor—defined as a ratio of the wetted section assigned on the entire plate surface, as stated by Eq. (46) [36]—should be introduced to evaluate the performance of the water film distribution.

$$\varphi = \frac{A_w}{A_{pl}} \quad (46)$$

where φ represents the coverage factor of the plate surface; A_w represents wet section for water membrane evaporation; A_{pl} represents the entire plate surface area.

5.1.2 Control equations

In contrast to previous approaches to modelling IEC fluids, this study combines the nozzle spray process with the water droplet contact and formation of water film process based on heat and mass exchange between air flows. Therefore, the model of the nozzle spray, water film formation and heat exchanger should be considered comprehensively. The specific formulations for the control principles are as follows:

(1) Conservation of momentum transfer

$$\frac{\partial}{\partial t}(\rho E) + \nabla \cdot (\rho u^2) = -\nabla P + \nabla \cdot (\mu(\nabla u + \nabla u^T)) + \rho g + F \quad (47)$$

(2) Conservation of mass

$$\frac{\partial}{\partial t}(\rho) + \nabla \cdot (\rho u) = 0 \quad (48)$$

(3) Conservation of energy

$$\nabla \cdot \sum_{k=1}^n (\alpha_k v_k (\rho_k E_k + p)) = \nabla \cdot (k_{eff} \nabla T) + S_E \quad (49)$$

(4) VOF multi-phase model

Due to the presence of both air and water flow in the IEC system during operation and the fact that the liquid has both drop and film forms, the multi-phase flow model needs to be applied here. Each numerical grid in the VOF model has a density and viscosity that were represented by Eqs. (50), (51) and (52).

$$\rho = \alpha_1 \rho_1 + \alpha_g + \rho_g \quad (50)$$

$$\mu = \alpha_1 \mu_1 + \alpha_g + \mu_g \quad (51)$$

$$\frac{\partial \alpha_{1/g}}{\partial t} + \vec{u} \cdot \nabla \alpha_{1/g} = 0 \quad (52)$$

(5) Discrete phase (spray droplets) model

In this study, the DPM model was used to complete the nozzle spray conditions above the heat exchanger, taking into consideration random collisions, coalescence and break-up. The discrete phase droplets will therefore be subject to inertia, the gas phase aerodynamic drag force, as well as gravity. By resolving the force balance equation represented by Eq. (53), the track of the droplets could be calculated using a joint Euler-Lagrangian approach.

$$\frac{d(\vec{X}_g)}{dt} = \vec{V}_g \quad (53)$$

where \vec{V}_g is the speed of droplet (m/s); and \vec{X}_g is the location of droplet (m).

The second law proposed by Newton is applied here to predict the speed of evaporating circular particles of water moving in a steady flow. Air and droplet connection via two methods

facilitate the exchange of mass and heat with air. Eq. (54), a mathematical formula, describes how a single droplet moves.

$$\frac{d(m_a \vec{F}_d)}{dt} = \vec{F}_D + \vec{F}_g \quad (54)$$

The drag force acts in the direction contrary to the relative speed of the moving droplet towards the wind. The size and shape of the water droplet, its relative speed to the airflow, and the property of the air all affect the force generated [129]. All these influencing factors are taken into account by the drag coefficient. For a circular drop, the drag force formulated by Eq. (55).

$$\vec{F}_d = -\frac{\pi}{8} C_D \rho_a D_d^2 \vec{V}_r |\vec{V}_r| \quad (55)$$

where C_D is the drag factor, and \vec{V}_r represents the relative speed of droplet ($m \cdot s^{-1}$).

(6) Eulerian Wall Film (EWF) model

The formation and flow of the water membrane covered along the plate surface should be considered in order to properly characterize the physical processes occurring inside the IEC wet channel. The water droplet injected by the nozzle then trapped by the plate could be seen as transfer to the water membrane and flow down along the wall surface, following the relationship as Eq. (56) and Eq. (57).

$$\frac{\partial \delta}{\partial t} + \nabla \cdot (\delta u_l) = \frac{\dot{m}_s}{\rho_l} \quad (56)$$

$$\dot{m}_s = \alpha_l \rho_l u_{l,n} \quad (57)$$

(7) Species transport model

The phase change process causes some heat mass movement in the wet channel of the IEC

by virtue of evaporation; hence the simulation must include the species transfer model developed by Eq. (58) in order to properly account for this.

$$\frac{\partial C_i}{\partial t} + \nabla J_i = R_i \quad (58)$$

5.1.3 Boundary conditions

The modelling of the overall IEC system relies on the application of the commercial CFD software Fluent, where the heat combined mass transfer between fluids and the evaporation process of the liquid film is considered while the spray is simulated to eject and contact with the heat exchanger plate to produce the continuous water membrane, thus the overall boundary conditions are explicitly represented as follows.

For the dry channel, the front side is used as the air inlet for the primary airflow while the back side is used as the air outlet in contrast. For the secondary air channel, the bottom side of the heat exchanger is defined as the secondary air entrance and the top side as the air outlet. In addition, based on previous assumptions, all panels included in the heat exchanger are set up as adiabatic walls. For the water film section, the inner plate of the wet channel is considered as an absorbable wall for the DPM model with Eulerian liquid film transformation and coupling under certain conditions. The structured grid is applied, and the meshing mode used in this model is depicted in Fig. 5.4. Besides, the water membrane had such a thin film thickness across the heat exchanger plate during the simulation time, so the flow characteristics of the film were captured using a finite mesh with dimensions not exceeding 0.1 mm for the region nearby the wall.

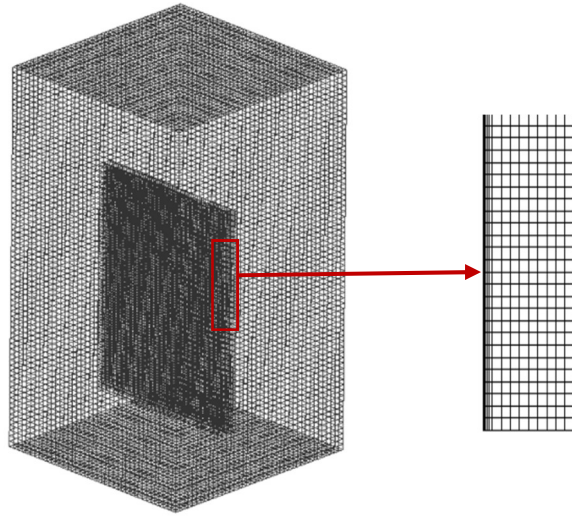


Fig. 5.4 Sketches for the division of the numerical model into meshes

5.2 Description of experimental system

A test bench was set up as depicted in Fig. 5.5 so as to validate the proposed simulation model. The three core components of the experimental system were a plate heat exchanger, a water supply equipment, and an air supply device, respectively. As an essential part of the IEC, the heat exchanger, which is built up of alternate dry and wet channels. Each aluminium plate that makes up the heat exchanger is the same size, $0.25 \times 0.4 \times 0.4\text{m}$, with the surface of each plate showing microscopic protrusions inwards and outwards, as well as every two aluminium plates meeting head to tail to form a 4 mm channel gap to support the flow of air through. When the experimental system is in normal operation, a fan set at the bottom of the heat exchanger supplies a continuous stream of dry secondary air upwards. At the same time, a nozzle built above supplied water into the heat exchanger in a counterflow configuration to the secondary airflow. During this process, some of the water droplets that are sprayed in the heat exchanger

come into contact with the heat exchanger walls and form a water membrane that slides down the walls. In order to allow the distribution of the water film covered on heat exchanger plates to be observed, a transparent panel of plastic is provided on the outermost side. In addition, the nozzles on top of the system will be mounted on slides so that the nozzles can be moved to different distances from the observable walls to support the validation work.

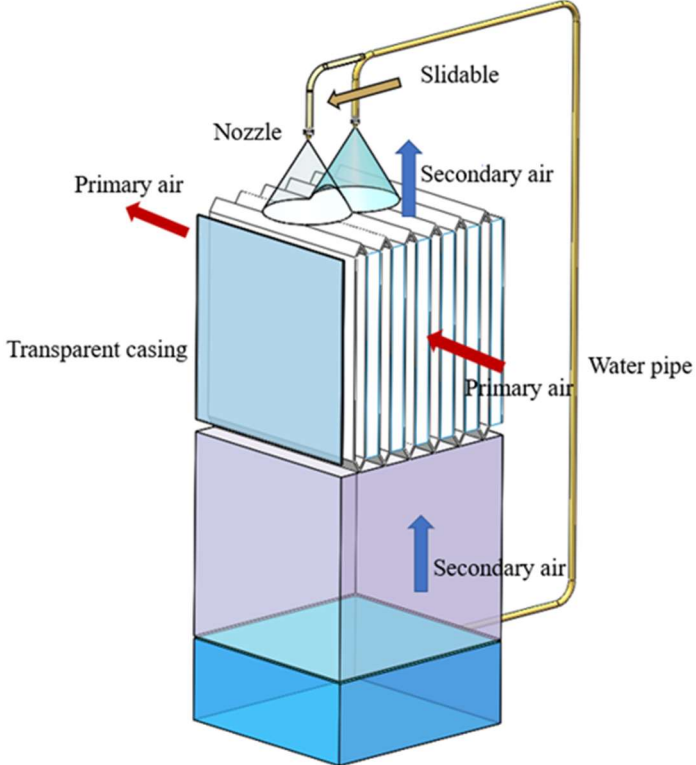


Fig. 5.5 The test bench for the IEC water spray system

5.3 Model validation

5.3.1 The proof of grid independence

The mesh computational model was subjected to the ICEM software in ANSYS work

bench. The water membrane had such a thin film thickness across the heat exchanger plate during the simulation time, so the flow characteristics of the film were captured using a finite mesh with dimensions not exceeding 0.1 mm for the area close to the wall. In general, the accuracy of the calculation increases with the quality of the grid, but the time taken increases when the number of grids is too large. The trade-off between computational accuracy and time cost is therefore critical and the most appropriate number of meshes needs to be determined in order to keep the accuracy of the results within reasonable limits while reducing computational time.

In Fig. 5.6, the coverage ratio calculated by the model at different numbers of grids is shown separately. It is evident that the calculated value clearly increases with the number of grids and then plateaus at grid number of 113200, which is therefore determined as the grid number for subsequent simulations.

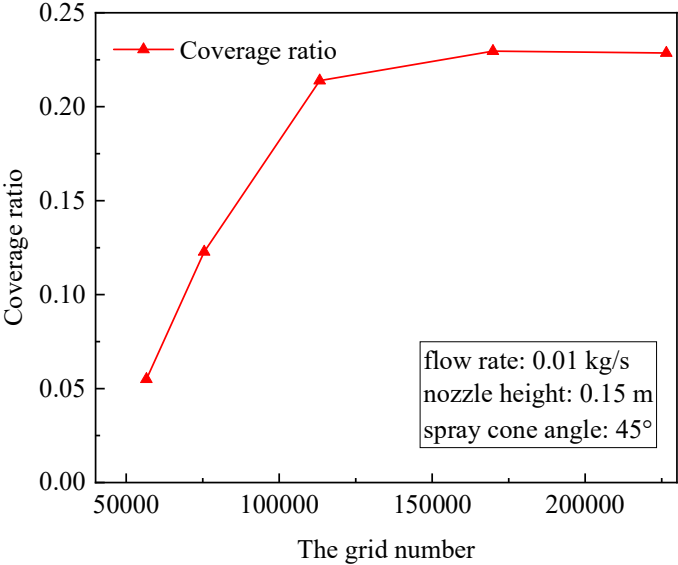


Fig. 5.6 Coverage factor at different accounts of grid

5.3.2 Water film coverage validation

In terms of coverage area occupied by water film, the suggested CFD-based water membrane distribution model was validated. The divided grid will be provided to help collect the water film covering area on the surface of plate. Fig. 5.7 (a) and (b) individually show the division sample of the genuine experimental plate and simulation mode. On this basis, ImageJ software was applied to identify the area of the heat exchanger plate covered by the water film (Fig. 5.7 (c)). The specific steps are to adjust the scale of the picture, then set the picture properties to grey scale display, and finally the contour of the wetted part is indicated by a line to obtain the accurate coverage area.

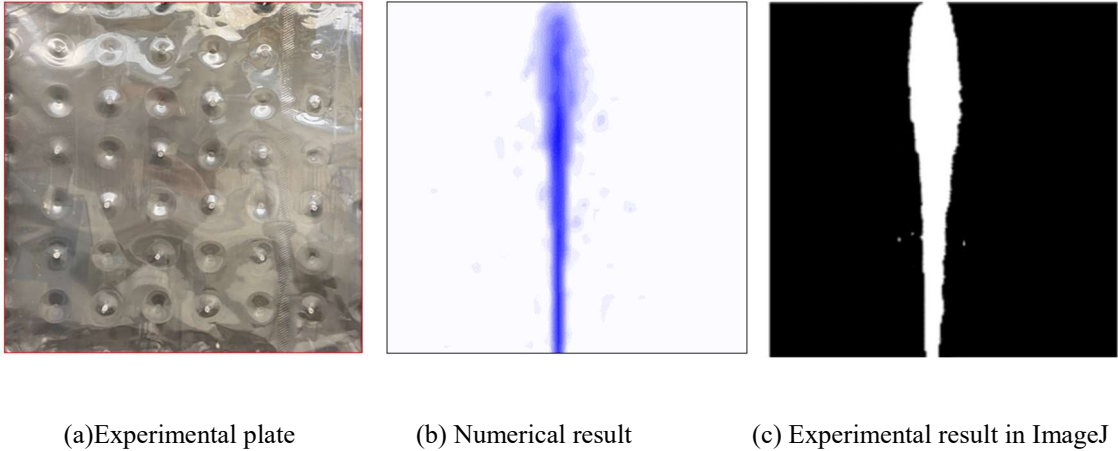


Fig. 5.7 Demonstration of the division sample

Besides, the water circulation in this experiment was primarily powered by a pump system located in the water reservoir. A flowmeter and a manometer are set up as measuring instruments on the section of the water pipe from the pump to the nozzle, respectively. The bracket limits the spray height to 0.15 m, and the frequency converter pump combined with a valve regulates the water flow in the pipe. Fig. 5.8 depicts the photos of instruments, and Table 5.1 has a

description of the feature of each tool.



(a) Flowmeter

(b) Pressure gage

Fig. 5.8 Photos of the test instruments

Table 5.1 Specifications of the instrument

Instrument	Parameter	Range	Accuracy
Flow meter	Flow rate of water	0-0.1 L/h	±1%
Manometer	Pressure	0-1500 kPa	±1%

Uncertainty analysis of the data from the test results is essential due to the errors introduced by the accuracy of the measurement equipment during the experiment [99], Eqs. (59), (60) provide methods on how to calculate the uncertainty of measurement models and experimental parameters, respectively.

$$U = f(x_1, x_2, x_3, \dots, x_n) \quad (59)$$

$$\delta U = \sqrt{\left(\frac{\delta U}{\delta x_1} \delta x_1\right)^2 + \left(\frac{\delta U}{\delta x_2} \delta x_2\right)^2 + \left(\frac{\delta U}{\delta x_3} \delta x_3\right)^2 + \dots + \left(\frac{\delta U}{\delta x_n} \delta x_n\right)^2} \quad (60)$$

where δU represents the entire uncertainty of the specified parameter, and δx_n is the

uncertainty of each measurement x_n . Based on the accuracy data of each testing equipment arranged in Table 5.1, the uncertainty of the coverage factor by the experimental assessment criteria is 2.31%.

The initial parameters of experimental test were applied in the simulation model as well. The experiments were carried out under the following conditions: $Q = 0.01 \text{ kg/s}$, $\alpha = 45^\circ$, and $H = 0.15 \text{ m}$. Fig. 5.9 reflects the simulation results for coverage compared to the experimental results and finds that these points lie within 20% of the deviation and that the maximum difference is 7.1%, which is acceptable for subsequent studies.

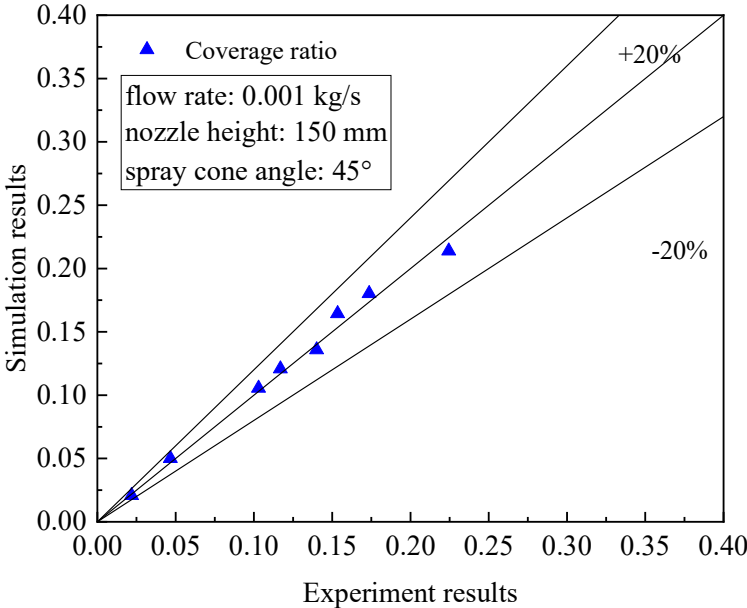


Fig. 5.9 Comparison between the tested and simulated data

5.3.3 IEC system validation

To combine the water film coverage area with the performance of the whole IEC system, another more complete model with validation experiment should be carried out. On the

foundation of section 6.2, the ICEM program in ANSYS was still used to build a numerical model of the mesh, taking into account the temperature and humidity factors with heat and mass transfer. Fig. 5.10 described the test rig of a complete IEC system, which consist primary air channel, secondary air channel and water spray system, and the fixed parameters of experimental setting were shown in Table 5.2. The entire setup was done in a lab with regulated humidity and temperature levels. Table 3 lists the test conditions and the details of the measurement equipment. A data logger recorded, showed, and recorded every piece of tested data, at 2-second intervals.

Table 5.2 Setpoint of the IEC for simulation

Parameter	Value	Units
Channel number	25	-
Channel gap	4	mm
The length of IEC	250	mm
No. of nozzles	2	-

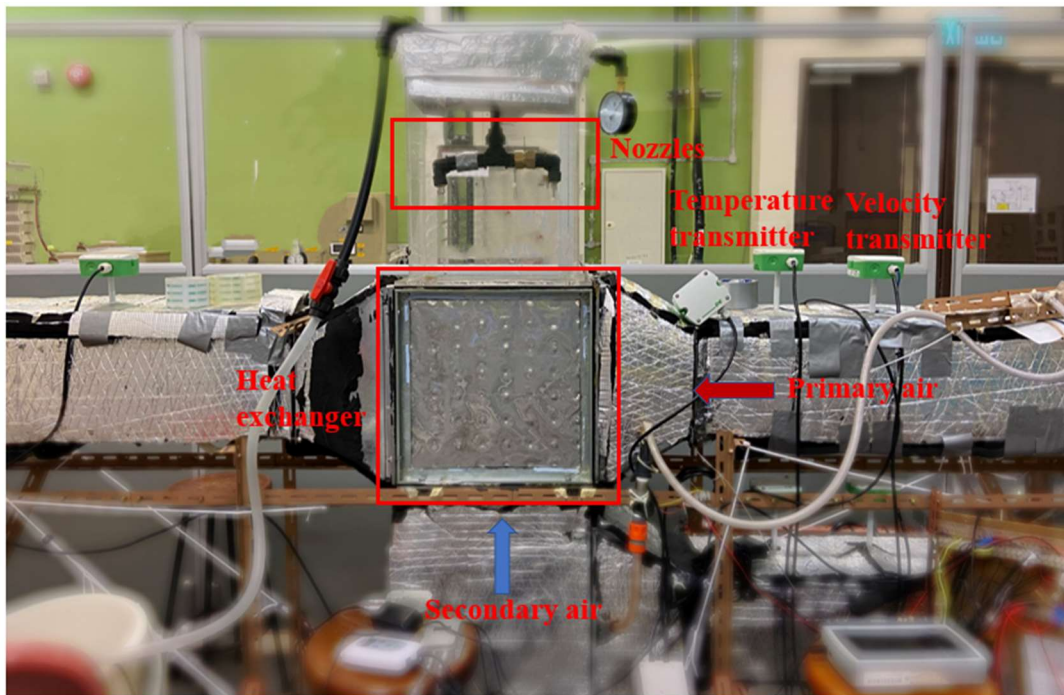


Fig. 5.10 The test bench for the complete IEC system

Table 5.3 Specifications of the test parameters

Instrument	Parameter	Range	Accuracy
Temperature	Temperature sensor EE160	-10-60 °C	$\pm 0.2\%$ °C
Relative humidity	Humidity sensor EE160	-15-95% RH	$\pm 2\%$ RH
Air speed	Velocity sensor EE65	0-0.17 m/min	$\pm 2\%$

According to Table 5.3 and Eqs. (59), (60), the results of uncertainty analyses could be determined. Based on the accuracy data of each testing equipment arranged in Table 5.3, the

uncertainty of the wet-bulb efficiency by the experimental assessment criteria is 4.2 %.

The same settings as section 6.2 were used for the water system in the experimental validation, and the other parameters of the air supply system were set as follows: $t_p = 35\text{ }^\circ\text{C}$, $RH_p = 50\%$, $u_p = 2\text{ m/s}$, $t_s = 24\text{ }^\circ\text{C}$, $RH_s = 60\%$, $u_s = 2\text{ m/s}$, $s = 4\text{ mm}$, $H = 0.4\text{ m}$, $L = 0.4\text{ m}$. Fig. 5.11 reflects the simulation results for coverage compared to the experimental results and finds that these points lie within 10% of the deviation and that the maximum difference is 8.2 %, which is acceptable for subsequent studies.

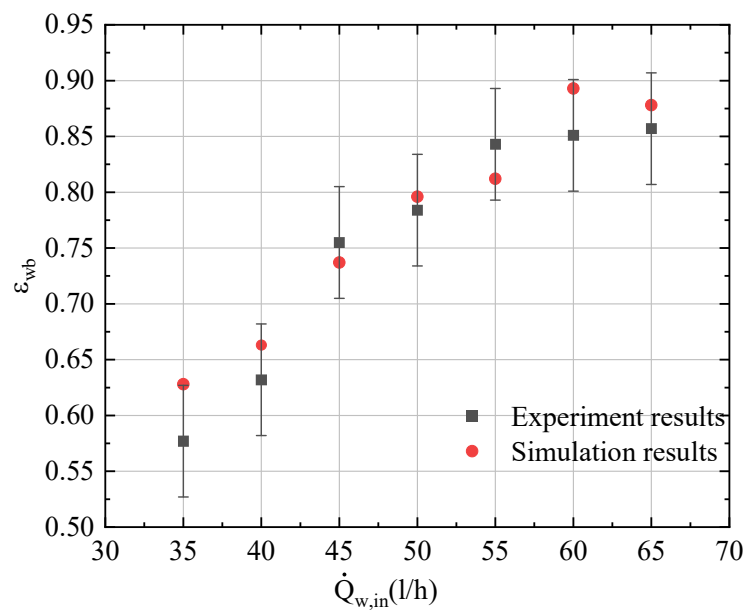


Fig. 5.11 The model verification results based on wet bulb efficiency

5.4 Results and discussions

A parametric analysis was carried out using the validated model to determine the effect of parameter variations in the nozzle on the area covered by the water membrane on the plate

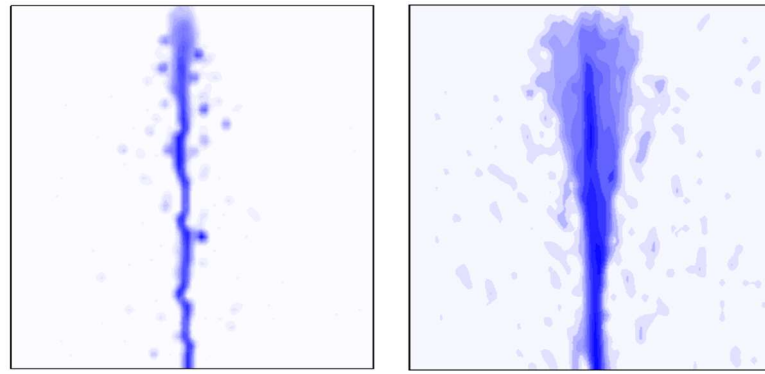
surface of the wet channel.

5.4.1 Influence for single nozzle

5.4.1.1 Droplet parameter

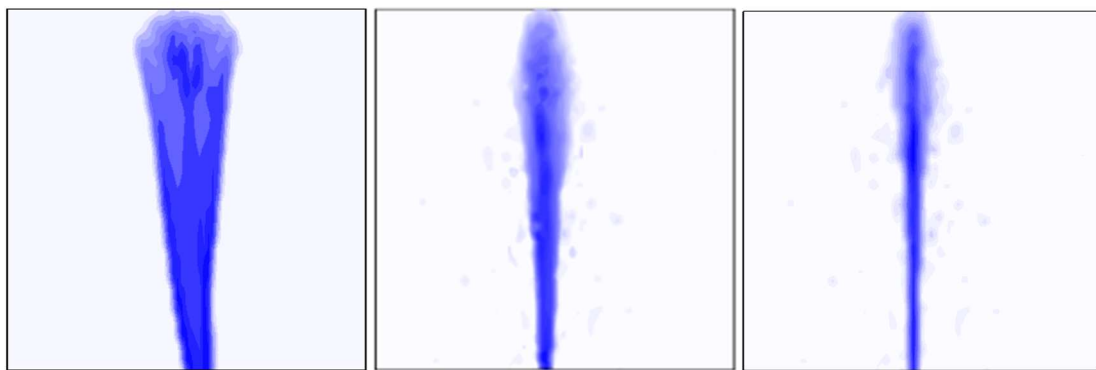
In contrast to the other adjustable parameters of the nozzle, the size of the spray droplet was identified as the key influence in this study as a determinant of whether it drifts or not, while the other parameters were kept constant in the initial simulation step. As shown in Fig. 5.12 and Fig. 5.13, the overall water film coverage increased significantly with rising the droplet diameter at the initial of the diameter expansion, reaching a peak of 0.22 with a diameter of 0.25 mm. Thereafter, as the droplet diameter increased, there was no longer an upward trend and the area covered by the water film instead continued to decrease.

Normally, with a constant flow rate and installation position of the nozzle, if the droplets released from the nozzle are much too small in size with a light weight, they are easily driven by the underside airflow supplied in the wet channel, which results in the droplets being carried away before they arrive at touch with the surface of plate. On the other hand, weight problems can result in droplets with too wide a diameter slipping out of the wetting channel before they arrive in touch with the plate surface. Thus, for the same supply of water rate, an inappropriate droplet size can worsen the area covered by water film, whereas an appropriate size can increase the wetted area up to 61.9%.



(a) 0.05 mm

(b) 0.15 mm



(c) 0.25 mm

(d) 0.35 mm

(e) 0.45 mm

Fig. 5.12 Impact of droplet size on the coverage area

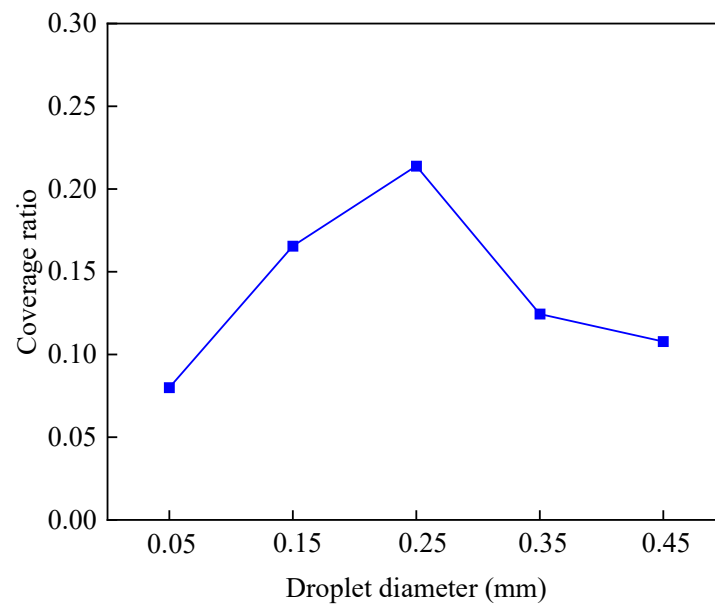


Fig. 5.13 Trend in the effect of droplet size on the coverage area

5.4.1.2 Spray characteristics

In order to evaluate the effect factor of single nozzle in reality, the fundamental spray characteristics should also be discussed. The actual design notes and previous studies have both proved that the flow rate, pressure, droplet diameter and spray cone angle of nozzles are interrelated factors. The main characteristic equations of the nozzle are as follows. According to Lefebvre and McDonell, the theoretical mass flow rate could be calculated as Eq. (61) [107].

$$\dot{m}_{th} = \rho A_o \left(\frac{2\Delta P}{\rho} \right)^{0.5} \quad (61)$$

The average droplet diameter is obtained from the following equation [89]:

$$d = 9.5d_j / (\Delta P_1 \sin(\alpha/2)) \quad (62)$$

Besides, the inviscid theory could be seen as the foundation of the correlation for spray cone angle which is formulated as Eq. (63) [90].

$$2\alpha = 334.32K^{-0.165} \left(\frac{D_s}{D_o} \right)^{-0.484} W_e^{0.043} Re_p^{-0.065} \quad (63)$$

Since the flow rate, pressure, droplet diameter and spray cone angle of nozzles are interrelated factors, it is necessary to balance the degree of variations between these factors while maximizing the nozzle performance. Eqs. (61) and (62) demonstrate that the spray flow increases with nozzle spray pressure while the width of the spray droplets decreases. Additionally, the spray cone angle exhibits a tendency of increasing and then dropping when the nozzle pressure and flow rate are raised, which is consistent with the actual design specification. Obviously, the spray droplet diameter is mainly influenced by the jet pressure at

the nozzle, and at constant pressure the droplet size is almost constant.

5.4.1.3 Spray cone angle and flow rate

According to the theory and experiments, a certain range of spray nozzle spray cone angle the larger the better, from angle increases at the same time, the wider the contact range it can spray. In addition, the larger flow rate supply gives the nozzle a denser droplet, which to some extent increases the area covered by the liquid film on the plate. However, due to the linked nature of the variables in the nozzle, it is not possible to avoid the impact on other factors by simply adjusting one factor in isolation. It is therefore essential to maximize the power of the spray in terms of film coverage and to balance the effects of each factor.

The size of the spray droplet diameter will be the primary consideration in this study in order to better control the smooth entry of the droplet into the airflow channel and the smooth contact with the wall. Based on the conclusions of the analysis in section 6.4.1.1, 0.25 mm should be set as the ideal droplet diameter to be pursued in the study. Besides, three common nozzles with spray diameter of 2.8 mm, 3.0 mm and 3.2 mm were selected as the main object of this study, and Fig. 5.14 reflects the parameter characteristics of the three nozzles in order from left to right according to the different pressures at once. With reference to the results shown in Fig. 5.14, although the droplet diameter (calculated by Eq. (61)) of all three nozzles is close to 0.25 mm at an operating pressure of 1.5 bar, but the spray cone angle of nozzle 1 is too small, while nozzle 3 can reach the maximum spray cone angle but the water consumption is too high. Therefore, the nozzle with a spray diameter of 3.0 mm will be the ideal object of study and its

operating condition will be set at a pressure of 1.5 bar, while the spray flow rate is 5.4 l/min, and the spray cone angle is 68°.

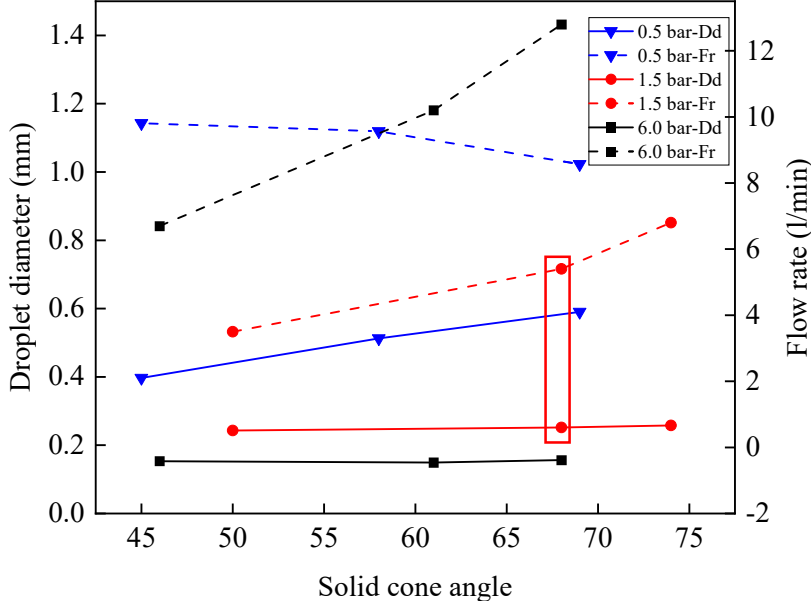


Fig. 5.14 The characteristics of nozzle spray

5.4.1.4 Shrinkage phenomenon

As the material of the heat exchanger is usually aluminum plate, and the spray medium is water with high tension, so as the water film slips, it will inevitably produce the phenomenon of liquid film contraction, making the liquid film away from the secondary airflow outlet the smaller the coverage area [67]. The water droplet membrane consists of the main part of the membrane thickness is basically uniform and there is a raised edge part of the composition. In the direction of flow, the length of the droplet membrane becomes smaller, representing the droplet film gradually shrinks. Thus, in the 3D model, the evaporative heat absorption process within the wet channel takes place only in the wetted area. However, in the 2D model it is unrealistic to assume that evaporation occurs over the entire heat exchanger, as it is not possible

to simulate film shrinkage. Due to the contraction of falling film in the direction of flow, it is evident from the 3D simulation that the evaporation process inside the moist channel is not uniform, as shown in Fig. 5.12. However, neither the film contraction nor the non-uniform mass transfer process can be depicted by a two-dimensional simulation, which clearly demonstrates the need for 3D simulations.

5.4.2 Influence for multi-nozzles

As the above discussion is based on a single-pass heat exchanger, whereas the actual IECs are always multi-pass heat exchangers, a simple discussion of the spray distribution placed vertically above the airflow channels is inadequate. This section will focus on the analysis of the heat exchanger channels that can be covered by a film of water when receiving water spray, from close to far apart from the nozzle. As the nozzle height is fixed at 0.15 m and the spray cone angle is 68° , the maximum distance covered by the outgoing spray is 80 mm, but based on practical conditions about 60 mm is already the limit. The progressive interval was therefore set to 20 mm and 0.25 mm was to be used as the defined droplet spray particle diameter. Fig. 5.15 illustrates the water film formed by the heat exchanger plate surface receiving a fixed single nozzle spray at different locations, and it can be seen that the best wetting situation of the plate surface occurs at a nozzle of 40 mm.

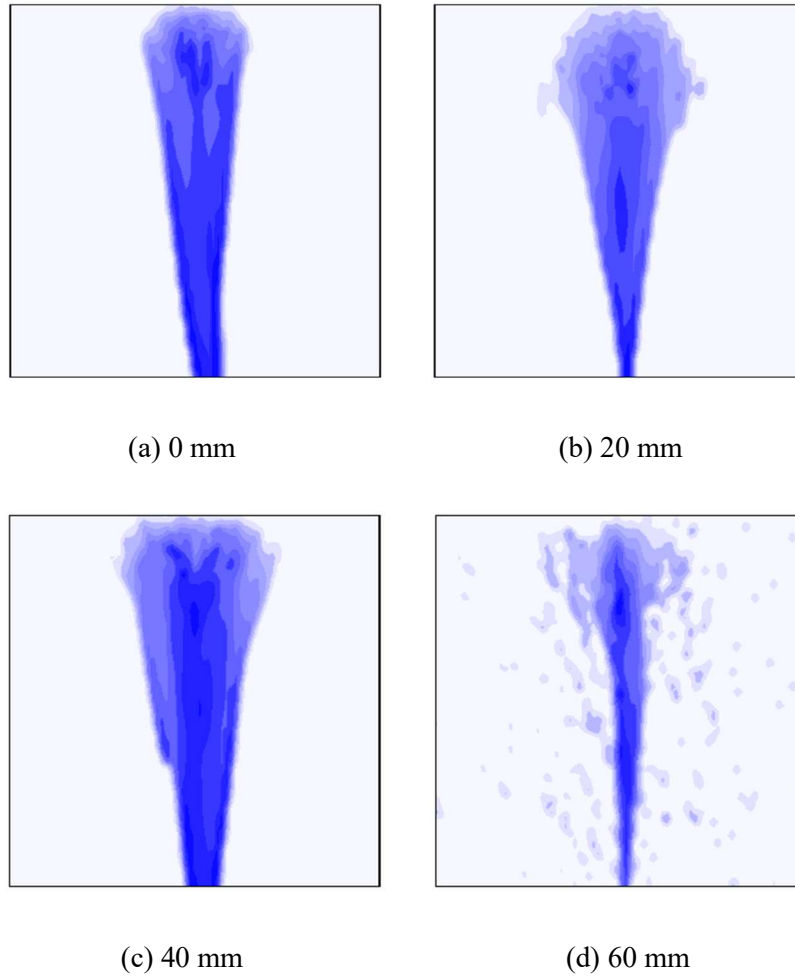


Fig. 5.15 Variation of single nozzle to plate distance

In order to determine the optimum spacing of multiple nozzles, the conditions for achieving maximum water film coverage will be evaluated here using two nozzles as an example and the fixed droplet injection particle size of 0.25 mm should be applied. As shown in Fig. 7.16, once the gap of the two nozzles is extended from 0 mm to 80 mm, the area covered by the water membrane on the surface of the plate rises from 0.32 to 0.53. Nevertheless, when the nozzle spacing exceeds 80 mm, the area covered by the water membrane reduces dramatically. This occurrence could be attributed to the fact that some droplets escape the boundary when the nozzles are placed too far apart, whereas when they are placed too close

together, many droplets collide and splash against one another, preventing the droplets from making contact with the plate and forming a thin film.

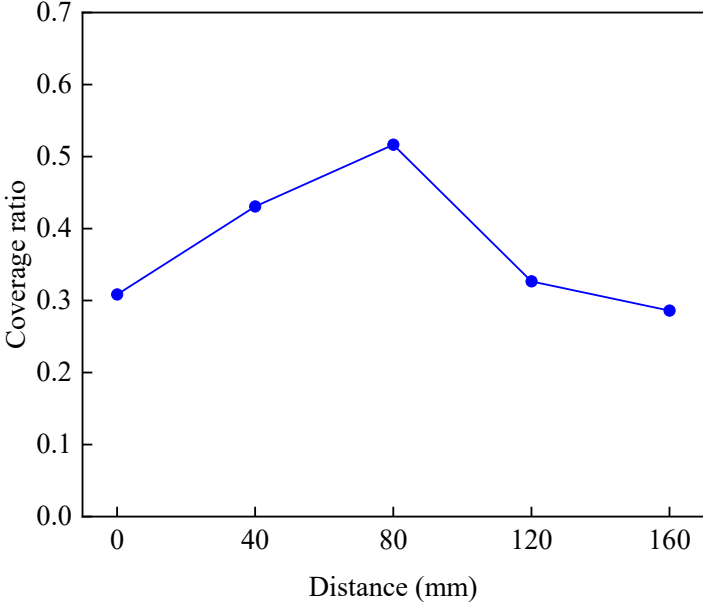


Fig. 5.16 Impact of distance between two nozzles on coverage factor

5.4.3 Influence on IEC performance

The mathematical model created by Yang et al. [109] was initially utilized here to evaluate the impact of the nozzle settings on the IEC performance. Fig. 5.17 illustrates how the diameter of droplet generated by the two identical nozzles alters the wet-bulb effectiveness. When the wet-bulb efficiency is 52% and the spray droplet size is 0.25 mm, the highest wet-bulb efficiency value is possible. This indicates that simply altering the area covered by the water film on the plate surface while maintaining the same working circumstances, a single parameter, the spray droplet size, may boost wet-bulb efficiency from 35% to 51%.

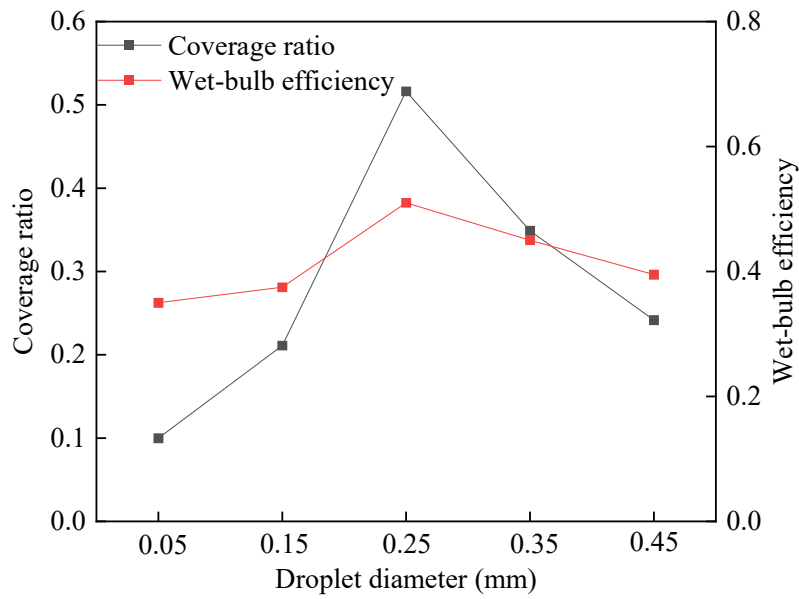
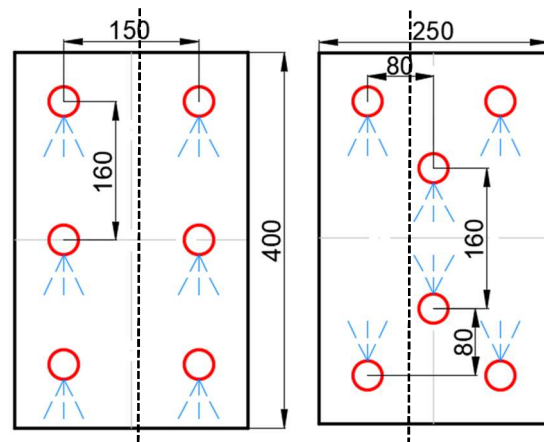


Fig. 5.17 Impact of droplet size on wet-bulb efficiency

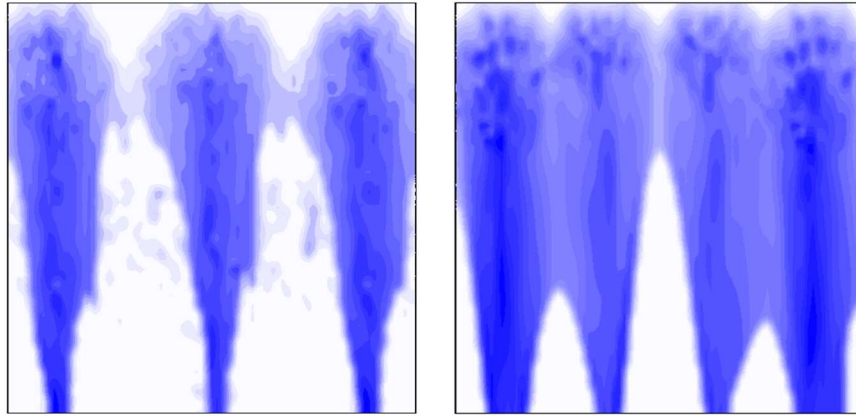
5.4.3.1 Optimal arrangement scheme

Based on the results and analysis in Section 6.1.2, an optimised nozzle arrangement scheme (Fig. 5.18 (a)) is proposed and a series of performance comparisons of the IEC system are made using the conventional linear arrangement scheme (Fig. 5.18 (b)) and parameter settings investigated experimentally by Antonellis et al. [110] as a reference.



(a) Conventional scheme (b) Optimized scheme

Fig. 5.18 Description of the two comparison arrangement schemes



(a) Conventional scheme

(b) Optimized scheme

Fig. 5.19 The coverage area situation of the two schemes

Fig. 5.19 (a) and (b) depict the state of the water film coverage on the plate surface of the heat exchanger furthest from the nozzle (position of the black line in Fig. 5.18) for the conventional and optimized schemes, and the water film coverage ratio are 0.72 and 0.91 respectively.

5.4.3.2 Temperature distribution

A case study was carried out at the intake air characteristics and heat exchanger specifications to illustrate the air temperature distribution of the IEC before and after the optimization:

$$t_p = 35 \text{ }^\circ\text{C}, RH_p = 50\%, u_p = 2 \text{ m/s}, t_s = 24 \text{ }^\circ\text{C}, RH_s = 60\%, u_s = 2 \text{ m/s}, s = 4 \text{ mm}, H = 0.4 \text{ m}, L = 0.4 \text{ m}.$$

The temperature distribution in primary air channel could be seen from Fig. 5.20. As shown in Fig. 5.20 (a) and (b), the temperature of the primary airflow drops significantly from the inlet end on the left to the outlet end on the right, and the temperature drop is more

pronounced close to the outlet of the secondary airflow. There are two main reasons for this phenomenon to occur here. Firstly, the air in the upper part of the wet channel is closer to the nozzle and therefore comes into contact with the spray earlier and more fully, producing a more intense heat mass transfer and resulting in a more dramatic temperature drop. Secondly, as discussed in the previous section, the area covered by the water film in the wetted channel is greatest near the inlet of the secondary air flow and converges as the water film flows downwards, resulting in a contraction of the water film and an inadequate evaporation response compared to the upper part of the channel. Furthermore, a comparison of the temperature distribution in the primary channel for nozzle arrangement schemes 1 and 2 confirms that the wider the area covered by the water film, the greater the gradient in temperature reduction, and that lower temperatures can be obtained at the exit of the gas stream when all other parameters are fixed.

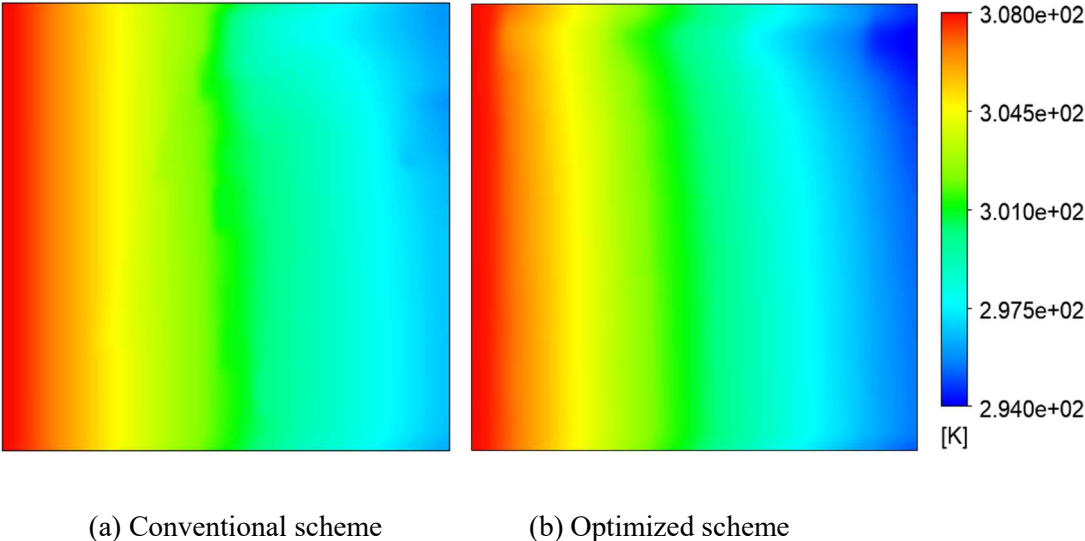


Fig. 5.20 Temperature distribution of primary air channel

Fig. 5.21 (a) and (b) describe the fluctuation of wet-bulb efficiency and COP for the IEC

with increasing inlet air temperature based on the two different nozzle arrangements, and it can be seen that the overall trend for both is progressively decreasing. However, the wet-bulb efficiency as well as COP values of the optimised IEC system are consistently greater than those of the conventional IEC system, and the improved results are both optimal at an inlet air temperature of 32°C, with increases of 15.1% and 17.6%, respectively.

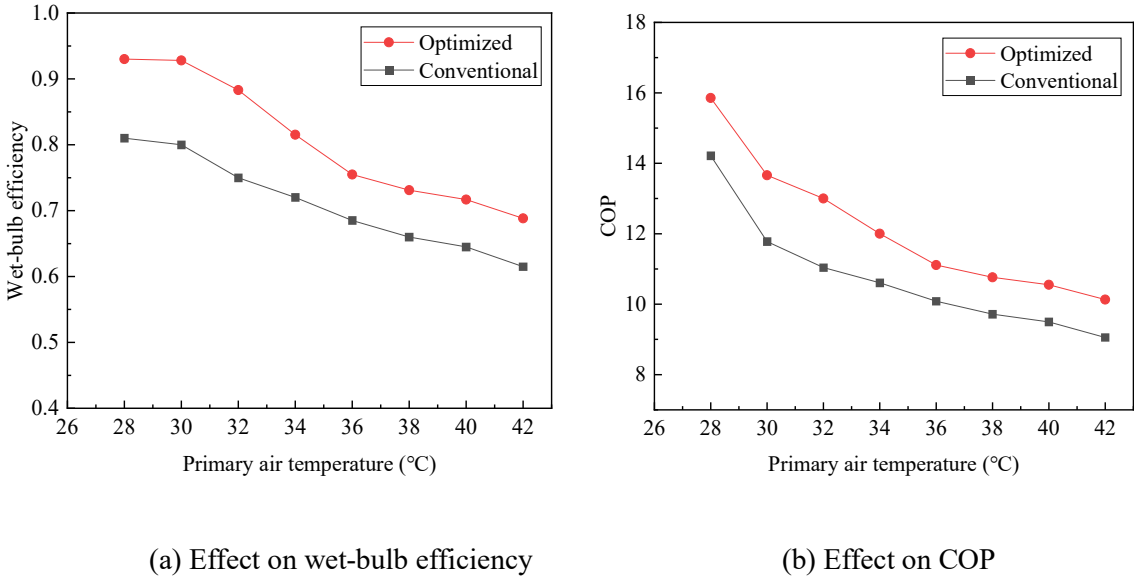


Fig. 5.21 Effect of inlet primary air temperature on the energy performance of the two IECs

5.4.3.3 Velocity of the secondary air

The impact of the secondary air velocity on the cooling capacity of the IEC with conventional and optimised nozzles is shown in (a) Effect on wet-bulb efficiency (b) Effect on COP

Fig. 5.22 (a) and (b). It is confirmed that the rise in secondary air velocity reduces the IEC to varying degrees regarding wet-bulb efficiency and COP. This is because the increase in secondary air mass flow rate reduces both the heat and mass transfer between the airflow and

the water membrane and with the airflow, as well as the lighter weight spray droplets being blown away. Similarly, the optimised IEC system consistently achieves higher wet-bulb efficiency and COP values than the conventional IEC system, and the improved results are both optimal at an inlet air velocity of 2 m/s, with increases of 10.4% and 14.9% respectively.

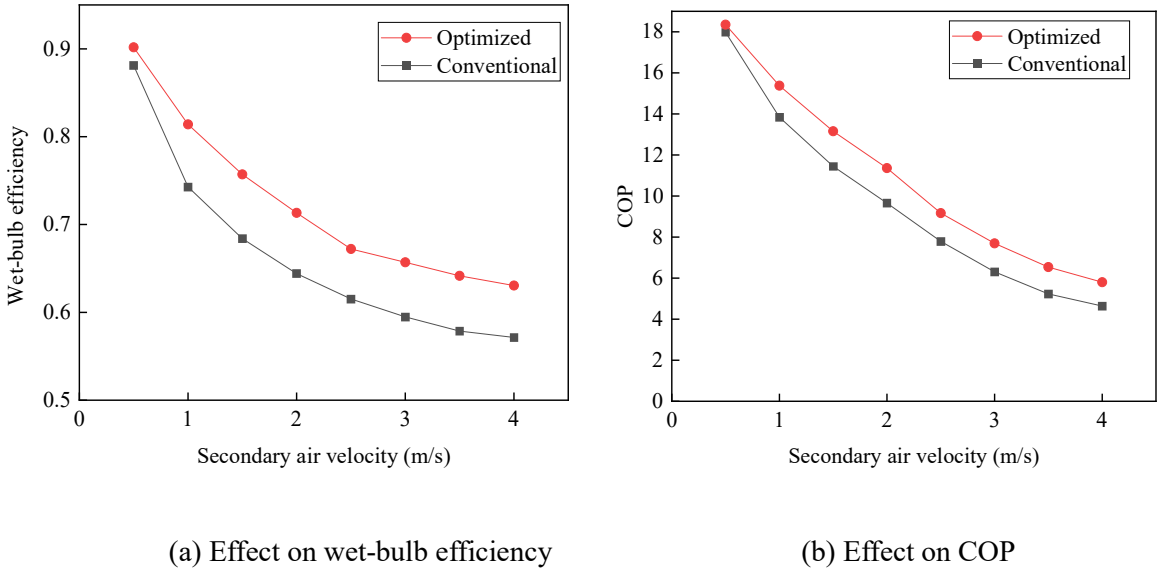


Fig. 5.22 Effect of secondary air velocity on the energy performance of the two IECs

5.5 Summary of this chapter

Considering the critical role of nozzle parameter settings in determining the water film coverage on the surface of IEC exchanger plates, this chapter introduces and validates a 3D CFD model to accurately assess the actual coverage factor of the water film, as well as the overall cooling performance of the IEC system. The thesis then evaluates the water film coverage on wet channel panels using different nozzle parameters and configurations. Based on these results, an optimal nozzle design is identified and compared with conventional designs.

The final analysis contrasts the ideal nozzle configuration, as suggested by the new IEC model, with traditional nozzle settings, focusing on wet-bulb efficiency and the COP of the IEC system.

The main findings from this chapter are summarized as follows.

- 1) The 3D CFD model developed in this chapter can accurately predict the IEC wet channel water film coverage and the overall performance of the IEC with an error of less than 7.2% and 8.1%, respectively.
- 2) The size of the spray droplets emitted by the water system is a critical factor for achieving an effective water film on the plate surface. A single nozzle can reach a maximum membrane coverage ratio of 0.22 with a droplet diameter of 0.25 mm, marking a 61.9% enhancement over the least effective scenario.
- 3) Optimal nozzle parameters for maximum coverage were determined to be a droplet diameter of 0.25 mm, a pressure of 1.5 bar, a flow rate of 5.4 l/min, and a spray cone angle of 68°.
- 4) When considering multiple nozzles, an 80 mm spacing was found to be the most effective layout, increasing coverage from 0.32 to 0.53 with two nozzles and boosting IEC system efficiency by 31.4% compared to the least favorable outcomes.
- 5) The refined IEC water distribution system employs a triangular nozzle arrangement based on distance analysis. This optimized configuration enhances water film coverage by 20.9% and significantly improves the temperature reduction in the primary airflow, using the same number of nozzles as the conventional setup.

6) While the IEC system's performance trends remain consistent with variations in primary air temperature and secondary air velocity for both conventional and optimized nozzle arrangements, the optimized solution enhances wet-bulb efficiency and COP by 15.1% and 17.6%, respectively, under optimal operating conditions.

CHAPTER 6 PERFORMANCE ASSESSMENT AND OPTIMIZATION OF WATER SPRAY STRATEGY FOR INDIRECT EVAPORATIVE COOLER BASED ON ARTIFICIAL NEURAL NETWORK MODELING AND GENETIC ALGORITHM

The 3D CFD model developed in Chapter 5 demonstrates reliable accuracy in predicting the performance of indirect evaporative cooler (IEC) systems under various shower designs. However, the requirements of model for high computational configurations and substantial computational resources render it impractical for widespread engineering applications. Consequently, there is a need for a more straightforward method to predict IEC performance and optimize spray strategies for diverse applications.

To address the particular challenge, this chapter introduces a novel approach that utilizes the principles of neural network theory to construct a predictive model based on backpropagation artificial neural networks (BP-ANN). The developed model is employed to investigate the impact of six main operating parameters of the water spray system on the IEC performance. Wet-bulb efficiency and pressure drop of secondary air channel are utilized as the performance evaluation indexes. The model is rigorously validated by relevant experimental data, enabling a comprehensive analysis of the influence of each parameter on the operational performance of the whole system. The significance of the influential parameters is evaluated through grey relational analysis. Furthermore, a multi-objective optimization approach employing a genetic algorithm (GA) is introduced to effectively determine the optimal

operating parameters of the IEC system.

This chapter is written based on a published paper of this thesis author. The paper is titled “*Performance prediction and optimization of cross-flow indirect evaporative cooler by regression model based on response surface methodology*” in *Applied Energy*.

6.1 Concept and model set up

6.1.1 Data preparation

The aim of this section of the thesis is to analyze the design parameters of the spray system that affect the working performance of IEC and develop a model capable of predicting and evaluating the performance of system under various operating conditions. Therefore, it is unnecessary to encompass all parameters related to energy and mass transfer involved in the operation of the IEC system. This reflects a key advantage of data-driven modeling, which only requires considering the major parameters that simultaneously vary during real-time operation to predict the performance. For a neural network system, defining the range of parameter variations is crucial as it allows the model and users to establish upper and lower limits for inputs, preventing the consideration of unrealistic values or operating conditions, which helps to maintain a manageable model structure, reducing training and prediction time significantly. Moreover, incorporating unrealistic operating conditions may lead the machine learning model to learn from conditions that do not exist in real-time system operation. This section primarily focuses on selecting the key parameters that may vary simultaneously during the operation of

the IEC spray system, along with the appropriate working ranges for these parameters.

6.1.1.1 Primary design parameters

On the basis of the investigations from relevant literature [30,31] and previous experimental researches [32,33], the primary design parameters of the spray system that affect the performance of IEC can be identified as follows: nozzle pressure, nozzle spacing, nozzle aperture, nozzle count, spray density, and air-to-water ratio of the secondary airflow in the spray system. These six parameters play a crucial role in identifying spray uniformity, system efficiency, and the secondary air channel pressure drop (which affects the cooling capacity and power consumption of IEC). Table 6.1 lists the main operating ranges for these six parameters.

Table 6.1 The primary working range of design parameters

No.	Input parameters	Minimum	Maximum
1	Nozzle pressure	0.05 MPa	0.2 MPa
2	Nozzle spacing	0 mm	300 mm
3	Nozzle aperture	2.5 mm	6 mm
4	Nozzle number	0	15
5	Spraying density	0.1 kg/(s·m ²)	2 kg/(s·m ²)
6	Air-water ratio	1	8

6.1.1.2 Evaluation indexes

In general, the performance of IEC is evaluated based on its ability to reduce the temperature of inlet air, which is referred to as temperature reduction capability. The extent of

temperature reduction is a key parameter to assess the energy-saving performance of IEC, and wet-bulb efficiency is commonly used as an evaluation metric [131]. However, in addition to the thermal performance of system, understanding the energy efficiency of IEC is also crucial. These aspects can be evaluated using common metrics defined by ASHRAE [132], such as the COP. In addition, the wet-bulb efficiency represents the cooling performance of the system, while COP represents the ratio of cooling capacity to the power input required, primarily influenced by temperature reduction and energy consumption, with energy consumption being mainly affected by the pressure drop in the secondary air channel [133][37]. Thus, the pressure drop of secondary air channel is another important performance parameter that arises when the airflow is distributed within the IEC. Velocity and friction are the key factors contributing to the occurrence of pressure drop within the IEC. Excessive pressure drop is generally considered unfavorable as it increases the demand for higher air velocities, resulting in higher power consumption by fans and lower COP values. On the other hand, it is crucial to overcome air resistance along the flowing channels to ensure efficient operation of the system. By managing the pressure drop effectively, the system can achieve improved energy efficiency while maintaining adequate air resistance for optimal heat transfer within the IEC. Therefore, in this study, wet-bulb effectiveness and pressure drop are selected as performance evaluation parameters for IEC, serving as the output (target) variables for the ML model. The specific calculation formulas are explained as follows [135].

The wet-bulb efficiency serves as a valuable metric for evaluating the overall operational performance of the IEC system [39, 40], as represented by Eq. (64).

$$\varepsilon_{wb} = \frac{t_{p,in} - t_{p,out}}{t_{p,in} - t_{wb,s}} \quad (64)$$

Employing a hydraulic calculation technique enables the estimation of the pressure drop, which in turn allows for the calculation of the power requirements for each fan:

$$f_{Re} = 96 * (1 - 1.3553\left(\frac{L}{S}\right) + 1.9467\left(\frac{L}{S}\right)^2 - 1.7012\left(\frac{L}{S}\right)^3 + 0.9564\left(\frac{L}{S}\right)^4 - 0.2537\left(\frac{L}{S}\right)^5) \quad (65)$$

$$d_e = \frac{2sL}{s + L} \quad (66)$$

$$\Delta P = \frac{f_{Re}L\rho u^2}{2Red_e} \quad (67)$$

Consequently, the energy expenditure attributable to the fans and water pump could be characterized as follows:

$$W_{fan} = \frac{Q \Delta P}{3600 \times 1000 \times \eta_0 \times \eta_1} \times K \quad (68)$$

$$W_{pump} = m_w g (h_{gravity} + h_{nozzles} + h_{valves}) \times K \quad (69)$$

The COP is utilized in this study to assess the energy efficiency of refrigeration under different optimized design parameters [138], and the corresponding formula for calculating the COP is as follows:

$$Q_p = m_p c_{pg} (t_{p,in} - t_{p,out}) \quad (70)$$

$$COP = \frac{Q_p}{W_{fan} + W_{pump}} \quad (71)$$

6.1.1.3 Collection of experimental data

An IEC is a device utilized to cool the airflow, typically referred to as the primary flow, by passing it through an air-to-air heat exchanger and simultaneously crossing it with a

secondary airflow that is humidified with spray water. In this study, experiments were conducted on a laboratory-scale prototype of the IEC system to simulate different operating conditions and generate an experimental dataset for training a neural network and validating the accuracy and reliability of the model. The complete IEC system used in the experiments consisted of the following components: a cross-flow heat exchanger, nozzles for supplying water to the secondary airflow, and a pumping device to increase the water pressure as shown in Fig. 6.1. In order to train a reliable model for analyzing the parameters of the IEC spray system, the main parameters adjusted during the experiments were nozzle pressure, nozzle spacing, nozzle aperture, nozzle count, spray density and air-water ratio. The remaining parameters, such as the specifications of the IEC and indoor temperature, were kept constant. The specific values are depicted in Table 6.2.

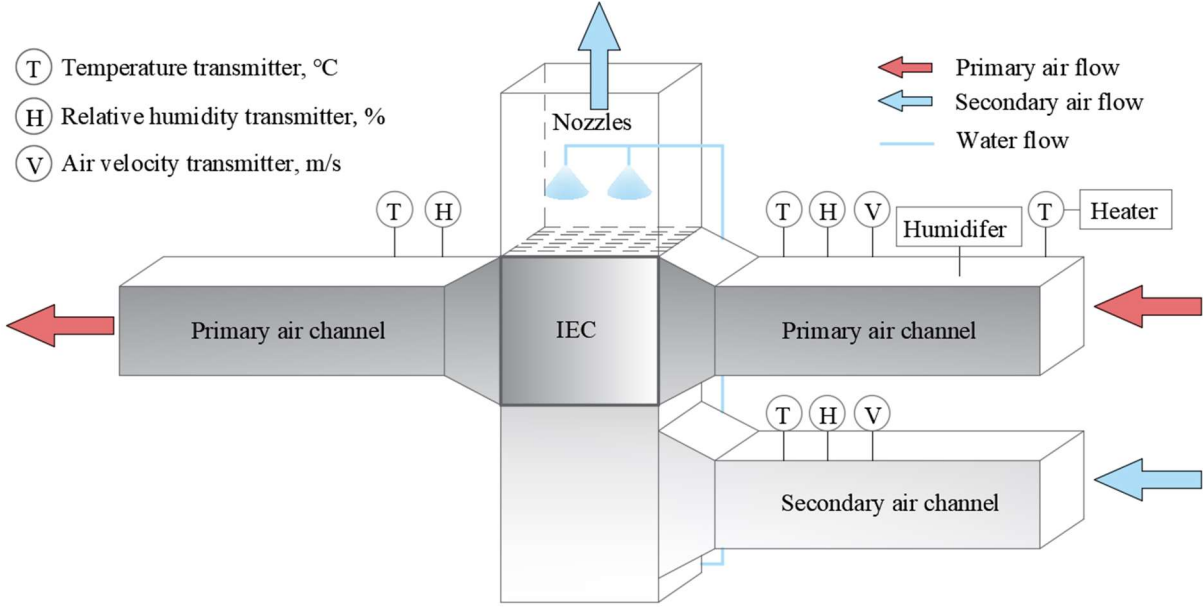


Fig. 6.1 Schematic diagram of the IEC system

Table 6.2 Specific values of IEC and experimental conditions

Item	Details
Material	Aluminium
Net length and width	400 mm
Plate thickness	0.15 mm
Plate gap	5 mm
Channel height	400 mm
t_p	35°C
RH_p	50%
t_s	24°C
RH_s	60%

6.1.2 IEC-ANN model set up

6.1.2.1 Introduction to algorithms

ANN is a simplified dynamic system that mimics biological neural networks through various interconnections and operates weight and activation functions to process information. The distribution of weights between neurons establishes connections and facilitates the process of information storage. Network learning encompasses the continuous adaptation of connection weights among neurons. The neural network applied in this study is the backpropagation algorithm. The basic learning algorithm of neural networks is the BP algorithm, also referred

to as the error backpropagation algorithm. This process involves two primary steps: forward propagation and error backpropagation. Through iterative weight and threshold adjustments, the network aims to minimize the error and enhance prediction accuracy.

6.1.2.2 Normalization of sample data

Given the extensive range of variations among the six selected input variables and two output variables in this research, it is crucial to normalize the training data to facilitate more effective network training [139]. Normalization involves mapping the data to a uniform range between 0 and 1. By normalizing the training data, it ensures that all variables contribute equally to the learning process, preventing any single variable from overpowering the training. Bringing the data within the range of [0, 1] enables the neural network to effectively learn the patterns and relationships within the data, ultimately leading to enhanced training and improved performance.

The formulas for normalization, denoted as Eq. (72) and Eq. (73), are as follows.

$$x = \frac{x_i - x_{\min}}{x_{\max} - x_{\min}} \quad (72)$$

$$y = \frac{y_i - y_{\min}}{y_{\max} - y_{\min}} \quad (73)$$

In these formulas, x represents the original input variable, and y represents the original output variable.

Besides, the network output data is back-normalized. Assuming that the network output model is y , the inverse normalization is processed as shown in the following equation.

$$y_i = y_{\min} + y * (y_{\max} - y_{\min}) \quad (74)$$

6.1.2.3 Details of the model setting

Considering the current data dimensionality and scale, a three-layer network with a hidden layer comprising 14 neurons, can effectively capture the relationship between the input and output variables. The final structure of the IEC-ANN model, programmed in MATLAB software, is depicted in Fig. 6.2. The dataset could be divided into three sections: the training dataset, validation dataset, and testing dataset, with portions of 70%, 15%, as well as 15%, correspondingly. The training dataset is employed to train the ANN model, the validation dataset is utilized to fine-tune the model and prevent overfitting, while the testing dataset is applied to assess the performance of the model. For the training process, a learning rate of 0.001 is set, which determines the step size for adjusting the weights during training. The number of epochs is configured as 200, indicating the total iterations of the training dataset passing through the network during the training process. The following equations describe the mathematical model of the neural network used in this thesis.

The input vector of the input layer is represented as,

$$X = (x_1, x_2, \dots, x_i, x_n)^T \quad (75)$$

The inputs, outputs and output vectors of each neuron in the hidden layer are expressed in turn with the help of the following formulas respectively,

$$net_j = w_{1j} \cdot x_1 + \dots + w_{nj} \cdot x_n \quad (76)$$

$$h_j = f(\text{net}_j - a_j) \quad (77)$$

$$H = (h_1, h_2, \dots, h_j, \dots, h_i)^T \quad (78)$$

The inputs, outputs, output vectors and desired output vectors of each neuron in the output layer are expressed in turn with the help of the following formulas respectively,

$$\text{net}_k = w_{1k} \cdot h_1 + \dots + w_{lk} \cdot h_l \quad (79)$$

$$o_k = g(\text{net}_k - b_k) \quad (80)$$

$$O = (o_1, o_2, \dots, o_k, \dots, o_m)^T \quad (81)$$

$$Y = (y_1, y_2, \dots, y_k, \dots, y_m)^T \quad (82)$$

where x_i signifies the input value of the network, y_i signifies the predicted value of the network, O_i signifies the output of the output layer, net_j signifies the input of each neuron, w_{nj} represents the value of the weights, H signifies the output vector of the implicit layer, O signifies the output vector of the output layer, and Y signifies the expected output vector of the output layer.

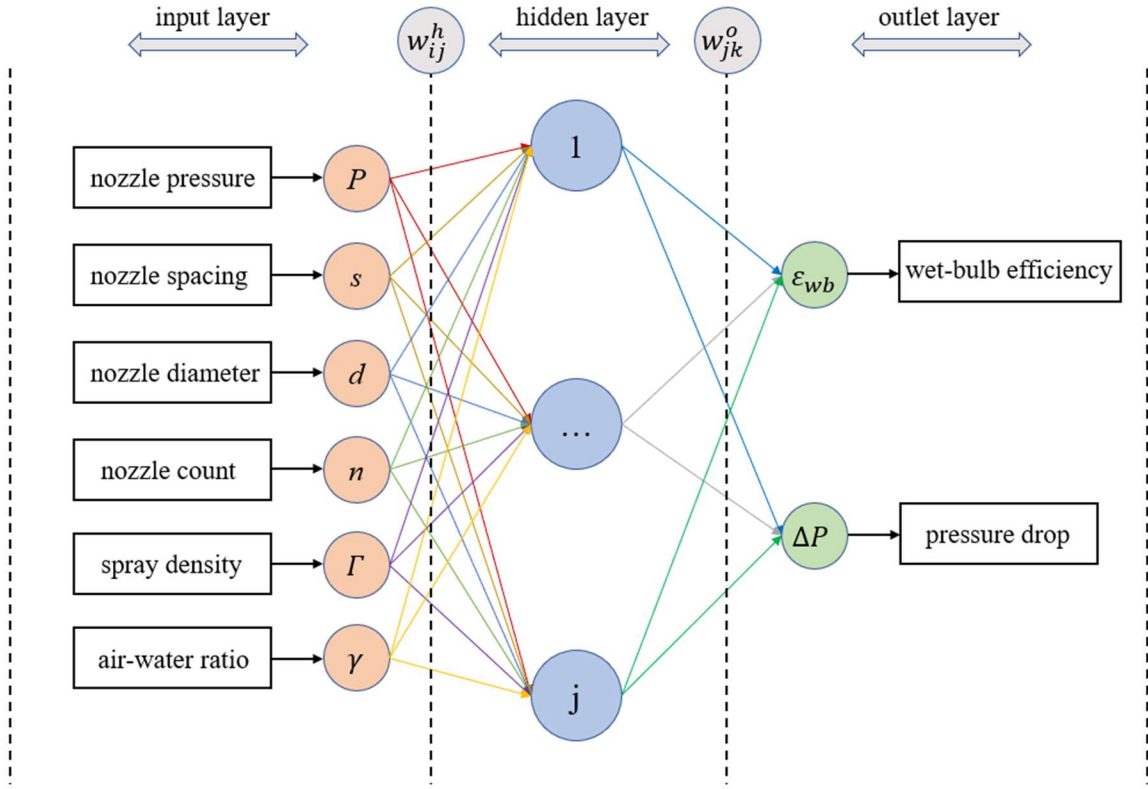


Fig. 6.2 Structure of the IEC-ANN model

6.1.2.4 Evaluation metrics of neural network

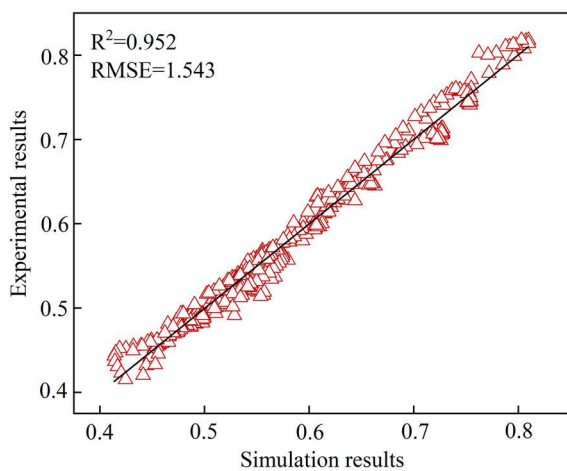
This study utilized widely recognized statistical indicators to assess the performance of the model. The metrics utilized include the coefficient of determination (r^2) as well as the root mean square error (RMSE) to assess the accuracy and predictive capability of the model, given as:

$$r^2 = \frac{[n \sum_{k=1}^n Y_P(k) Y_T(k) - \sum_{k=1}^n Y_P(k) \sum_{k=1}^n Y_T(k)]^2}{[n \sum_{k=1}^n Y_P(k)^2 - (\sum_{k=1}^n Y_P(k))^2][n \sum_{k=1}^n Y_T(k)^2 - (\sum_{k=1}^n Y_T(k))^2]} \quad (83)$$

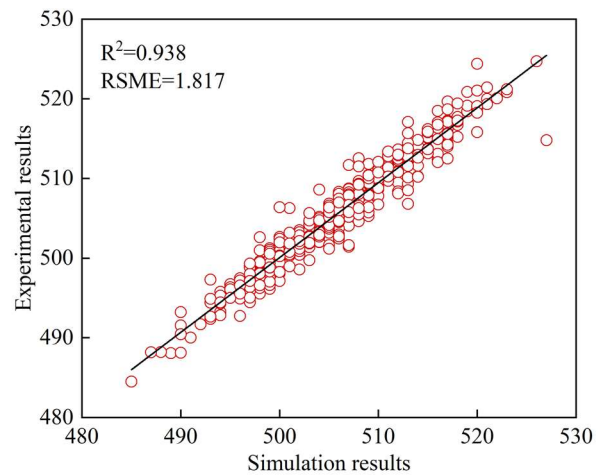
$$RMSE = \sqrt{\frac{\sum_{k=1}^n (Y_P(k) - Y_T(k))^2}{n}} \quad (84)$$

6.1.3 Validation

To validate the predictions of the ANN model established in this study, the regression coefficient r^2 and RSME value are used as evaluation metrics to assess the accuracy of the predictions. A higher r^2 value indicates better generalization ability of the ANN model, and when $r^2=1$, it represents the best-case scenario where the simulated output of the ANN model matches the target values. Fig. 6.3 illustrates the linear regression plots for the test data samples, showcasing the relationship between wet-bulb efficiency, pressure drop, and the corresponding points distributed along contour lines. The majority of points closely align with the contour lines, indicating a strong correlation. Additionally, the final r^2 values are 0.952 and 0.938 separately, while the RSME values are 1.543 and 1.817 Pa. The results demonstrate that the developed ANN model possesses a high level of accuracy, enabling precise predictions of wet-bulb efficiency. Overall, the findings highlight the exceptional performance of the ANN model in capturing the relationship between input variables and output variables, providing reliable and robust predictions.



(a) Validation results for ϵ_{wb}



(b) Validation results for ΔP

Fig. 6.3 Validation results of the proposed IEC-ANN model

6.2 Results and discussions

6.2.1 Effect of variations in a single factor

Within this segment, the impact of various design parameters of the IEC spray system on its performance is evaluated. Specifically, the effect of each parameter on the wet-bulb efficiency and pressure drop of the IEC system is examined, while keeping ambient temperature and humidity constant. The major design and operating parameters of the IEC system in this thesis are enumerated in Table 6.3. To analyze the individual influence of each parameter on the performance of IEC system, one parameter was systematically varied while keeping all other parameters constant. This approach allows for a comprehensive understanding of how changes in specific design or operating parameters affect the wet-bulb efficiency and air channel pressure drop of the IEC system. The findings provide valuable insights for enhancing the design of IEC spray systems.

Table 6.3 Parameter setting of IEC base system

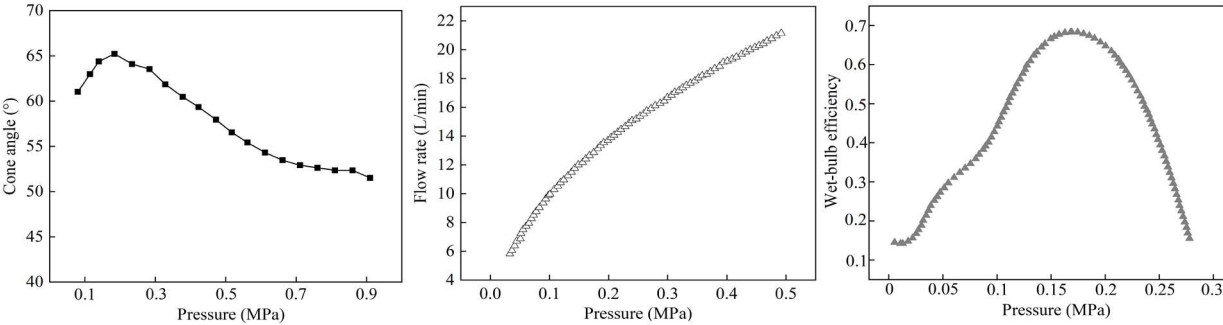
Item	Nozzle pressure	Nozzle spacing	Nozzle Aperture	Nozzle number	Spraying density	Air velocity	Height
Value	0.1 MPa	80 mm	6 mm	8	0.4 kg/(m ² ·s)	2 m/s	330 mm

6.2.1.1 Nozzle characteristics parameters

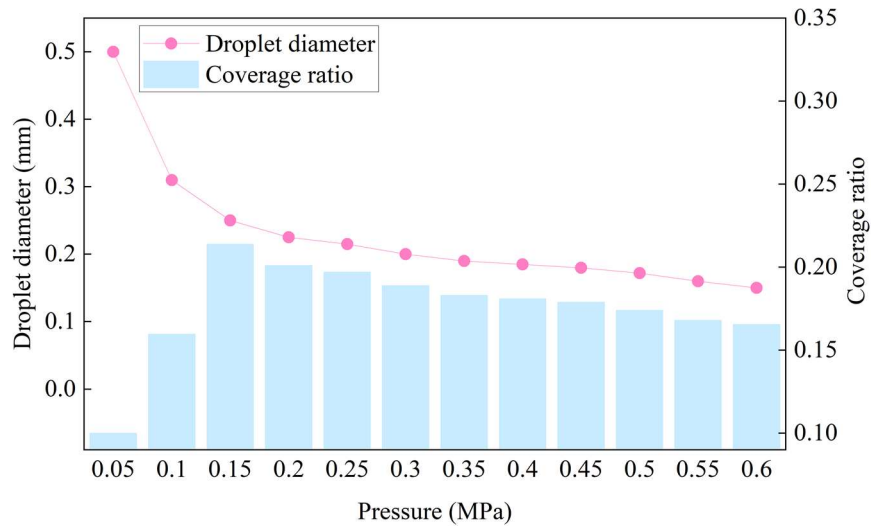
Extensive experimental data consistently demonstrates that the spray angle and flow rate of nozzles exhibit systematic variations in response to changes in inlet pressure across various scenarios. Manufacturers typically offer product catalogs that specify the pressure range for each nozzle model, along with the corresponding spray cone angle and flow rate [43,44]. Fig. 6.4 illustrates the variations in spray cone angle and flow rate of the nozzles used in this study at different pressure values. In Fig. 6.4 (a), it is apparent that the spray cone angle exhibits an initial rise followed by a subsequent decrease as the inlet pressure of the nozzle increases. The peak value of 67° is achieved at a pressure of 0.15 MPa. Fig. 6.4 (b) demonstrates the increasing trend of spray flow rate with the rise in pressure. Furthermore, Fig. 6.4 (c) depicts the comprehensive impact of these three interconnected factors on the IEC efficiency. The graph indicates that the wet-bulb efficiency reaches its peak around a pressure value of 0.15 MPa before declining, aligning with the trend of spray cone angle variations. This finding confirms that a larger spray cone angle leads to broader spray coverage and a more uniform distribution of droplets. Conversely, excessively concentrated spray can result in increased water film thickness, elevated overall pipe resistance, and hindered heat transfer, thereby reducing the cooling effectiveness of the IEC system. Overall, these study results emphasize the interplay between nozzle pressure, spray cone angle, and flow rate, as well as their combined influence on wet-bulb efficiency of a whole IEC system.

Correspondingly, as depicted in Fig. 6.4 (d), with all other influencing parameters held

constant, increasing the nozzle pressure results in a gradual decrease in the diameter of the spray droplets. According to the impact of droplet size on the coverage ratio of the water film in the wet channel of IEC [16], an indirect trend is observed where the water film coverage ratio initially increases and then decreases with pressure, peaking at 0.15 MPa. This trend is consistent with the changes in wet-bulb efficiency. Moreover, the water flow through the nozzle also increases with enhanced pressure, leading to an enlarged water film coverage area within the IEC wet channel. Simultaneously, the increase in local thickness of the water film could impede heat transfer to a certain extent, resulting in a reduction in wet-bulb efficiency for the same coverage area.



(a) Effect of pressure on cone angle (b) Effect of pressure on flow rate (c) Effect of pressure on ϵ_{wb}



(d) Effect of pressure on droplet diameter and coverage ratio

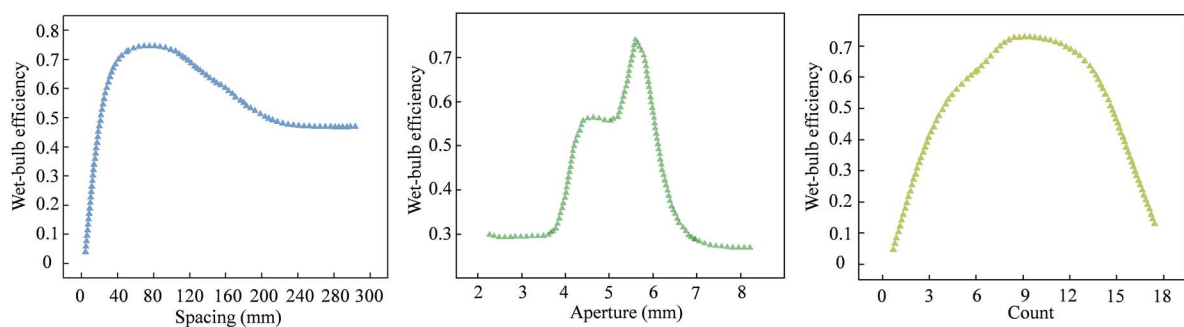
Fig. 6.4 The effect of nozzle pressure variations

Based on Fig. 6.5 (a), it can be observed that under constant conditions, the wet-bulb efficiency of the IEC system initially increases with an increase in nozzle spacing. However, once the spacing exceeds 80 mm, the efficiency starts to decline. This behavior can be attributed to the interaction between nozzle spacing and spray coverage. In the ideal scenario with a constant spray cone angle, the coverage area of droplets is assumed to be fixed and uniform. When the nozzle spacing is too small, the spray coverage areas from multiple nozzles overlap excessively. This leads to a narrower overall coverage area and reduces the cooling efficiency of the IEC system. Additionally, when the spacing between two nozzles is too close, the sprayed droplets collide, altering their original trajectories. As the nozzle spacing increases, the total spray coverage area reaches a peak and then decreases due to excessively wide spacing. This decline in efficiency is likely because the coverage becomes more scattered and less concentrated, resulting in reduced cooling efficiency. Consequently, careful consideration of the nozzle spacing is of utmost significance in the design of an IEC system for optimizing the

wet-bulb efficiency.

Additionally, Fig. 6.5 (b) reveals that under the same conditions, the wet-bulb efficiency of the IEC system initially increases with an increase in nozzle aperture, while then decreases after the aperture larger than 6 mm. This could be attributed to the fact that the interplay between nozzle aperture and its impact on water flow rate and droplet characteristics. With a larger nozzle aperture, there is a greater flow area, resulting in reduced resistance and an increased water flow rate. This initially leads to improved efficiency as more water is available for cooling. However, as the aperture continues to increase, the droplets become heavier and fail to make direct contact with the surface of the heat exchanger, resulting in the formation of a non-ideal water film. Moreover, when the water film becomes excessively thick, it becomes challenging to atomize, resulting in a decrease in wet heat exchange efficiency. Therefore, there exists an optimal range of nozzle aperture that balances the benefits of increased water flow rate and the formation of an ideal water film for efficient heat exchange in the IEC system. Besides, it is noteworthy that a plateau phase of wet-bulb efficiency occurs when the nozzle aperture is expanded from 4 mm to 5 mm. This phenomenon could be attributed to the slight increase in water flow through the nozzle when the aperture is enlarged from 4 mm to 5 mm, under constant nozzle water pressure. Concurrently, there is a discernible reduction in the spray cone angle, which results in the wet-bulb efficiency remaining essentially unchanged. As the nozzle aperture continues to increase from 5 mm to 6 mm, the water flow further escalates, and the spray cone angle begins to widen accordingly. Consequently, the wet-bulb efficiency progressively improves until it reaches its peak value.

Furthermore, from Fig. 6.5 (c), it is apparent that under constant conditions, the cooling efficiency of the IEC system demonstrates an initial increase as the number of nozzles increases, but it starts to decline when $n \geq 10$ and reaches its peak at $n=10$. This behavior can be attributed to the interaction between the number of nozzles and the resulting water flow velocity and coverage area of the water membrane formed by the nozzles. Initially, as the number of nozzles increases, the water flow velocity and the coverage area of the water film formed by the nozzles increase. This leads to a more uniform distribution of water droplets and generally higher heat exchange efficiency. However, when the number of nozzles becomes too high, interference and overlap of the water films occur, affecting the atomization process and reducing the wet heat exchange efficiency. Therefore, there is an optimal range of nozzle quantity, and the cooling efficiency reaches its peak when $n=10$. Beyond this optimal point, the interference and overlap of water films hinder the atomization process, resulting in a decrease in wet heat exchange efficiency.



(a) Effect of nozzle spacing on ϵ_{wb} (b) Effect of nozzle aperture on ϵ_{wb} (c) Effect of count on ϵ_{wb}

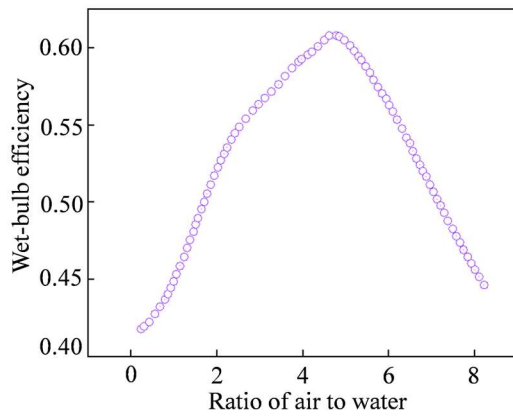
Fig. 6.5 The effect of three other nozzle parameters variations

6.2.1.2 Operation characteristics parameters

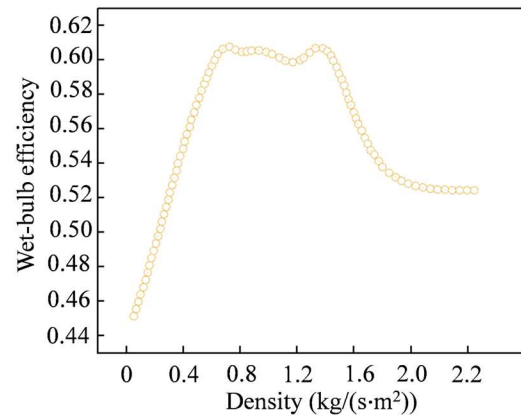
The data presented in Fig. 6.6 reveals the relationship between the air-to-water ratio, wet bulb efficiency, and channel pressure drop in a plate heat exchanger. When the spray water flow rate remains constant, elevating the air-to-water ratio results in higher air velocities in the secondary air channels. Consequently, this augmentation enhances both the convective heat transfer effectiveness and mass transfer coefficient, thereby optimizing the efficiency of the plate heat exchanger and improving the overall evaporative cooling effect. The study identified an air-to-water ratio of 4.86 as the optimal point for achieving the highest efficiency in the plate heat exchanger. At this ratio, the secondary air velocity is 3 m/s, and the heat transfer performance is optimal. However, exceeding this ratio leads to excessive secondary air, which disrupts the formation of a water membrane on the surface of the plate heat exchanger. This disruption creates dry areas on the water film, ultimately reducing the heat transfer effectiveness of the exchanger. It is worth noting that increasing the air-to-water ratio beyond the optimal value not only fails to improve the heat transfer efficiency but also increases the pressure drop in the secondary air duct and the power consumption of the IEC system. Hence, it is necessary to carefully consider the air-to-water ratio to strike a balance between enhancing the heat transfer effectiveness and energy efficiency of the IEC.

According to the data presented in Fig. 6.7 (a), the efficiency of the plate heat exchanger exhibits a positive correlation with the water spray rate, particularly when the spray water density remains below 0.81. Within this range, it is observed that augmenting the water spray

rate enhances the effectiveness of the heat exchanger. Nevertheless, once the spray water density surpasses $0.81 \text{ kg}/(\text{s}\cdot\text{m}^2)$, further increments in the flow rate do not result in a subsequent increase in the efficiency of the plate heat exchanger. This behavior is attributed to the inability of the spray water in the secondary air channels to form stable flow on the fins of the indirect plate heat exchanger at low spray densities. Many dry regions can be observed on the fins throughout the channel, resulting in poor heat transfer performance. At this particular stage, elevating the spray water flow rate plays a crucial role in mitigating the occurrence of dry regions on the fins, leading to a notable enhancement in the heat transfer effectiveness of the plate heat exchanger. Nevertheless, once the spray density reaches a certain threshold, the water film on the fins becomes saturated, rendering further increments in the spray density impractical for enhancing the heat transfer efficiency of the plate heat exchanger. Additionally, as illustrated in Fig. 6.7 (b), the presence of a thicker water film leads to blockage in the secondary air channels, increasing air resistance and the energy consumption of the secondary air fans. Therefore, finding the optimal spray water density is essential to strike a balance between establishing a stable water film and minimizing the occurrence of dry regions on the fins, ultimately maximizing the heat transfer efficiency.

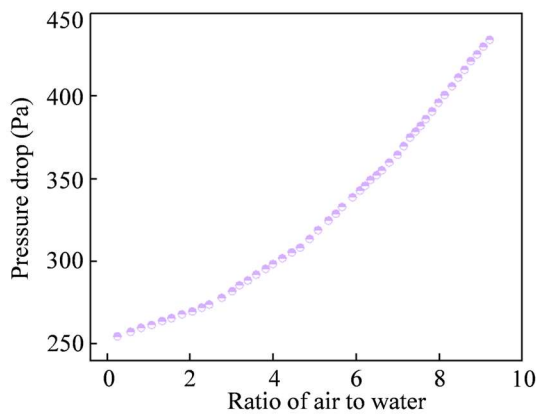


(a) Effect of air to water ratio on ϵ_{wb}

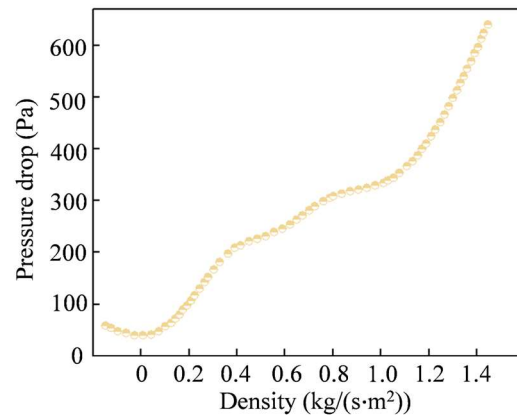


(b) Effect of spray density on ϵ_{wb}

Fig. 6.6 The effect of operation parameters on ϵ_{wb}



(c) Effect of air to water ratio on pressure drop



(d) Effect of spray density on pressure drop

Fig. 6.7 The effect of operation parameters on pressure drop

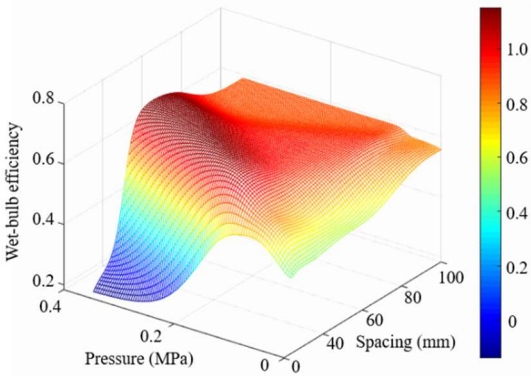
6.2.2 Combined effect of variations in two factors

Taking into account the interdependence or constraints among the six design parameters of the IEC spray water system and the different impacts on IEC performance when two related factors are simultaneously changed, this section analyzes the effects on IEC performance when two related factors are simultaneously changed through surface plots generated by the proposed IEC-ANN model.

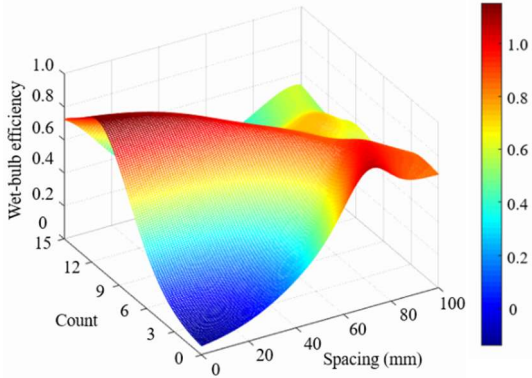
Based on the data presented in Fig. 6.8 (a), it is evident that the IEC performance attains its highest point at a nozzle spacing of 80 mm, after which it gradually declines and stabilizes. When the spacing is small, increasing the pressure rapidly brings the IEC performance to its peak and then decreases rapidly. At a spacing of 80 mm, the performance reaches its global maximum at a nozzle pressure of 0.15 MPa. Subsequently, further changes in pressure and spacing have minimal impact on the IEC wet-bulb efficiency and remain lower than the previously achieved maximum. Therefore, compared to pressure, the spacing is the dominant factor influencing the IEC performance. Based on the information depicted in Fig. 6.8 (b), it could be deduced that when the number of nozzles is small, altering the nozzle spacing has minimal impact on the IEC performance. However, when the number of nozzles exceeds 4, increasing the nozzle spacing leads to an initial increase followed by a decrease in the wet-bulb efficiency of the IEC. Moreover, as the number of nozzles increases, the performance peak occurs more quickly. However, compared to the number of nozzles, the impact of spacing is much smaller. Once the number of nozzles reaches a critical value, the effect of changing the spacing becomes negligible. At this point, the IEC performance stabilizes, and further increasing the number of nozzles does not provide any additional benefits to the overall effectiveness.

Fig. 6.8 (c) shows that at lower pressures, a larger nozzle aperture results in better cooling capabilities for the IEC system. However, at higher pressures, the cooling capabilities of the IEC system diminish with an increase in nozzle aperture. This is because higher pressure corresponds to higher jet velocities, and in such cases, the water spray system does not need to

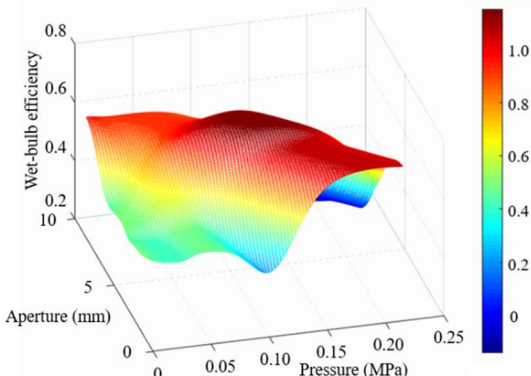
rely on increasing the nozzle aperture to achieve higher flow velocities, which would result in an excessively thick water film on the surface. Research findings indicate that the optimal performance of the IEC system can be attained by setting the pressure at 0.15 MPa and utilizing a nozzle aperture of 6 mm. Similarly, as demonstrated in Fig. 6.8 (d), when the number of nozzles is set at 10, the performance of the IEC system increases to a peak and then decreases as the nozzle aperture increases. The performance tends to stabilize when the number of nozzles reaches 10. In conclusion, to attain the best performance, it is recommended to use a combination of 10 nozzles with a 6 mm nozzle aperture.



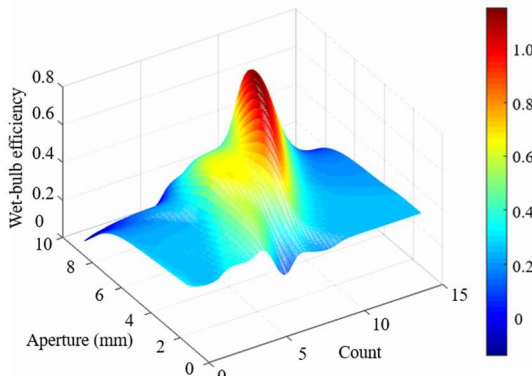
(a) Effect caused by spacing and pressure



(b) Effect caused by spacing and count



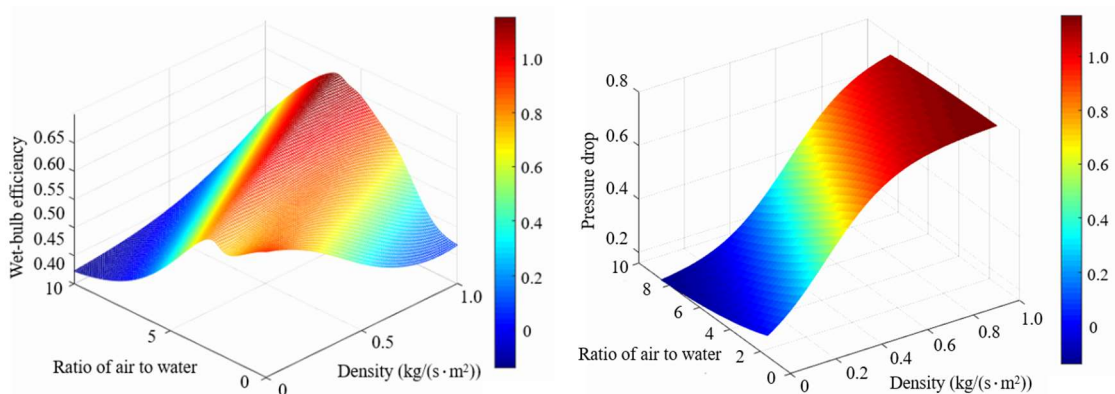
(c) Effect caused by aperture and pressure



(d) Effect caused by aperture and count

Fig. 6.8 The combined effect of two nozzle characteristics factors on ε_{wb}

As depicted in Fig. 6.9, the performance of the IEC system initially improves with an increase in the air-to-water ratio, but it quickly deteriorates after reaching a peak. Additionally, with an increase in spray density, the performance peak occurs later but at a higher level. Therefore, to minimize pump power consumption, the optimal choice for spray density is $0.82 \text{ kg}/(\text{s}\cdot\text{m}^2)$, while the air-to-water ratio should be 5.37. Furthermore, in terms of airflow resistance in the secondary air channel, it continuously increases with an increase in the air-to-water ratio and spray density. In conclusion, to achieve optimal performance and energy efficiency, it is recommended to select a spray density of $0.82 \text{ kg}/(\text{s}\cdot\text{m}^2)$ and an air-to-water ratio of 5.37 for the IEC system. Additionally, if the air-to-water ratio and spray density are appropriately matched, the IEC system has the potential to achieve the desired wet bulb efficiency while maintaining the lowest resistance and energy consumption in the secondary air channel.



(a) Combined effect on ε_{wb}

(b) Combined on pressure drop

Fig. 6.9 The combined effect of two nozzle operation factors on ε_{wb} and pressure drop

6.2.3 Analysis of the influence of input variables on the output variable

Grey relational analysis is a multifactor statistical method utilized to measure the degree of correlation between factors. It is probable for dynamic process analysis and can compensate for the limitations of traditional statistical methods, making it highly applicable.

Based on the correlation calculation formula, Table 6.4 lists the correlation values of the six input variables. To provide a more intuitive comparison of the effects of the six input variables, Fig. 6.10 presents them in the form of a bar chart. Through the comparison of the correlation between the six input variables and the output variable, it can be observed that the air-to-water ratio has the greatest influence on the evaporation efficiency of the output variable. The nozzle count follows as the second most influential factor, followed by water density, nozzle pressure, nozzle spacing, and nozzle aperture, in descending order. Although the nozzle aperture has the smallest impact, with a correlation coefficient of 0.5228, which is greater than 0.5 [141], it remains an important parameter in the analysis.

Table 6.4 The influence of input variables on the output variable

Parameters	Pressure	Spacing	Aperture	Count	Density	Ratio
Influence	0.6758	0.5958	0.5228	0.7187	0.7064	0.8534

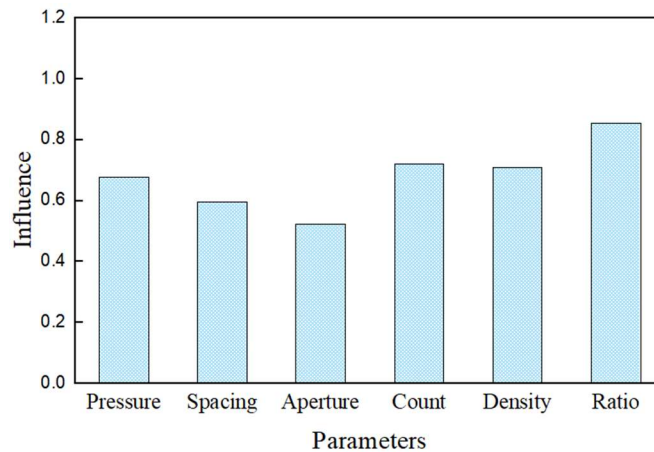


Fig. 6.10 The importance of different design parameters

6.2.4 Optimization of IEC-ANN model based on genetic algorithm

6.2.4.1 Genetic algorithm

Genetic algorithms are highly effective for addressing non-continuous, non-linear, and multi-objective problems, showcasing robust global optimization capabilities. When applying genetic algorithms to such problems, four key aspects need to be carefully considered: determining the basic operating parameters, chromosome encoding and decoding, evaluating individual fitness, and implementing the three genetic operators. By following these critical steps and understanding the main process of genetic algorithms, implementing a genetic algorithm using MATLAB becomes relatively simple, and its accuracy has been proved in various researches [46,47]. In this thesis, an approach is proposed for utilizing a genetic algorithm to search for the optimal control strategy of an IEC spray water system.

6.2.4.2 Multi-objectives optimization

In this thesis, the GA is employed as the algorithmic optimization approach to explore the

full capability of the IEC system by determining the optimal values of operational and design variables. The relationship between cost and iteration count is also investigated to further explore the behavior of the GA.

The selection of wet-bulb efficiency and pressure drop in the secondary air channel as the objective parameters in this thesis is motivated by their ability to simultaneously take into consideration the economic and engineering aspects of the IEC system. This approach aims to optimize the system by minimizing power consumption while maximizing cooling performance. Although maximizing wet bulb efficiency would result in the lowest supply air temperature for the IEC system, it is important to consider the potential increase in power consumption due to high spray flow rates and airflow. Focusing on a single objective may overlook crucial trade-offs and lead to suboptimal solutions. Therefore, employing a multi-objective optimization strategy is essential to attain the optimal equilibrium between these objectives.

The optimization function comprises of both a fitness as well as a constraint function. The trained ANN model from Section 2 serves as the fitness function to be improved, establishing the factors and optimization objectives of the problem. The constraint function enforces the specified parameter intervals as limitations on the fitness function. In the current GA approach, input variables are treated as genotypes, while output variables are regarded as phenotypes. The six input parameters of the developed ANN model are selected as decision variables. In each iteration, the selection function identifies the most advantageous genes as parent genes for the next iteration and applies multi-point crossover to them. Additionally, random genes are

introduced to the population through mutation mechanisms. Various criteria could be specified to halt this process, and in this study, a maximum iteration count of 200 was chosen. Fig. 6.11 illustrates the flowchart of the GA, and the cost function employed in this thesis is defined as follows:

$$J(P, s, d, n, \Gamma, v) = W_1 \frac{\varepsilon_{wb}}{R\varepsilon_{wb}} + W_2 \frac{\Delta P}{R\Delta P}$$

where W represents the weights assigned to each objective, $R\varepsilon_{wb}$ and $R\Delta P$ are utilized for normalizing the output values or objectives.

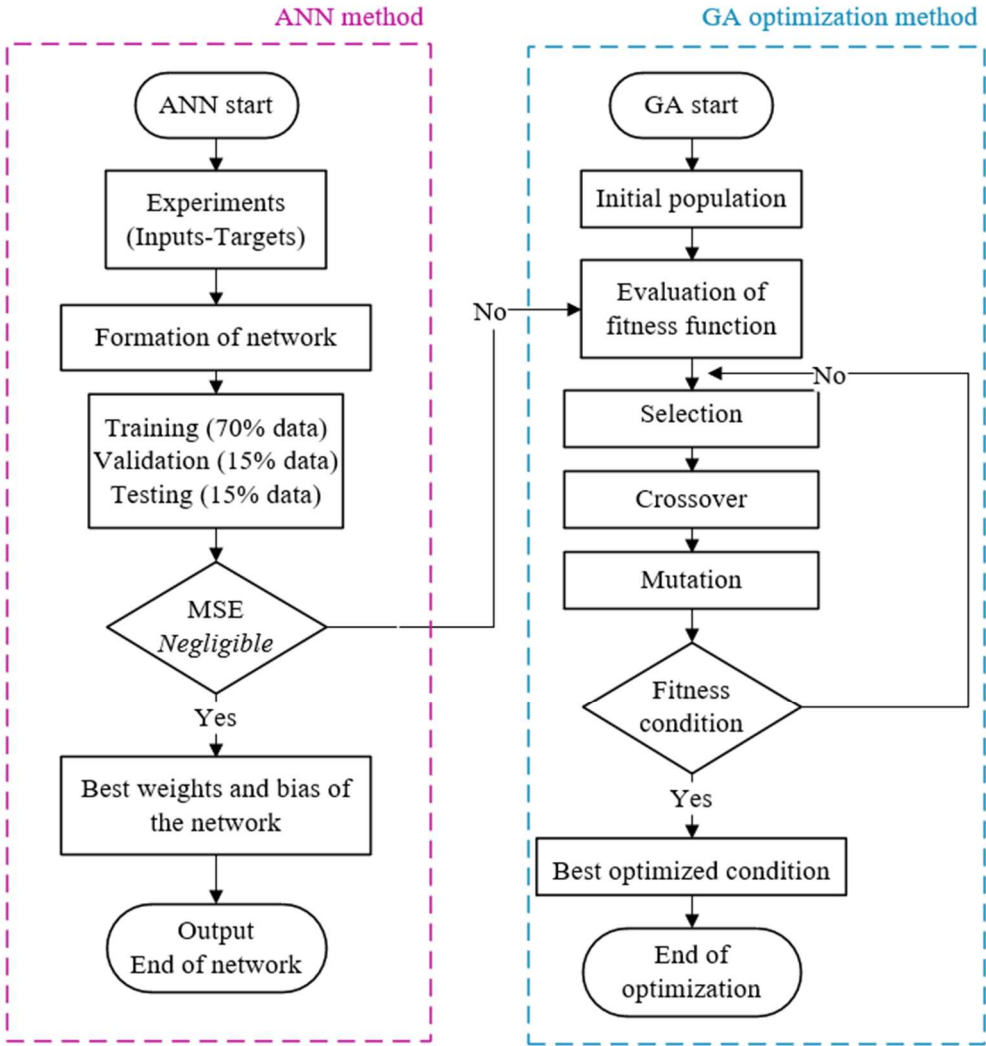


Fig. 6.11 The flow of GA-ANN optimization

Using the typical specifications of IEC units commonly found in laboratories and air-conditioned machine rooms as an example, the GA-ANN model is applied to optimize the operational parameters. The objective is to maximize the cooling efficiency of the IEC while maintaining a relatively low pressure drop in the secondary air duct. During commissioning operations, the operating parameters are controlled within the ranges shown in Table 6.5.

Table 6.5 The range of design parameters

Parameters	Pressure	Spacing	Aperture	Count	Density	Ratio
Range	0.05-0.2MPa	0-300 mm	2.5-6 mm	0-15	0.1-2 kg/(s·m ²)	1-8

6.2.4.3 Results derived from GA

Table 6.6 presents the results of multi-objective optimization using GA, showcasing various operational and design parameters of the IEC system while preserving the optimal COP value. The findings reveal that among the three weight distributions considered, an equal-weight distribution yields the best conditions for optimizing IEC performance. This distribution significantly enhances both the COP value and cooling capacity while maintaining a lower pressure drop range. However, if cooling capacity is prioritized as the primary objective ($W_1 = 0.75$), there is a slight improvement in wet-bulb efficiency, but a substantial increase in pressure drop contributes to higher energy consumption and a significant decline in the COP value. Conversely, prioritizing pressure drop as the main objective ($W_2 = 0.75$) results in a reduction in both cooling capacity and wet bulb efficiency. Therefore, an equal-weight distribution is

determined as the optimal approach for optimizing system performance, as it strikes a balance between the objectives and yields the best overall results. Under this condition, the optimal operating parameters include a nozzle pressure of 0.15 MPa, spacing of 85 mm, aperture of 6 mm, count of 11, spray density of 0.85 kg/(s·m²) and air velocity of 2 m/s (converted from air-water ratio), at which time the wet-bulb efficiency was 0.85, the pressure drop was 210 Pa, and the COP was 12.4, which is an increase of 23.2% in comparison with the base system.

Table 6.6 The optimization results derived from GA

Design weight			Design variables						Objectives		
No.	W ₁	W ₂	Pressure (MPa)	Spacing (mm)	Aperture (mm)	Count	Density (kg/(s·m ²))	Velocity (m/s)	ϵ_{wb}	ΔP	COP
1	0.75	0.25	0.15	60 mm	6 mm	14	1.5	3.5	0.86	328	10.35
2	0.5	0.5	0.15	85 mm	6 mm	11	0.83	2.8	0.85	210	12.4
3	0.25	0.75	0.15	95 mm	6 mm	8	0.31	1.7	0.77	97	7.71
Base system			0.1	80 mm	6 mm	8	0.44	2.0	0.81	117	9.52

For a complete IEC system, numerous operational parameters can significantly impact the equipment's performance and efficiency. Therefore, it is crucial to establish appropriate operational parameters to ensure the system operates optimally. Based on years of operational experience, the general ranges for IEC operational parameters are as follows: nozzle pressure of 0.05-0.2 MPa, nozzle spacing of 0-100 mm, nozzle aperture of 1-10 mm, number of nozzles

ranging from 0 to 12, spray density of 0-10 kg/(s·m²), and air-to-water ratio ranging from 0 to 10. However, in practical engineering, adjusting operations can be time-consuming and may not always yield the desired results. In such cases, utilizing pre-adjustment operational data and employing a GA-ANN model to optimize IEC operational parameters can offer several advantages. It enables the quick determination of more favorable combinations of operational parameters and enhances the cooling efficiency of the unit. The obtained optimal parameters, as revealed by the model results, generally fall within the range of design parameters, aligning with real-world considerations. The results derived from the model provide theoretical guidance for IEC operational parameters and contribute to the practical significance of debugging work.

Besides, the GA-ANN model established in this thesis innovatively focuses on the spray system of the IEC, hence the selection of model input parameters is concentrated on the influencing factors of the spray system and the state of the wet channel, with the temperature and humidity of the airflow being constant. Future work will involve the development of ANN models for different spray parameters under various climatic conditions to achieve a more comprehensive analysis and optimization of the IEC system. Additionally, the proposed GA-ANN model is based on data from a conventional plate-type cross-flow IEC, limiting its predictive capability to the cooling performance of this specific IEC type. Therefore, it is imperative not to mix data from different types of IECs (such as tubular IECs) during the modeling process.

6.3 Summary of this chapter

This chapter focuses on creating a machine learning (ML) model to predict the performance of IEC systems by accounting for six critical factors related to spray operation. A comprehensive dataset, which includes operational, design, and performance parameters of IEC systems, was developed. The significance of these factors was analyzed using grey relational analysis. Additionally, genetic algorithms were used to optimize the system's operational parameters. By appropriately weighting performance parameters, the study effectively reduced energy consumption while enhancing overall energy performance. These findings provide important insights for designing and operating IEC systems in an energy-efficient and sustainable manner. Below is a summary along with some concluding remarks:

- 1) The developed three-layer IEC-ANN model, focusing on the conditions of water spray operation, shows high predictive accuracy with coefficients of determination of 0.952 for wet-bulb efficiency and 0.938 for the pressure drop in the secondary air channel. The RMSE values are 1.543 and 1.817 Pa, respectively.
- 2) When altering individual factors, increases in nozzle pressure, aperture, count, spacing, spray density, and secondary air velocity tend to enhance wet-bulb efficiency up to a certain point before declining. However, the pressure drop rises continuously with increased spray density and air velocity.
- 3) At lower pressures, larger nozzle apertures improve the IEC system's cooling effect. However, at higher pressures, the cooling performance diminishes as the nozzle aperture

increases. The ranking of the six influential factors from most to least important is: air velocity > nozzle spacing > nozzle pressure > spray density > nozzle count > nozzle aperture.

- 4) Using genetic algorithms based on the ANN model, a multi-objective optimization of the IEC water system was performed to maximize energy efficiency while minimizing pressure drop. The optimal parameters were found to be: nozzle pressure of 0.15 MPa, spacing of 85 mm, aperture of 6 mm, count of 11, spray density of 0.85 kg/(s·m²), and air velocity of 2 m/s. Under these conditions, the wet-bulb efficiency is 0.85, the pressure drop is 210 Pa, and the COP is 12.4, which represents a 23.2% improvement over the baseline system.

In summary, this chapter offers a detailed analysis of how nozzle operating parameters affect the performance of IEC systems. It presents a cost-effective method for achieving optimal performance under various operational conditions through multi-objective optimization. The proposed configuration enhances cooling efficiency while reducing energy consumption, offering valuable guidance and a theoretical foundation for future IEC system optimizations through improvements in water distribution systems.

CHAPTER 7 PERFORMANCE ANALYSIS AND NOZZLE SETTING OPTIMIZATION OF IEC FOR ENERGY RECOVERY IN DATA CENTERS

In contrast to the conventional arrangement, IECs as heat recovery units are often arranged in a diamond shape inside the air handling units (AHUs) of data centers (DCs), an approach that facilitates the flexible use of space and integration within the units in a more compact form. The use of CFD simulations allows an integrated analysis of the coupling of hydrodynamic, thermal and mass properties, which helps to improve the evaporation performance of IECs.

In this chapter, a 3D simulation model of a diamond-shaped IEC containing a water spray system is developed to compare and analyze the air-water arrangement schemes in the IEC system currently used in DC power generation, and the corresponding characteristics are explored from the perspective of CFD technology to determine the effects of nozzle configurations on the formation of a water film and evaporation in the wet channel. Then, a parametric analysis of the nozzle setup schemes is carried out according to the performance indexes to summarize the nozzle arrangement and the air-water distribution scheme that achieves the optimal performance. Last, the effects of enhancement methods are analyzed for hydrophilic and fiber coating simulations.

This chapter is written based on a published paper of this thesis author. The paper is titled *“Improving the performance of indirect evaporative cooler for energy recovery from the perspective of nozzle configuration: A CFD model analysis”* in *Journal of Building*

7.1 Description of numerical model

7.1.1 Description of the model geometry

Different from the conventional IEC placement (Fig. 7.1 (a)), IECs which installed as a heat recovery unit in the AHU of DCs are often distributed in a diamond shape due to their compactness and flexible arrangement, as exemplified in Fig. 7.1 (b). The baseline model was set up in the Space claim unit embedded in the ANSYS work bench, and the coverage factor of the water film on the surface of the wet channel will be taken into consideration as a major research aspect in this thesis. For focused investigation, the model will be built assuming that the properties of water and air are constant with the incompressible element and the plate of the IEC is adiabatic [38].

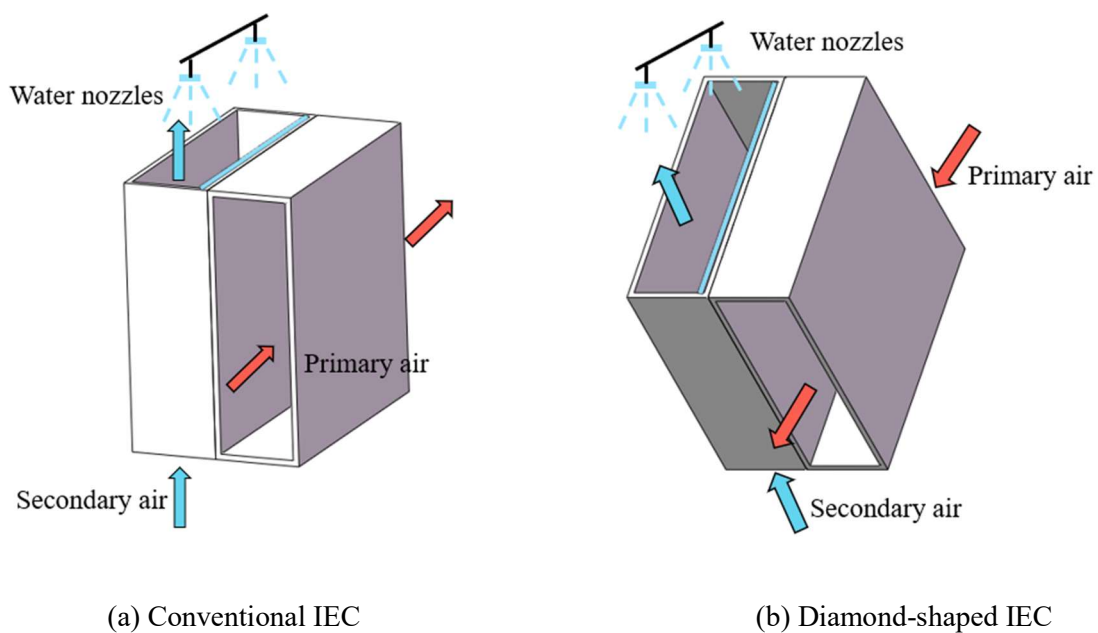


Fig. 7.1 Two types of IEC models set up in work bench

7.1.2 Mathematical bases of CFD approach

The following is a list of the control three types of conservation equations for momentum, mass conservation and energy respectively.

$$\frac{\partial}{\partial t}(\rho E) + \nabla \cdot (\rho u^2) = -\nabla P + \nabla \cdot (\mu(\nabla u + \nabla u^T)) + \rho g + F \quad (85)$$

$$\frac{\partial}{\partial t}(\rho) + \nabla \cdot (\rho u) = 0 \quad (86)$$

$$\nabla \cdot \sum_{k=1}^n (\alpha_k v_k (\rho_k E_k + p)) = \nabla \cdot (k_{eff} \nabla T) + S_E \quad (87)$$

For the selection of turbulence mode, the Reynolds number of the air treated in this investigation was the range of 5,000-13,000 with the water film less than 400. Therefore, the flow form of the falling water film and treated air were laminar and turbulent respectively. Based on the reference of Fluent user's guide [111], RNG (Renormalization group) turbulence model was chosen to simulate the behavior of the fluid dynamics in the IEC. The controlling equations for the turbulent kinetic energy as well as its dissipation rate could be determined as follows.

$$\frac{\partial}{\partial t}(\rho k) + \frac{\partial}{\partial x_i} \cdot (\rho k u_i) = \frac{\partial}{\partial x_j} \cdot \left(\alpha_k \mu_{eff} \frac{\partial k}{\partial x_j} \right) + G_k + G_b - \rho \varepsilon - Y_M + S_k \quad (88)$$

$$\frac{\partial}{\partial t}(\rho \varepsilon) + \frac{\partial}{\partial x_i} \cdot (\rho \varepsilon u_i) = \frac{\partial}{\partial x_j} \cdot \left(\alpha_\varepsilon \mu_{eff} \frac{\partial \varepsilon}{\partial x_j} \right) + C_{1\varepsilon} \frac{\varepsilon}{k} \cdot (G_k + C_{3\varepsilon} G_b) - C_{2\varepsilon} \rho \frac{\varepsilon}{k} - R_\varepsilon + S_\varepsilon \quad (89)$$

Owing to the presence of evaporation in the wet channel of IEC, the phase change process produces a degree of heat and mass transfer, hence the simulation needs to

incorporate the species transfer model formulated by Eq. (90). For the species transport, the description are as follows.

$$\frac{\partial}{\partial t}(\alpha_q \rho_q x_{k,q}) + \nabla \cdot (\alpha_q \rho_q \vec{u} x_{k,q} - \alpha_q D_{k,q} \nabla x_{k,q}) = S_{l,g,k} \quad (90)$$

The Volume of Fluid (VOF) model, which is originally the most widely used falling film interface capture model has undergone a series of refinements and has matured since its development [67]. The description equation for the volume fraction could be shown in Eq. (91).

$$\frac{\partial \alpha_{1/g}}{\partial t} + \vec{u} \cdot \nabla \alpha_{1/g} = 0 \quad (91)$$

Based on solving Eq. (91) to acquire the volume fraction within each involved section, Eqs (92), (93) and (94) illustrate that the associated thermal characteristics could also be determined.

$$\rho = \alpha_1 \rho_1 + \alpha_g \rho_g \quad (92)$$

$$\mu = \alpha_1 \mu_1 + \alpha_g \mu_g \quad (93)$$

$$\lambda = \alpha_1 \lambda_1 + \alpha_g \lambda_g \quad (94)$$

The DPM (Discrete Phase Model) will be used to simulate the operating status of the nozzles in the IEC water system, including the trajectory of the spray droplets from being ejected, to falling into the wet channel, to finally colliding with the wall or leaving the wet channel.

The trajectory of droplets can be determined based on a combined Euler-Lagrangian

method by solving the force balance equation written as Eq. (95).

$$\frac{d(\vec{X}_g)}{dt} = \vec{V}_g \quad (95)$$

The movement description of a single droplet is described by Eq. (96).

$$\frac{d(m_d \vec{F}_d)}{dt} = \vec{F}_D + \vec{F}_g \quad (96)$$

For a circular drop, the drag force formulated by Eq. (97).

$$\vec{F}_d = -\frac{\pi}{8} C_D \rho_a D_d^2 \vec{V}_r |\vec{V}_r| \quad (97)$$

The EWF (Eulerian Wall Film) model could be used to describe the process by which water droplets in contact with the wet channel wall are trapped by the plate to form a thin water film attached to the plate and flow down the plate, following the relationship of Eqs. (98) and (99).

$$\frac{\partial \delta}{\partial t} + \nabla \cdot (\delta u_l) = \frac{\dot{m}_s}{\rho_l} \quad (98)$$

$$\dot{m}_s = \alpha_l \rho_l u_{l,n} \quad (99)$$

Finally, interfacial mass transfer also needs to be considered due to the phase change reaction resulting from the evaporation of the liquid in the wet channel. In this process, the local mass transfer coefficients as well as the total mass transfer coefficients are reflected by Eqs. (100), (101) and (102), respectively.

$$h_{m,g} = 2 \sqrt{\frac{D_g}{\pi t_c}} \quad (100)$$

$$h_{m,l} = 2 \sqrt{\frac{D_l}{\pi t_c}} \quad (101)$$

$$\frac{1}{K} = \frac{1}{h_{m,g}} + \frac{1}{\psi h_{m,l}} \quad (102)$$

Based on the total mass transfer factor K, the mass source component and the energy component at the phase surface could be determined by Eqs. (103) and (104).

$$S_{lg,k} = K (d_g - d_e) A \quad (103)$$

$$S_E = \sum_{k=0}^{m-1} S_{lg,k} H_{lg,k} \quad (104)$$

7.1.3 Simulation settings

The schematic diagram of IEC and computational domains are illustrated in Fig. 7.2. The whole model is consisting of two domains to describe the direction and state of gas-liquid flow in the dry and wet channels respectively. The finite control volume method could be applied to deal with the control equations. Since gravity is not negligible, the weight-pressure discretization method is used [41]. The SIMPLE method is applied for the pressure-velocity coupling and then the pressure interpolation technique (PRESTO!) is used [42]. In the calculation domain for the wet channel, the inlet and outlet of the secondary airflow are at a certain distance compared to the heat exchanger prototype, allowing the nozzle model, which is located inside the external boundary of the heat exchanger, to deliver a smooth spray into the wet channel. Therefore, the continuously fed spray contacts the plate surface and forms a continuous film of water flowing along the wall lead by gravity. The wet air flows beside the water film in a downstream, counterflow or staggered flow. Since the differential temperature between the water membrane and the secondary air flow, heat absorption by evaporation of the liquid occurs in the channel. The entire channel is the computational domain of the cross-flow because of the asymmetry of the air flow and the water flow. On the other hand, for the computational domain of the dry channel, the primary

airflow enters from the upper right and condensation occurs when the humidity is too high, then the airflow undergoes cooling and dehumidification before leaving the dry channel from the lower left. The dimensions of all calculation domains are 620×620 mm (L \times H). As shown in Fig. 7.2, the grid size in the area close to the plate surface should be fine enough in order to ensure a correct interface description. The mesh size in the interface region is less than 0.1 mm.

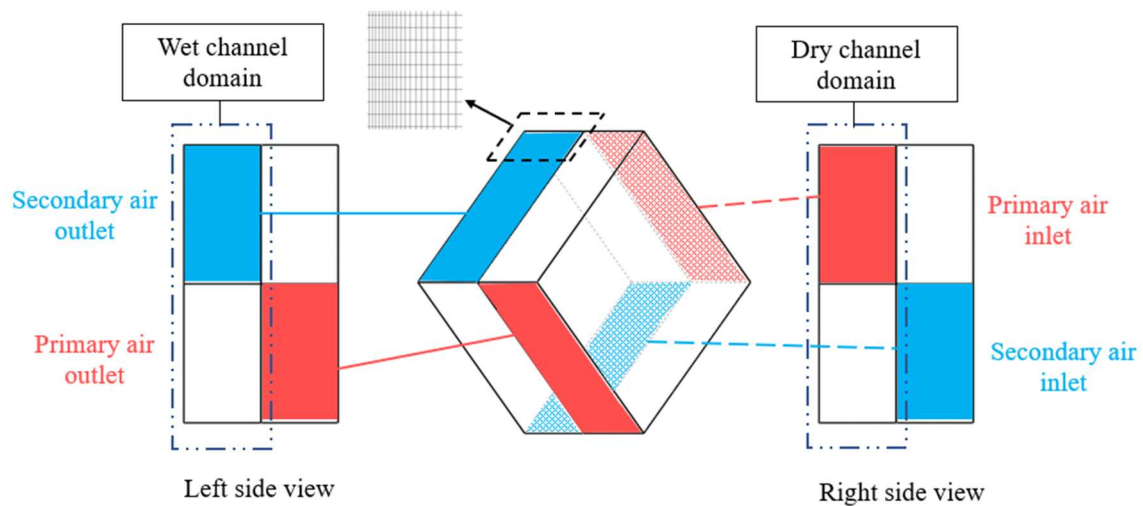


Fig. 7.2 Geometry, mesh and boundary conditions in simulations

7.1.4 Grid independence verification

To complete the simulation of the mathematical model, the base model created in Space claim needs to be meshed. As the key point of this study is the water membrane that forms on the plate surface when the spray droplets come into contact with the wet channel, the film is quite thin and flows slowly down the wall surface by gravity. To accurately obtain the distribution of the film on the surface and the flow characteristics, a fine size grid with a size

of less than 0.1 mm was selected in the area close to the plate surface. It is well known that the results of the model calculations will be closer to the true value due to the increase in the number of meshes, and the mesh quality is higher while the time cost of the program to run the calculation is also higher. Therefore, a reasonable balance between mesh quality and computational time is required, and grid independence is verified to select the number of meshes that are close enough to the exact value. For the air side, the velocity of inlet primary air was set at 3.7 m/s, the absolute humidity was set at 10 g/kg, and the temperature was determined as 35°C. For the water side, the water supply flow rate was selected to be 65 L/h. Fig. 7.3 compares the water membrane coverage factor on the wet channel wall and the primary air output temperature for different grid quantities. It is clear that both evaluation parameters initially deviate significantly with the grid mass and then level off at a grid number of 450,000. Thus, this grid structure was selected for further simulations so as to maintain a balance between simulation accuracy and processing time.

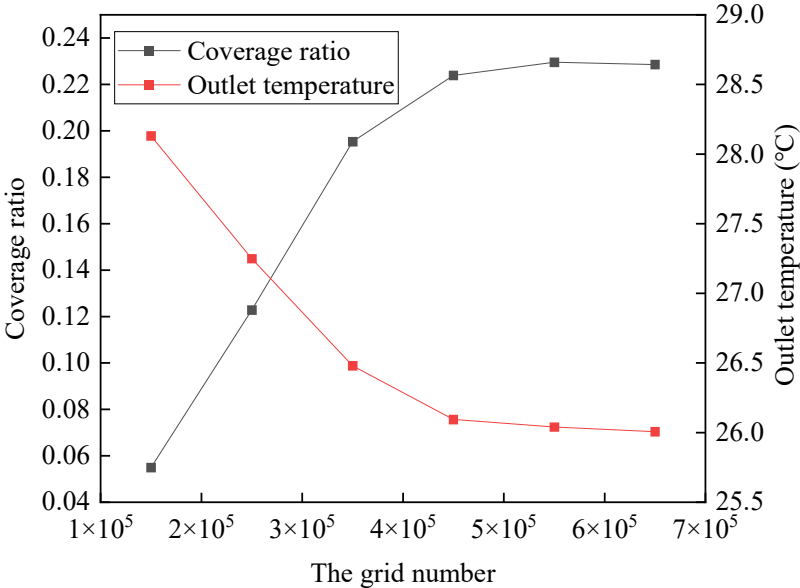


Fig. 7.3 Coverage ratio and outlet temperature at different accounts of grid

7.1.5 Description of exergy analysis

The determination of dead state conditions is significant for exergy analysis. A constant atmospheric condition is frequently used as the benchmark environment [113]. Nevertheless, there is still exergy accessible when the atmosphere is not completely filled with air. Water would be able to spontaneously disperse into the unsaturated air and finally achieve saturation through such a moist air process. As a result, the dead state in this essay is referred to as saturated outside air.

The exergy used to reach thermal, mechanical and chemical equilibrium with the atmosphere during indirect evaporative cooling process can be written as [146]:

$$e_t = e_{th} + e_{me} + e_{ch} \quad (105)$$

The combination of dry air and water vapor found in humid air makes it an ideal gas. The following equation was developed by Wepfer et al. to represent the entire flow exergy of moist air per kilogram of dry air [115]:

$$Ex_a = (C_{P,DA} + \omega C_{P,V}) \left[T - T_0 \left(1 - \ln \frac{T}{T_0} \right) \right] + T_a \left[(1 + 1.608\omega) \ln \left(\frac{1 + 1.608\omega_0}{1 + 1.608\omega} \right) + 1.608\omega \ln \frac{\omega}{\omega_0} \right] \quad (106)$$

The exergy balance for the basic heat exchanger is shown in Fig. 7.4. As there is no work being produced for the reaction process of IEC system, the exergy balance for the IEC is determined as follows:

$$(m_i e_{1,a} + m_{w,i} e_{w,a}) = (m_f e_{2,a} + m_3 e_{3,a}) + I \quad (107)$$

Consequently, the exergy efficiency of the IEC is depicted as:

$$\eta_e = 1 - \frac{I}{(m_i e_{1,a} + m_{w,i} e_{w,i})} \quad (108)$$

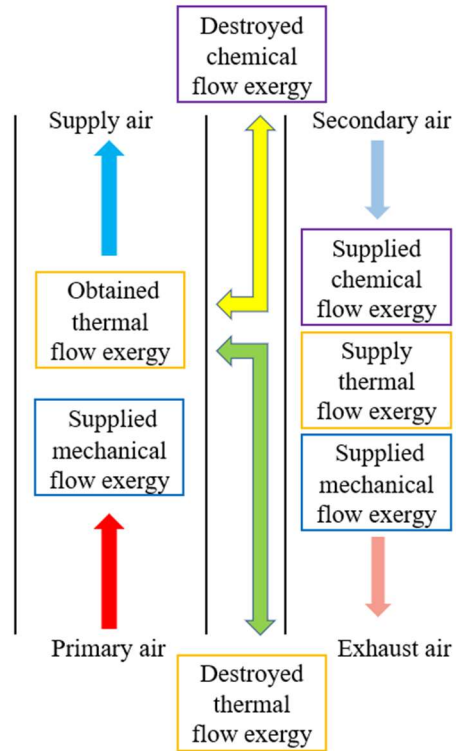


Fig. 7.4 The schematic diagram of exergy analysis

7.2 Model validation

7.2.1 Validation of the water spray system

The accuracy of the CFD model developed in this thesis for a diamond-shaped IEC is verified based on a comparison and analysis of the simulation data with the field trial data in the literature by De Antonellis et al [29]. In the experiments, the fluctuation of the wet-bulb efficiency of the diamond-shaped IEC (TOP/SIDE configuration) was investigated when the water spray flow rate was varied. The temperature drops at the supply air outlet compared to

the inlet at different flow rates was compared under the fixed inlet air characteristics, heat exchanger geometry and heat transfer coefficients provided in the literature. According to Fig. 7.5, the trend of primary airflow temperature drop with water supply flow is the same in both sets of data, and the maximum difference is less than 10%, hence the CFD model fits the water system and temperature drop to the required degree.

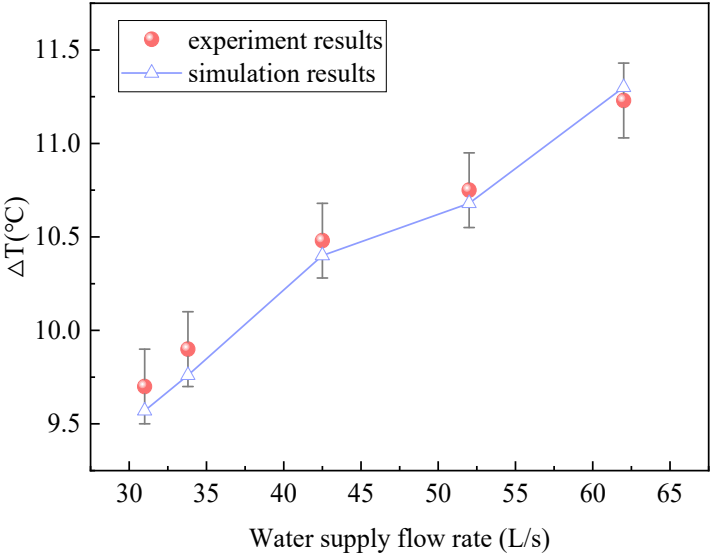


Fig. 7.5 Comparison between the tested and simulated data based on temperature difference

7.2.2 Validation of film thickness

As was noted in section 2.3, the main form of downward flow of the water film formed by the aggregation of liquid droplets inside the IEC wet pass due to gravity is wavy laminar flow. The average membrane thickness of the Nusselt-based liquid film theoretical laminar flow could be determined by the analytical equation of the film, as shown in the following equation [51],

$$\delta_w = \left(\frac{3\nu_w Re_w}{g} \right)^{1/3} \quad (109)$$

This section compares the average membrane thickness values derived from this simulation model with the estimated results of the preceding analytical equation, and the outcomes are displayed in Fig. 7.6, with the purpose of confirming the accuracy of the suggested CFD model in terms of flow. It is obvious that the simulated results and the estimated outcomes of the empirical equation correspond well. Therefore, it is accurate to simulate the water film flow formation in the IEC wet channel using the current model.

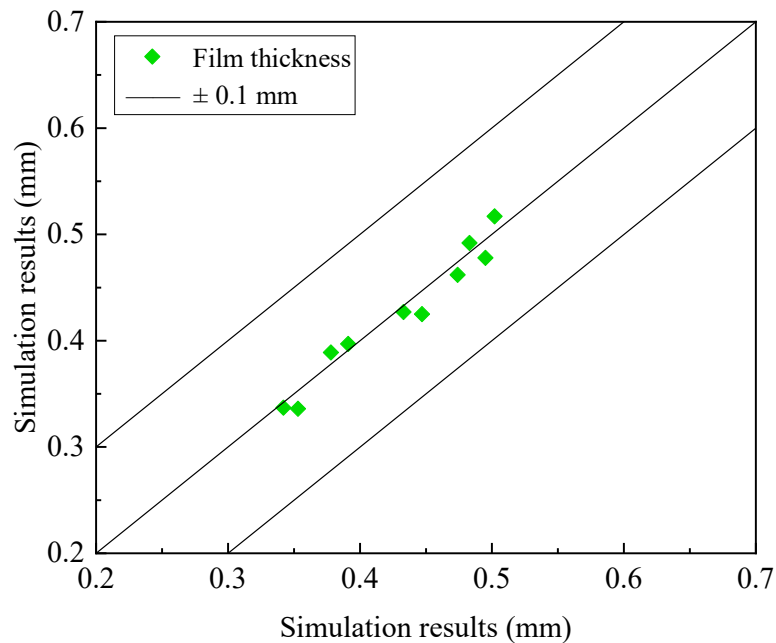


Fig. 7.6 Validation of film thickness between simulation results and Nusselt empirical formula

7.2.3 Validation of IEC system

To gain a fuller understanding of the precision of the model in foretelling the performance of the overall IEC system, tested data from an IEC combined with AHUs set up at a printing

facility in Hong Kong was also considered for validating. In this project, the IEC was made of aluminum sheets with a thickness of 0.5 mm, and a total of 90 channel pairs of fresh air and return air were placed in a width of 0.8 m space. By referring to the fresh air demand of 3312 m³/h, the area of each heat exchange plate is designed as 0.384m² with a dimension of 0.62 m × 0.62 m. The total heat exchanger area of this IEC is 69.1 m².

To collect the operation and performance data of the IEC system for performance analysis, a data monitoring system. A variety of kinds of senders are required to transmit real-time measured data to a data logger and Table 7.1 lists the specific parameters of these instruments. The data measured by these transmitters was collected in every 5 minutes.

Table 7.1 Specifications of the test parameters

Sensor	Parameter	Range	Accuracy
T&R Transmitters	Temperature,	-10-60 °C	± 0.25% °C
	Humidity	-15-95% RH	± 2.0% RH
ΔP Transmitters	Air velocity	0-15 m/s	± 1%

With the purpose of identify the reliability of the test results, the uncertainty introduced by the errors of the quantified instruments used during the experiment needs to be analyzed. The method Eqs. (110) and (111) for calculating the uncertainty of the measurement equipment and the experimental factors according to the error analysis guidelines provide how to calculate the uncertainty of the measurement equipment and the experimental factors respectively [52, 53].

$$U = f(x_1, x_2, x_3, \dots, x_n) \quad (110)$$

$$\delta U = \sqrt{\left(\frac{\delta U}{\delta x_1} \delta x_1\right)^2 + \left(\frac{\delta U}{\delta x_2} \delta x_2\right)^2 + \left(\frac{\delta U}{\delta x_3} \delta x_3\right)^2 + \dots + \left(\frac{\delta U}{\delta x_n} \delta x_n\right)^2} \quad (111)$$

On the account of the accuracy data of each testing equipment arranged in Table 7.1, the uncertainty of the wet-bulb efficiency by the experimental assessment criteria is 2.47%.

The initial parameters of field test were applied in the simulation model as well. The experiments were conducted under the following conditions: $t_p = 35 \text{ }^\circ\text{C}$, $RH_p = 50\%$, $u_p = 2 \text{ m/s}$, $t_s = 24 \text{ }^\circ\text{C}$, $RH_s = 60\%$, $u_s = 1.5 \text{ m/s}$, $s = 4 \text{ mm}$, $H = 0.5\text{m}$, $L = 0.5 \text{ m}$. Fig. 7.7 reflects the comparison of the simulated results of wet bulb efficiency with the experimental results, and according to the results it was found that the deviations of these points are within 10%, and the maximum difference is 8.6%, Consequently, the proposed CFD model is proved acceptable for subsequent research.

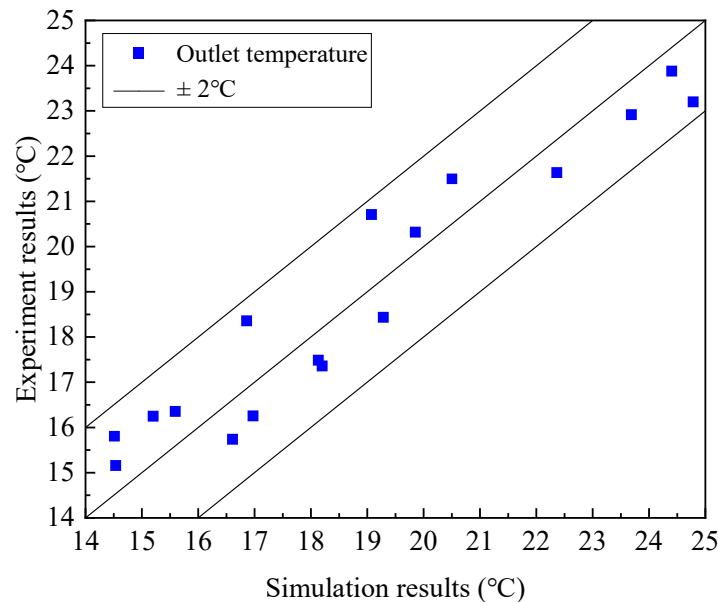


Fig. 7.7 The model verification results based on the outlet temperature of primary airflow

7.3 Effects of nozzle configuration on cooling characteristics

With a view to better and more specifically enhance the performance of the IEC as a heat recovery unit for AHUs in DCs and to determine the best nozzle design solution for the diamond-shaped IEC, this section put forward a comprehensive analysis of the air-water configuration on the basis of CFD modelling, in terms of both the installation position of the nozzles and the direction of the airflow relative to the water flow.

7.3.1 Four schemes of nozzle configuration

On the basis of the literature summaries and surveys of actual AHU heat recovery devices in DCs with taking into account the installation space with flexible arrangement of IECs, the common nozzle setting configurations can be summarized into the four types illustrate in Fig. 7.8, namely upper side configuration, lower side configuration, top configuration and bottom configuration. In addition, existing researches on the heat and mass transfer case of IEC showed that the evaporative response in the wet channel is stronger in the counterflow case compared to the configuration with air-water flowing in the same direction, owing to the fact that the secondary air and water streams in the wet channel are in contact with water more fully and for a longer period of time. Therefore, this section analyzed the performance of four nozzle configuration options founded on the premise of air-water reverse flow, and the superior option would be determined through systematic analysis.

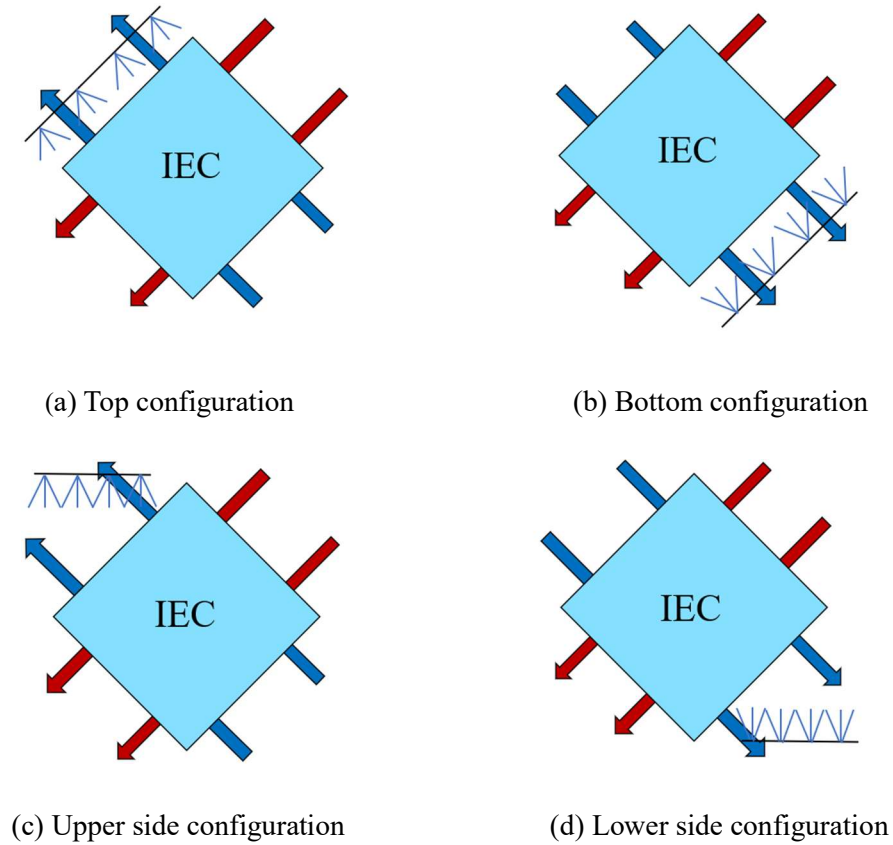


Fig. 7.8 The schematics of the four nozzle configurations

7.3.2 Performance evaluation of different nozzle configurations

7.3.2.1 Determination of the test water flow rate

In advance of comparing different nozzle system setup scenarios, the water supply flow rate should be determined when the water film attached to the wetted channel wall tends to be at the maximum wetting ratio. According to the experimental data of De Antonellis et al., the trend of IEC wet-bulb efficiency with water supply flow rate can be derived as shown in Fig. 7.9 [56]. In general, the wet -bulb efficiency of diamond-shaped IEC usually grows with the increase of water supply flow rate and stabilizes at a maximum value when the flow rate arrives 65 L/s, thus 65 L/s is determined as the simulated flow rate value.

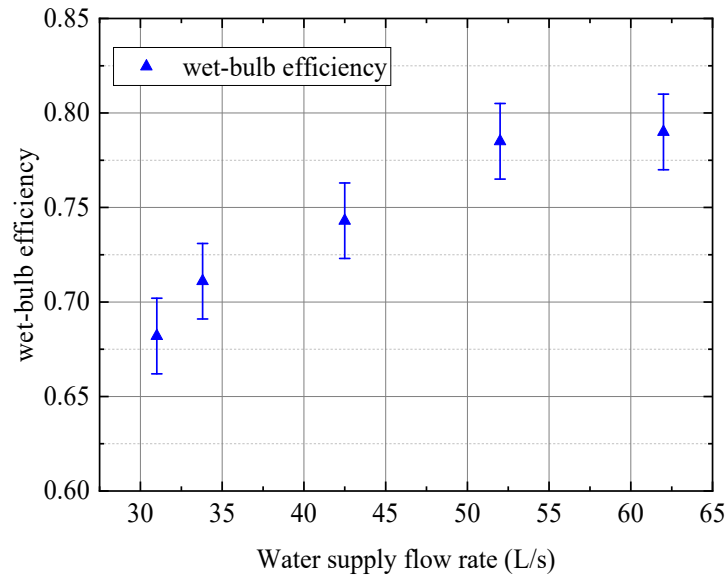


Fig. 7.9 The determination of test spray flow rate

Besides, with reference to the previous study on the uniformity of spray distribution, a full cone nozzle with an outlet diameter of 2.4 mm was used as the subject of this thesis on the water film coverage [21]. Similarly, since this type of nozzle achieves the most ideal spray distribution at a spray cone angle of 45° , this operating parameter is also applied in the simulation of this thesis. In addition, according to the actual design instructions and previous studies have proven that the nozzle flow rate, pressure, droplet diameter and spray cone angle are interrelated factors. The main characteristic equations of the nozzle are as follows. According to Lefebvre and McDonnell, the theoretical parameters of spray can be calculated as Equation (112), (113) and (114) [55].

$$\dot{m}_{th} = \rho A_o \left(\frac{2\Delta P}{\rho} \right)^{0.5} \quad (112)$$

$$d = 9.5d_j / (\Delta P_1 \sin(\alpha/2)) \quad (113)$$

$$2\alpha = 334.32K^{-0.165} \left(\frac{D_s}{D_o}\right)^{-0.484} W_e^{0.043} Re_p^{-0.065} \quad (114)$$

Therefore, it is clear that after the spray cone angle and flow rate are determined, the remaining parameters can be specified as shown in Table 7.2. Water supply temperature that is the temperature of liquid water at room temperature 20°C.

Table 7.2 The specifications of the nozzle

Nozzle type	Orifice diameter (mm)	Volumetric flow Rate (L/s)	Pressure (bar)	Spray angle (°)	Water temperature (°C)
Full cone	2.4	220	1.5	45	20

Finally, for the smooth operation of the wet channel simulation and the subsequent further comparison of IEC performance, the air and water conditions of the IEC need to be identified first, with the following parameter conditions:

$$t_p = 35 \text{ }^\circ\text{C}, RH_p = 50\%, u_p = 2 \text{ m/s}, t_s = 24 \text{ }^\circ\text{C}, RH_s = 60\%, u_s = 1.5 \text{ m/s}, s = 4 \text{ mm}, H = 0.5 \text{ m}, L = 0.5 \text{ m}$$

7.3.2.2 Comparison of four configurations on water film coverage

Fig. 7.10 depicts the simulated water film coverage levels within the IEC wet channel for each of the four scenarios with different nozzle configurations.

For the horizontal configurations (top and bottom), the distribution pattern of the water membrane in the wet channel is similar to that of the conventional IEC (square), with minor

differences due to the direction of the secondary air flow since a change from the conventional reverse flow to a 45° direction of flow. Furthermore, on account of the characteristics of the diamond-shaped IEC under study, the horizontal configuration, although providing a good flow of water film, concentrates the water film more on the side with the position of nozzles installation, while the plate surface near the primary airflow outlet is not sufficiently wetted. This disadvantage is even more serious in the bottom configuration of the nozzle scheme. As a result of the inevitable gravitational forces, the nozzles need to be set at a higher water pressure in order to deliver the spray droplets into the upper part of the wet channel. However, when the spray pressure is too high, the droplets tend to atomize making it difficult to form a water film in contact with the walls. Therefore, for the lower configuration, the water film is not uniformly distributed in the upper left side of the diamond-shaped IEC, and is subject to the gravity factor even if the right side of the heat exchanger where the nozzle is set is not sufficiently wetted.

For the side configuration of the nozzle, IEC wet channel wall water film distribution of uniformity and coverage compared to the forward configuration is better, whether the nozzle with upper or lower installation. In the case of nozzle for the side on the configuration, the overall distribution of water film tends to spray direction, that is, 45° . At the same time, the water film is affected by gravity and slips along the vertical direction when it comes in contact with the wall, thus the water film is more uniformly distributed and covers a wider area. Likewise, as a consequence of the direction of the nozzle spray, the upper right side of the wet channel is also mostly covered by the water membrane. In contrast, the lower side of the nozzle configuration produces a narrower water film. However, again, due to the direction of the water

spray, the comprehensive water film distribution performance is still better than the vertical installation of the nozzle in the case of downward flow of the water film.

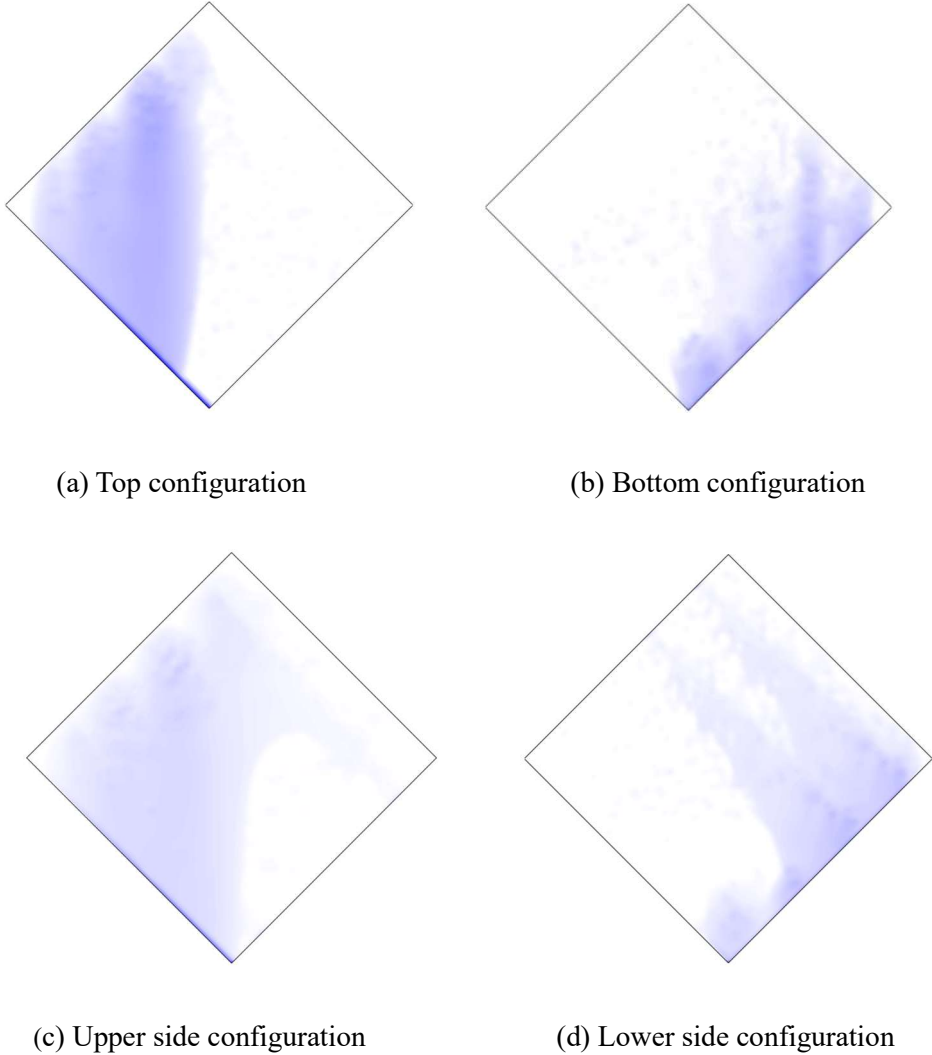
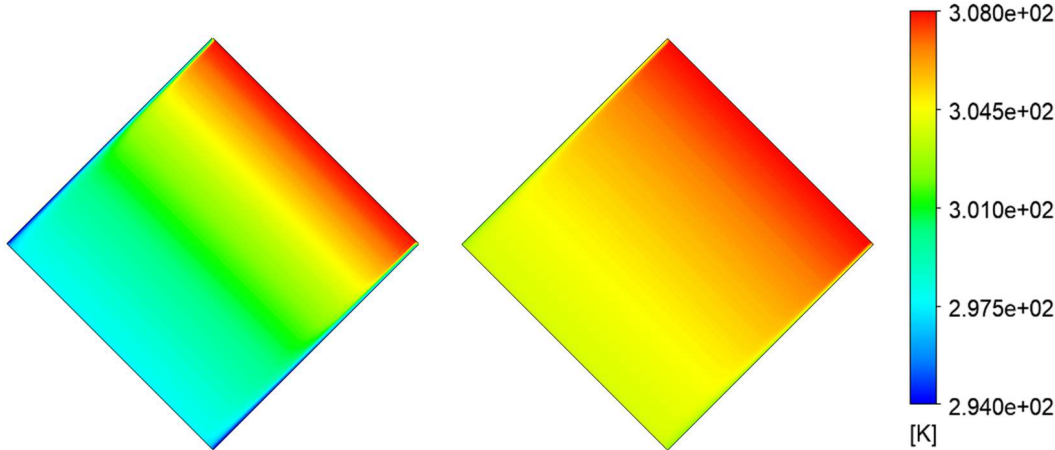


Fig. 7.10 The water film distribution of the four nozzle configurations

7.3.2.3 Comparison of four configurations of temperature distribution

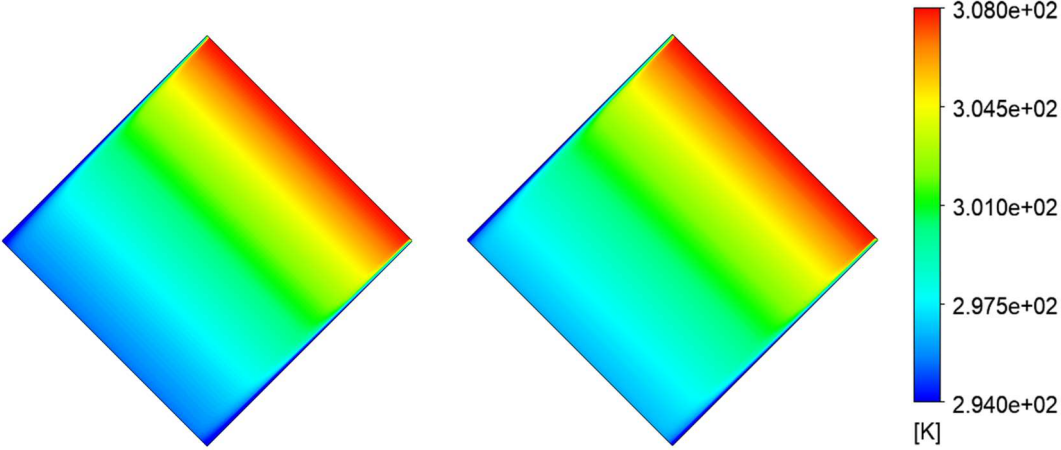
Fig. 7.11 illustrates the temperature distribution states within the IEC primary airflow channel for four different nozzle configuration schemes. It is clear that the degree of temperature drop in the primary airflow temperature within the dry channel is closely related

to the percentage of water film coverage within the wet channel. Among them, the IEC with nozzles in the upper side configuration can achieve the minimum outlet temperature of the primary air, and the magnitude of temperature will be significantly more intense and compact inside the heat exchanger channel. This is due to the most intense evaporation process inside the wet channel and the most pronounced cooling effect of the heat exchanger plate, with the primary air being correspondingly more fully cooled in the dry channel. Conversely, the nozzles in the bottom configuration have the worst temperature drop for the same environment and energy consumption due to the most inferior wetting rate.



(a) Top configuration

(b) Bottom configuration



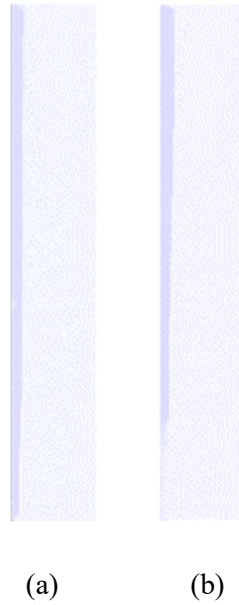
(c) Upper side configuration

(d) Lower side configuration

Fig. 7.11 The primary temperature distribution of the four nozzle configurations

7.3.2.4 Comparison of configurations of axial characteristics

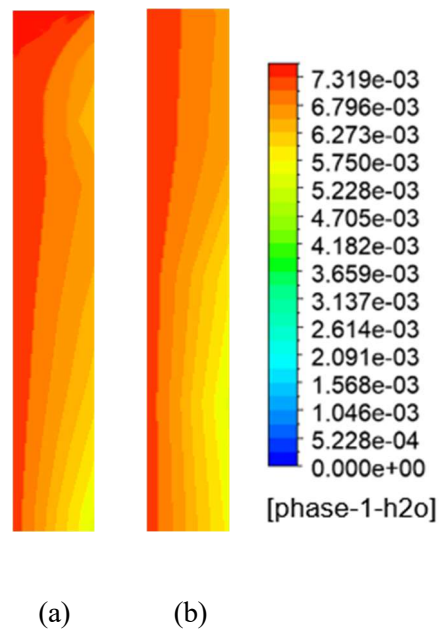
On the basis of the relative flow directions of the water film and the airflow, the four nozzle configurations could be grouped into two main categories, respectively, the upper and lower spray forms. Therefore, in this section, the upper and lower side configurations are selected as representatives for the water flow and temperature distribution on the plate surface in the thickness direction. The results of this model are allowed to investigate the state of water film formation and the effect of heat mass exchange within the wet channel, as depicted in Fig. 7.12. Surface tension, gravity and viscous forces all contribute to the flow of the water film. In the initial stage, the water film forms higher thickness in the upper part of the channel section due to surface tension and viscous forces. Due to gravity, the velocity of the water film increases, resulting in the formation of a continuous film on the surface of plate. In addition to the uniform basic characteristics of water film formation, it is clear that by comparing the results of water film distribution between the two water distribution methods that the installation position of the nozzle affects the state of the film formed. In this case, the upper side configuration yields a smooth and diffuse continuous water film, while the lower side configuration results in a partially thicker water film and incomplete water film coverage due to aggregation from uneven gravity distribution.



(a) Upper side configuration (b) Lower side configuration

Fig. 7.12 The film formation of two configurations

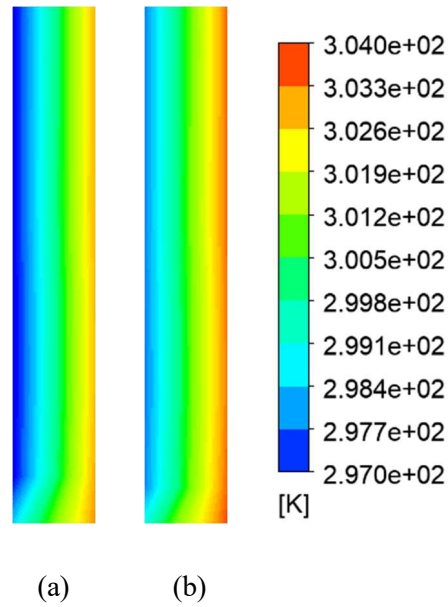
Besides, the effect of heat and mass transfer on the water vapor content and channel temperature could also be easily analyzed. As shown in Fig. 7.13, the water vapor concentration in the secondary airflow in the wet channel of the upper side configuration is significantly higher than that in the lower side configuration. The mass transfer process between the water membrane and the airflow is smoother and faster, and the final water membrane transfers more mass to the airflow as a result. This is owing to the thinner and more uniform distribution of the water membrane covered on its plate surface.



(a) Upper side configuration (b) Lower side configuration

Fig. 7.13 The water vapor content distribution of two configurations

Correspondingly, Fig. 7.14 shows the temperature trends inside the wet channel for each of the two scenarios. It is clear that the temperature drop is stronger for the upper side configuration, reaching an average value of 25.5 °C at the outlet, while for another one it is 26.8 °C. Such a result is based on the principle of IEC operation, where the evaporative heat absorption by the water film allows the secondary airflow to transfer heat to the water film thus achieving the desired temperature drop of the airflow. Corresponding to the upper analysis, the temperature drop is the same as the increasing trend of water vapor concentration. Furthermore, it is evident that the film temperature does not change due to the heat absorbed from the airflow.



(a) Upper side configuration (b) Lower side configuration

Fig. 7.14 The temperature distribution of two configurations

7.3.2.5 Specific gaps in the four configurations

Moreover, Fig. 7.15 summarized the specific values of the water film coverage coefficient and the primary airflow temperature variation along the wet channel surface for the four cases. Obviously, the temperature drop in the primary airflow typically follows the same trend as the water film coverage coefficient of the wet channel. The best results are achieved in the upper side configuration, while the water film coverage ratio and temperature drop are 0.76 and 24.1°C, respectively, with a 59.2% and 27.4% improvement compared to the worst configuration directly. In addition, a small expansion of the wetted area at such low wetting rates also leads to a relatively high temperature rise, while further optimization is no longer apparent when wetting is already more uniform and close to the maximum.

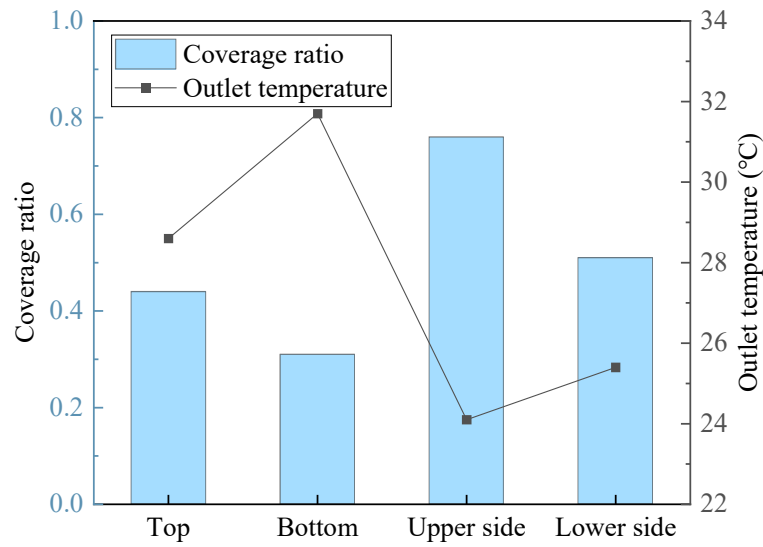


Fig. 7.15 The coverage ratio and outlet temperature of four configurations

7.4 Approaches for cooling performance enhancement

7.4.1 Performance enhancement by hydrophilic coating

The wettability of the plate surface inside IEC wet channel is determined by a combination of nozzle configurations and plate surface characteristics, while the contact angle is a crucial parameter for affecting the wetted area by water on a certain surface. In general, the three-phase equilibrium of the gas, liquid, as well as solid phases in the measuring environment determines the contact angle value. The interfacial tension of the water phase and the surface energy of the solid phase are what determine the contact angle, thus decreasing the interfacial tension of the liquid or rising the surface energy of the solid surface could enhance the wetting ratio of the descending film. Previous studies have shown that the addition of a new hydrophilic coating to the IEC wet channel surface can reduce the contact angle between the droplets and the heat exchanger plate surface, thus improving the uniformity of droplet distribution. Therefore, this

section will further investigate and analyze the wet channel using standard epoxy resin coating and IEC with well-dispersed hydrophilic coating, respectively.

Firstly, the contact angles of the wet channel walls of IEC with conventional epoxy resin coating and new hydrophilic paint were determined to be 77.8° and 57.8° , respectively [116]. Then, the contact angle of the additional hydrophilic coating was applied as the initial setting parameter of the heat exchanger wet channel wall boundary by EWF setting in the simulation of the CFD model proposed in this study. Fig. 7.16 (a) demonstrates the water membrane distribution on the plate surface of the IEC wet channel with a coated counterflow arrangement. There is no doubt that the shrinkage of the descending membrane on the plate surface of the IEC wet channel is significantly reduced for a 20° reduction in contact angle, with a relative increase of 14.5% in water film coverage from 0.76 to 0.87. Correspondingly, the evaporative heat absorption phenomenon of the secondary airflow in the wet channel is also more adequate as exemplified in Fig. 7.16 (b). Consequently, the temperature drop response of the primary airflow is also greater, from 24.1°C to 22.4°C , a relative increase of 7.4%. The improvement mechanism of the hydrophilic coated IEC is based on optimization for the contact state of water droplets and heat exchanger walls thus expanding the contact area and mass transfer area within the water film and the secondary airflow, the area of water in contact with the surface of the plate rises while the area available for evaporation of the water spray film is also enhanced. The end result is an increase in IEC wet-bulb efficiency and an overall increase in heat exchange capacity.

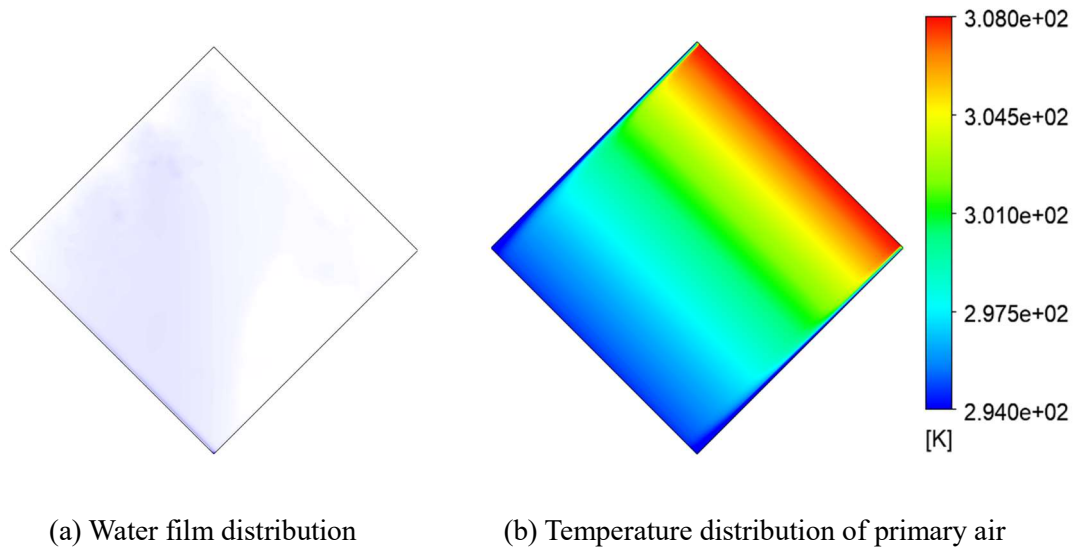


Fig. 7.16 The performance improved by hydrophilic coating

7.4.2 Performance enhancement by fiber coating

With the aim of improving the poor wetting of conventional aluminum and polymer IECs, another proven method is the proposal to attach a fiber coating to the walls of the IEC in order to enhance the wetting circumstances through its great water diffusion. The results showed that the fiber coating considerably improved the wetting conditions, with a contact angle of 0° between the spray droplets and the wall surface, and that the water film distribution as well as wetting rate on the surface of the plate were optimized [117]. The outlet air temperature of IEC can be left unaffected by the enhanced thermal resistance of the fiber covering when running in totally wet conditions. Maintaining the wet channel surface wetness is therefore a necessary condition for the use of fiber coatings. Additionally, to increasing surface wetness, the fiber coating has water conservation properties that make it possible to apply water spray for IEC intermittently.

Consequently, the ratio of water film coverage simulated in the IEC model based on the fiber coating can be considered as 1. Fig. 7.17 (a) elucidates the water membrane distribution in the diamond-shaped IEC wet channel with the additional fiber coating. Undoubtedly, with a contact angle of 0° and no water film shrinkage, the water film almost completely covers the heat exchanger wall from top to bottom, which is a 31.6% improvement compared to the original IEC with aluminum plate. In addition, the temperature drops in the primary air indicated by Fig. 7.17 (b) is greater, from 24.1°C to 20.7°C , a relative increase of 16.4%. The improvement mechanism of the fiber-coated IEC is manifested in two ways: first, the distribution of the water film in the wet channel benefits from a more uniform distribution of the diffusion phenomenon of the fiber material than that of the hydrophilic coating; second, the water retention capacity of the fiber material ensures the possibility of indirect water injection, thus achieving lower power demand of pump and higher COP of IEC system.

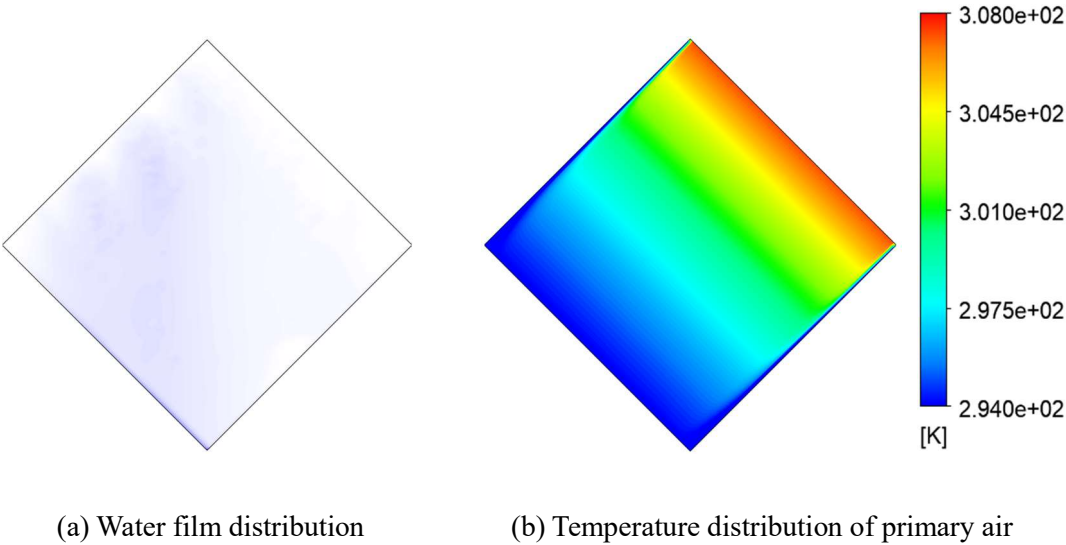
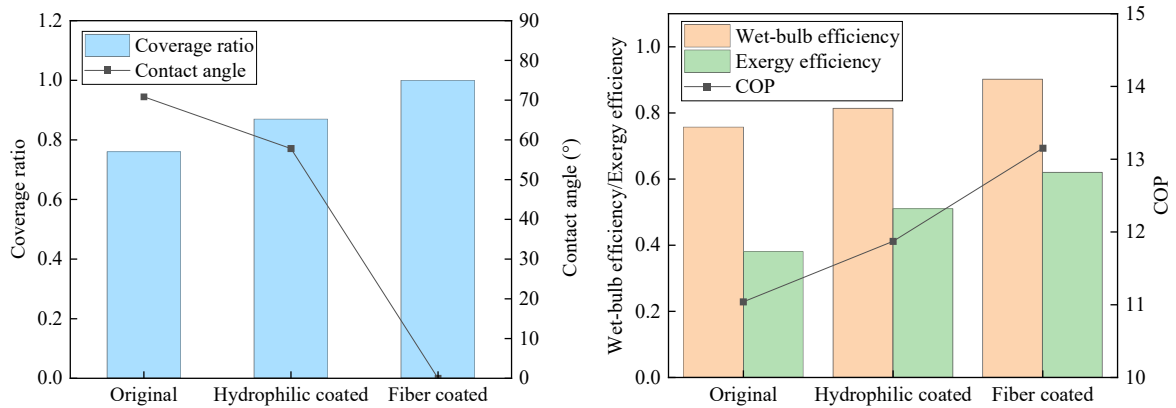


Fig. 7.17 The performance improved by fiber coating

7.4.3 Assessment of the degree of enhancement

Comparing the performance of the original solution with that of the two performance enhancement solutions, it is apparent that from the Fig. 7.18 (a) both the hydrophilic coating applied to the wet channel walls and the additional fiber coating increase the wetting ratio of the walls by decreasing the contact angle between the droplets and the wall surface. In addition, the fiber coating increases the diffusion rate of the water film compared to the hydrophilic one, thus achieving a wetting ratio close to 1, which is regarded as complete wetting. Accordingly, as shown in Fig. 7.18 (b), when the wetting rate is increased, the wetted surface of the wet channel has a larger contact area with the secondary air flow, the evaporation and heat absorption reaction is more intense and the temperature drop on the surface is more dramatic. As a consequence, the wet-bulb efficiency of the IEC was optimized for both the increased hydrophilic and fiber coating on the plate surface, by 5.7% and 14.5% respectively. Moreover, on account of the water conservation capacity of the fiber coating, which allows for indirect spraying, the energy requirement of the pump is reduced, resulting in a further increase in the COP value of 16.1%. Furthermore, due to the improved cooling capacity, the exergy efficiency of the diamond-shaped IEC with additional enhancement coating has been improved by 24.2% and 33.7% respectively without any other external energy consumption. Thus, the enhancement of the wetting ratio of the IEC wet channel by a functional coating, thus enhancing the evaporative heat absorption process, is always an effective way of heat transfer enhancement.



(a) Effect on coverage ratio and contact angle

(b) Comparison of the three performance indexes

Fig. 7.18 The performance comparison among original, hydrophilic coating and fiber coating

7.5 Summary of this chapter

This chapter aims to develop a comprehensive CFD model to explore the air-water flow dynamics, as well as the heat and mass transfer capabilities of a diamond-shaped IEC equipped with a water spray system. Incorporating theoretical foundations, computational domains, model validation, and parameter studies, the thesis identifies the optimal nozzle arrangement and assesses performance enhancements. Strategies such as hydrophilic and fiber coatings are proposed to improve efficiency, and the energy savings of IEC-DX as well as LDD-IEC-DX system in DCs are shown. Key findings and conclusions are summarized as follows:

- 1) In the IEC system, increasing the water supply flow rate enhances the water film coverage up to a point. Beyond a flow rate of 65 L/s, the coverage plateaus at its maximum, and further increases in flow rate do not improve the wetting rate but merely raise pump power consumption.

- 2) The performance of the IEC is significantly affected by the surface wetting coefficient due to its inherent heat transfer mechanism. For the diamond-shaped IEC, positioning the nozzles on the upper side yields the largest water film distribution area in the wet channel and the most substantial temperature reduction, showing improvements of 59.2% and 27.4%, respectively, compared to the least effective configuration.
- 3) The application of hydrophilic coatings on the wet channel plates reduces the contact angle of water droplets, diminishing the contraction of the water film and thereby increasing coverage. This enhancement leads to a 14.5% increase in water film coverage and a 7.4% rise in COP compared to a conventional aluminum plate IEC.
- 4) Fiber coatings, by virtue of their diffusion properties, not only extend the wetted area but also enable intermittent water spraying in the IEC, which cuts down on system power usage. With this approach, water film coverage is boosted by 31.6%, and the wet-bulb efficiency of IEC is enhanced by 16.1% over the initial setup.

CHAPTER 8 CONCLUSIONS AND RECOMMENDATIONS FOR FUTURE WORK

Considering that nozzle arrangement is a critical influencing aspect in the water distribution of the IEC system, this thesis firstly developed and validated a spray volumetric flux distribution model that includes the spray inclination angle. Based on this model, an existing IEC model was modified. Then, a novel 3D CFD model was firstly developed and verified to consider the actual coverage factor of water film including the cooling performance of the whole IEC system. Based on these two developed models, the effects of the original and optimized nozzle arrangement schemes and nozzle setting parameters on the thermodynamic performance as well as the energy performance of the IEC system are compared, demonstrating the superiority of the nozzle optimization scheme and providing a reference for further performance optimization of the IEC system. Then, a ML-based prediction model was developed to accurately estimate the performance of the IEC system, and GA was applied to optimize the IEC-ANN model to achieve efficient performance while maintaining low energy consumption. Moreover, a CFD model based on a diamond-shaped IEC explores the air-water flow, heat and mass transfer capabilities of the IEC as a heat recovery unit and specifies the optimal nozzle configuration and performance. Several enhancement strategies, including hydrophilic and fiber coatings, are also proposed. The enhancement characteristics of wet bulb efficiency, external energy efficiency, and COP values, as well as the enhancement mechanisms, are explained. Last, the energy savings of IEC-DX as well as LDD-IEC-DX system in DCs located in hot and humid regions are identified. The main conclusions are as follows.

8.1 Summary of the research findings and contributions

8.1.1 Development of numerical model for nozzle optimization of IEC with experimental validation

Considering that nozzle arrangement is a critical influencing aspect in the water distribution of the IEC system, Chapter 4 firstly developed and validated a spray volumetric flux distribution model that includes the spray inclination angle. Based on this model, an existing IEC model was modified and verified by experimental data from published literature. Then, the uniformity coefficient and coverage ratio of the different spray schemes were in-depth compared on the fixed size IEC by changing the nozzle arrangement distance and the installation inclination angle. The superiority of the optimized water distribution scheme was determined as well. Finally, the wet-bulb effectiveness, cooling capacity as well as COP value of the IEC system were compared between the original single-line arrangement of the nozzle and the optimal scheme based on the modified IEC model. The main conclusions are as follows:

- 1) The optimal spray distribution for a single cone spray nozzle scheme has the largest coverage ratio at a spray cone angle of 45° and an inclination angle of 30° , where the uniformity and coverage ratio are 1.49 and 0.47, respectively.
- 2) Multi-nozzle arrangement strategies are proposed for improving IEC's performance. For the IEC with 400 mm length and width, the optimal nozzle arrangement scheme is the scheme with four nozzles separated by 160 mm along the centerline, where its uniformity and coverage ratio were 0.74 and 0.72, respectively.

- 3) With the same water flow rate supplied (220 L/h), the optimized centerline scheme could increase the wettability factor of the IEC plate surface from 0.48 to 0.89 compared to the single-line arrangement of IEC water spray, reflecting the superiority of more uniform spray distribution.
- 4) The optimized nozzle scheme with four nozzles distributed at the centerline 160 mm apart recovers more energy due to a more uniform spray distribution for better wettability. The COP was increased up to 16% using this optimized nozzle arrangement scheme, which indicates the importance of a reasonable nozzle layout and provides a reference of spray system design for future studies and engineers for the application of this technology in air-conditioning systems.

8.1.2 Development and validation of CFD model for IEC considering water film formation with spray parameter analysis

In light of the fact that nozzle parameter setting is a crucial impact point in the water film coverage area of the IEC exchanger plate surface, Chapter 5 firstly proposed and verified a 3D CFD model to consider the actual coverage factor of water film including the cooling performance of the whole IEC system. Then, this thesis compares the water film coverage area of wet channel panels with various nozzle parameters and different arrangements. On the basis of the findings, an ideal nozzle design solution is found and contrasted with the traditional one. The final comparison was made between the ideal plan based on the proposed IEC model and the conventional setting of the nozzles in terms of wet-bulb efficiency and COP value of the

IEC system. The following are the primary conclusions:

- 1) The diameter of the spray droplets provided by the water system is an important aspect of the water membrane on the plate surface. For a single nozzle, a peak membrane coverage ratio of 0.22 could be achieved for a spray droplet diameter of 0.25 mm, with an improvement of 61.9% over the worst case scenario.
- 2) Based on the characteristics of the nozzles, the nozzle parameters for optimum coverage area were set at a droplet diameter of 0.25 mm, a pressure of 1.5 bar, a flow rate of 5.4 l/min and a spray cone angle of 68°.
- 3) For the presence of multiple nozzles, a spacing of 80 mm was tested and determined to be the optimum arrangement, improving coverage from 0.32 to 0.53 with two nozzles, while increasing IEC system efficiency by 31.4% compared with the worst results.
- 4) The optimized IEC water distribution system is based on a triangular arrangement of multiple nozzles according to the distance analysis. Compared to conventional settings, the optimized solution provides 20.9% better water film coverage and a significant increase in temperature drop in the primary airflow for the same number of nozzles.
- 5) For the conventional and optimized nozzle setting scheme, the IEC operating performance follows the same trend with the variation of primary air temperature and secondary air velocity. However, the optimized solution can increase the wet-bulb efficiency and COP by 15.1% and 17.6% respectively under the optimum operating conditions.

8.1.3 Performance assessment and optimization of water spray strategy for IEC based on ANN modeling and GA

Chapter 6 aims to develop a ML-based prediction model for accurately estimating the performance of IEC systems by considering six influential factors associated with spray operation. A large dataset consisting of operational, design, and performance parameters of IEC systems is thus constructed, and the importance of the influential factors was determined using grey relational analysis. Furthermore, the study employed genetic algorithms to optimize the operational parameters of the system. By assigning appropriate weights to performance parameters, it successfully reduced energy consumption while achieving better energy performance. These research findings offer valuable insights into designing and operating IEC systems in a sustainable and energy-efficient manner. The following is a summary and list of some concluding remarks:

- 1) The constructed three-layer IEC-ANN model related to the operating conditions water spray shows sufficient predictive power with coefficients of determination of 0.952 and 0.938 for the wet-bulb efficiency and pressure drop of secondary air channel, respectively, while the RMSEs are 1.543 and 1.817 Pa, correspondingly.
- 2) For changing a single factor, the effects of increasing the nozzle pressure, aperture, count, spacing, spray density and secondary air velocity on the wet-bulb efficiency all tend to increase to a peak and then continue to decay, while the pressure drop increased continuously with the increase of the spray density and air velocity.

- 3) As a result of the interplay of influencing factors, it can happen that at low pressures, the larger the nozzle aperture, the better the cooling effect of the IEC system, while at high pressures, the cooling performance of the IEC system decreases as the nozzle aperture increases. The importance of the six performance influencing factors, ranked from high to low, is as follows, air velocity > nozzle spacing > nozzle pressure > spray density > nozzle count > nozzle aperture.
- 4) A multi-objective optimization of the IEC water system was carried out utilizing GA based on the ANN model, with the aim of achieving the highest system energy efficiency with a low pressure drop. The optimal process parameters determined are nozzle pressure of 0.15 MPa, spacing of 85 mm, aperture of 6 mm, count of 11, spray density of 0.85 kg/(s·m²) and air velocity of 2 m/s, at which time the wet-bulb efficiency is 0.85, the pressure drop is 210, and the COP is 12.4, which is an increase of 23.2% in comparison with the base system.

Overall, this section contributes to a comprehensive analysis of the relationship between nozzle operating parameter settings and IEC system performance. It presents an economically efficient approach for achieving capacity matching under varying operational conditions through multi-objective optimization. Additionally, the proposed configuration improves system cooling efficiency by appropriately allocating weights to influential parameters while reducing energy consumption. As a result, this research provides valuable guidance and a theoretical basis for further optimizing IEC performance through enhancements in the water

distribution system.

8.1.4 Performance analysis and nozzle setting optimization of IEC for energy recovery in data centers

The purpose of the Chapter 7 is to develop a CFD model to investigate the air-water flow, heat and mass transfer capabilities of a diamond-shaped IEC with the water spray system. Through the inclusion of theoretical principles, computational domains, model verification and parameter analysis, the optimal nozzle configuration and performance were discovered. Several enhancement strategies, including hydrophilic coating and fiber coating, were also proposed. The enhancement of wet-bulb efficiency, exergy efficiency and COP value with characteristics as well as enhancement mechanisms were explained. The following is a summary and list of some concluding remarks:

- 1) With the IEC at a lower flow rate in the water supply system, the water film coverage reflects a more significant expand with the increase of the flow rate. However, when the water supply flow rate arrives 65 L/s, the water membrane coverage gradually stabilizes at the maximum value, and further increasing the flow rate does not benefit the wetting rate excepting increasing the power consumption of the pump.
- 2) Due to the nature of the IEC heat transfer mechanism, its performance is largely influenced by the surface wetting coefficient. For the diamond-shaped IEC, the nozzles are installed as upper side configuration when the water film distribution area in the wet channel is the largest and the temperature drop is the best, with 59.2% and 27.4%

improvement over the worst case, respectively.

- 3) Benefit from the addition of hydrophilic coatings on the plate surface of wet channels, the contact angle between the water droplets and the plate surface is reduced, thus weakening the shrinkage effect of the water film, resulting in an increase in the water film coverage. Compared with the conventional aluminum plate IEC, the water film coverage and COP are increased by 14.5% and 7.4%, respectively.
- 4) Moreover, the diffusion-based properties of the fiber coating in addition to expanding the wetted area also make intermittent spraying of IEC possible, thus reducing the power consumption of the system. Compared to the initial solution, the water film coverage increased by 31.6% and the wet-bulb efficiency of IEC improved by 16.1%.

8.2 Recommendations for future work

Based on the above studies, this thesis draws some innovative conclusions, but the spray optimization of IEC is still deficient in some aspects. Possible directions for future research and applications are presented here:

- 1) The primary focus of this thesis is on the common cross-flow plate IECs, which may not be applicable to other special types, such as tubular IECs. Thus, extensive experimentation across various IEC types is necessary to generalize the findings.
- 2) The optimization of spray systems for IECs utilizing porous materials such as ceramics or fabrics has not been fully realized. Further refinement of the spray strategy,

leveraging the benefits of intermittent spraying with further spray optimizations, could significantly reduce the energy consumption of IEC systems.

- 3) For the three operational modes of IEC systems in data centers, it is crucial to regulate the start and stop cycles of the water spray system to meet indoor temperature and humidity requirements while minimizing the energy consumption of the air conditioning system.
- 4) The GA-ANN model established in this thesis innovatively focuses on the spray system of the IEC, hence the selection of model input parameters is concentrated on the influencing factors of the spray system and the state of the wet channel, with the temperature and humidity of the airflow being constant. Future work will involve the development of ANN models for different spray parameters under various climatic conditions to achieve a more comprehensive analysis and optimization of the IEC system. Additionally, the proposed GA-ANN model is based on data from a conventional plate-type cross-flow IEC, limiting its predictive capability to the cooling performance of this specific IEC type. Therefore, it is imperative not to mix data from different types of IECs (such as tubular IECs) during the modeling process.
- 5) Current research on nanofluids in IECs is limited to the reliable applicability of homogeneous modeling, where empirical correlations of water-nanoparticle mixtures are used as proxies for the thermophysical properties of the spray water. The interaction between aqueous fluids and nanoparticles and the improvement of water film coverage

and evaporation effects in IEC have not been comprehensively investigated.

References

- [1] IEA. Financing Clean Energy Transitions in Emerging and Developing Economies. 2021.
- [2] IEA. The future of cooling in China. 2019.
- [3] Pérez-Lombard L, Ortiz J, Pout C. A review on buildings energy consumption information. *Energy Build* 2008;40:394–8. <https://doi.org/10.1016/j.enbuild.2007.03.007>.
- [4] Yang H, Shi W, Chen Y, Min Y. Research development of indirect evaporative cooling technology: An updated review. *Renew Sustain Energy Rev* 2021;145:111082. <https://doi.org/10.1016/j.rser.2021.111082>.
- [5] Min Y, Chen Y, Yang H. A statistical modeling approach on the performance prediction of indirect evaporative cooling energy recovery systems. *Appl Energy* 2019;255:113832. <https://doi.org/10.1016/j.apenergy.2019.113832>.
- [6] Rampazzo M, Lionello M, Beghi A, Sisti E, Cecchinato L. A static moving boundary modelling approach for simulation of indirect evaporative free cooling systems. *Appl Energy* 2019;250:1719–28. <https://doi.org/10.1016/j.apenergy.2019.04.087>.
- [7] Cooling performance measurement of two cross-flow indirect evaporative coolers in general and regenerative operation modes. *Appl Energy* 2017;195:268–77. <https://doi.org/10.1016/j.apenergy.2017.03.053>.
- [8] Park JY, Kim BJ, Yoon SY, Byon YS, Jeong JW. Experimental analysis of dehumidification performance of an evaporative cooling-assisted internally cooled liquid desiccant dehumidifier. *Appl Energy* 2019;235:177–85. <https://doi.org/10.1016/j.apenergy.2018.10.101>.
- [9] Min Y, Chen Y, Shi W, Yang H. Applicability of indirect evaporative cooler for energy recovery in hot and humid areas: Comparison with heat recovery wheel. *Appl Energy* 2021;287:116607. <https://doi.org/10.1016/j.apenergy.2021.116607>.
- [10] Chen Y, Yan H, Luo Y, Yang H. A proportional–integral (PI) law based variable speed technology for temperature control in indirect evaporative cooling system. *Appl Energy* 2019;251:113390. <https://doi.org/10.1016/j.apenergy.2019.113390>.
- [11] Cui X, Yan W, Liu Y, Zhao M, Jin L. Performance analysis of a hollow fiber membrane-based heat and mass exchanger for evaporative cooling. *Appl Energy* 2020;271:115238. <https://doi.org/10.1016/j.apenergy.2020.115238>.
- [12] Lin J, Bui DT, Wang R, Chua KJ. On the fundamental heat and mass transfer analysis of the counter-flow dew point evaporative cooler. *Appl Energy* 2018;217:126–42. <https://doi.org/10.1016/j.apenergy.2018.02.120>.

- [13]Shi W, Min Y, Ma X, Chen Y, Yang H. Performance evaluation of a novel plate-type porous indirect evaporative cooling system: An experimental study. *J Build Eng* 2021;48:103898. <https://doi.org/10.1016/j.jobe.2021.103898>.
- [14]Zhou Y, Zhang T, Wang F, Yu Y. Performance analysis of a novel thermoelectric assisted indirect evaporative cooling system. *Energy* 2018;162:299–308. <https://doi.org/10.1016/j.energy.2018.08.013>.
- [15]Shahzad MW, Burhan M, Ybyraiymkul D, Oh SJ, Ng KC. An improved indirect evaporative cooler experimental investigation. *Appl Energy* 2019;256:113934. <https://doi.org/10.1016/j.apenergy.2019.113934>.
- [16]Gurubalan A, Maiya MP, Geoghegan PJ. A comprehensive review of liquid desiccant air conditioning system. *Appl Energy* 2019;254:113673. <https://doi.org/10.1016/j.apenergy.2019.113673>.
- [17]Chen Y, Luo Y, Yang H. A simplified analytical model for indirect evaporative cooling considering condensation from fresh air: Development and application. *Energy Build* 2015;108:387–400. <https://doi.org/10.1016/j.enbuild.2015.09.054>.
- [18]Chen Y, Yang H, Luo Y. Parameter sensitivity analysis and configuration optimization of indirect evaporative cooler (IEC) considering condensation. *Appl Energy* 2017;194:440–53. <https://doi.org/10.1016/j.apenergy.2016.06.121>.
- [19]Min Y, Chen Y, Yang H. Numerical study on indirect evaporative coolers considering condensation: A thorough comparison between cross flow and counter flow. *Int J Heat Mass Transf* 2019;131:472–86. <https://doi.org/10.1016/j.ijheatmasstransfer.2018.11.082>.
- [20]Shi W, Min Y, Chen Y, Yang H. Development of a three-dimensional numerical model of indirect evaporative cooler incorporating with air dehumidification. *Int J Heat Mass Transf* 2022;185:122316. <https://doi.org/10.1016/j.ijheatmasstransfer.2021.122316>.
- [21]Ren C, Yang H. An analytical model for the heat and mass transfer processes in indirect evaporative cooling with parallel/counter flow configurations. *Int J Heat Mass Transf* 2006;49:617–27. <https://doi.org/10.1016/j.ijheatmasstransfer.2005.08.019>.
- [22]Adam A, Han D, He W, Chen J. Numerical analysis of cross-flow plate type indirect evaporative cooler: Modeling and parametric analysis. *Appl Therm Eng* 2021;185:116379. <https://doi.org/10.1016/j.applthermaleng.2020.116379>.
- [23]Sun T, Huang X, Chen Y, Zhang H. Experimental investigation of water spraying in an indirect evaporative cooler from nozzle type and spray strategy perspectives. *Energy Build* 2020;214:109871. <https://doi.org/10.1016/j.enbuild.2020.109871>.
- [24]Guilizzoni M, Milani S, Liberati P, De Antonellis S. Effect of plates coating on performance

of an indirect evaporative cooling system. *Int J Refrig* 2019;104:367–75. <https://doi.org/10.1016/j.ijrefrig.2019.05.029>.

[25]De Antonellis S, Cignatta L, Facchini C, Liberati P. Effect of heat exchanger plates geometry on performance of an indirect evaporative cooling system. *Appl Therm Eng* 2020;173:115200. <https://doi.org/10.1016/j.applthermaleng.2020.115200>.

[26]Duan Z, Zhan C, Zhang X, Mustafa M, Zhao X, Alimohammadisagvand B, et al. Indirect evaporative cooling: Past, present and future potentials. *Renew Sustain Energy Rev* 2012;16:6823–50. <https://doi.org/10.1016/j.rser.2012.07.007>.

[27]Liu S. A Novel Heat Recovery / Desiccant Cooling System 2008:227.

[28]D. Zhang, Huang, X., Wu Z. Experimental study on optimization of spraying water density of evaporative cooling. *Xi'an Inst Eng Sci Technol* 2006;20:191–4.

[29]De Antonellis S, Joppolo CM, Liberati P. Performance measurement of a cross-flow indirect evaporative cooler: Effect of water nozzles and airflows arrangement. *Energy Build* 2019;184:114–21. <https://doi.org/10.1016/j.enbuild.2018.11.049>.

[30]Al-Zubaydi AYT, Hong G. Experimental study of a novel water-spraying configuration in indirect evaporative cooling. *Appl Therm Eng* 2019;151:283–93. <https://doi.org/10.1016/j.applthermaleng.2019.02.019>.

[31]Shi W, Yang H, Ma X, Liu X. Performance prediction and optimization of cross-flow indirect evaporative cooler by regression model based on response surface methodology. *Energy* 2023;283:128636. <https://doi.org/10.1016/j.energy.2023.128636>.

[32]Adam A, Han D, He W, Amidpour M. Analysis of indirect evaporative cooler performance under various heat and mass exchanger dimensions and flow parameters. *Int J Heat Mass Transf* 2021;176:121299. <https://doi.org/10.1016/j.ijheatmasstransfer.2021.121299>.

[33]Hao JH, Chen Q, Li X, Zhang MQ, Yuan F. A new modeling and analysis method of the indirect evaporative heat exchanger based on the heat current perspective. *Appl Therm Eng* 2019;163:114331. <https://doi.org/10.1016/j.applthermaleng.2019.114331>.

[34]Farmahini-farahani M, Pasdarsahri H. Exergy Analysis of Evaporative Cooling for Optimum Energy Consumption in Diverse Climate Conditions 2011;3:9–20.

[35]Ma X, Shi W, Yang H. Study on water spraying distribution to improve the energy recovery performance of indirect evaporative coolers with nozzle arrangement optimization ☆. *Appl Energy* 2022;318:119212. <https://doi.org/10.1016/j.apenergy.2022.119212>.

[36]Yang M, Ma H, Ma S, Nong A, Zhang Y, Ma Y. Effect of surface wettability on air parameters and performance of indirect evaporative cooler in the presence of primary air

condensation. *J Build Eng* 2022;45:103535. <https://doi.org/10.1016/j.jobe.2021.103535>.

[37]Li X, Zhu G, Liu M, Guo C, Lv J, Wang L. Theoretical study on the wetting rate in wet channel of dew-point evaporative cooler based on Marangoni effect. *J Build Eng* 2023;73:106806. <https://doi.org/10.1016/j.jobe.2023.106806>.

[38]Mohammed RH, El-Morsi M, Abdelaziz O. Indirect evaporative cooling for buildings: A comprehensive patents review. *J Build Eng* 2022;50:104158. <https://doi.org/10.1016/j.jobe.2022.104158>.

[39]Kian C, Md J, Islam R, Kim N, Muhammad C, Shahzad W. *Green Energy and Technology: Advances in Air Conditioning Technologies*. 2021.

[40]Li WY, Li YC, Zeng L yue, Lu J. Comparative study of vertical and horizontal indirect evaporative cooling heat recovery exchangers. *Int J Heat Mass Transf* 2018;124:1245–61. <https://doi.org/10.1016/j.ijheatmasstransfer.2018.04.041>.

[41]Cui X, Chua KJ, Yang WM, Ng KC, Thu K, Nguyen VT. Studying the performance of an improved dew-point evaporative design for cooling application. *Appl Therm Eng* 2014;63:624–33. <https://doi.org/10.1016/j.applthermaleng.2013.11.070>.

[42]Yu Jianlin, Jin Liwen, Cao Qi, Wang Yiyi WY. Mass Transfer outside a Horizontal Tube for an Indirect Evaporative Cooler. *J Xi'an Jiaotong Univ* 1999;33:68–71.

[43]Braun, J E, Klein, S A, and Mitchell JW. Effectiveness models for cooling towers and cooling coils. *ASHRAE Trans* 1989;95:164–74.

[44]Camargo JR, Ebinuma CD, Silveira JL. Experimental performance of a direct evaporative cooler operating during summer in a Brazilian city. *Int J Refrig* 2005;28:1124–32. <https://doi.org/10.1016/j.ijrefrig.2004.12.011>.

[45]Zhao X, Liu S, Riffat SB. Comparative study of heat and mass exchanging materials for indirect evaporative cooling systems. *Build Environ* 2008;43:1902–11. <https://doi.org/10.1016/j.buildenv.2007.11.009>.

[46]Sofia E, Putra N, Kosasih EA. Development of indirect evaporative cooler based on a finned heat pipe with a natural-fiber cooling pad. *Heliyon* 2022;8. <https://doi.org/10.1016/j.heliyon.2022.e12508>.

[47]Fikri B, Sofia E, Putra N. Experimental analysis of a multistage direct-indirect evaporative cooler using a straight heat pipe. *Appl Therm Eng* 2020;171:115133. <https://doi.org/10.1016/j.applthermaleng.2020.115133>.

[48]Anisimov S, Pandelidis D, Jedlikowski A, Polushkin V. Performance investigation of a M (Maisotsenko)-cycle cross-flow heat exchanger used for indirect evaporative cooling. *Energy*

2014;76:593–606. <https://doi.org/10.1016/j.energy.2014.08.055>.

[49]Ham SW, Jeong JW. DPHX (dew point evaporative heat exchanger): System design and performance analysis. *Energy* 2016;101:132–45. <https://doi.org/10.1016/j.energy.2016.02.019>.

[50]Wang L, Zhan C, Zhang J, Zhao X. Optimization of the counter-flow heat and mass exchanger for M-Cycle indirect evaporative cooling assisted with entropy analysis. *Energy* 2019;171:1206–16. <https://doi.org/10.1016/j.energy.2019.01.099>.

[51]De Antonellis S, Joppolo CM, Liberati P, Milani S, Molinaroli L. Experimental analysis of a cross flow indirect evaporative cooling system. *Energy Build* 2016;121:130–8. <https://doi.org/10.1016/j.enbuild.2016.03.076>.

[52]De Antonellis S, Joppolo CM, Liberati P, Milani S, Romano F. Modeling and experimental study of an indirect evaporative cooler. *Energy Build* 2017;142:147–57. <https://doi.org/10.1016/j.enbuild.2017.02.057>.

[53]Zhou B, Lv J, Zhu M, Wang L, Liang L, Chen Q. Simulation study of a thin membrane inclined automatic wicking dew-point evaporative cooling device. *J Build Eng* 2023;72:106601. <https://doi.org/10.1016/j.job.2023.106601>.

[54]Al-Zubaydi AYT, Hong G. Experimental study of a novel water-spraying configuration in indirect evaporative cooling. *Appl Therm Eng* 2019;151:283–93. <https://doi.org/10.1016/j.applthermaleng.2019.02.019>.

[55]Jin Q, Yu Y, Xia Y. Experimental study on heat transfer characteristics of spray cooling system with plate-fin heat exchanger. *Exp Heat Transf* 2023;00:1–13. <https://doi.org/10.1080/08916152.2023.2204314>.

[56]Zhou B, Lv J, Zhu M, Wang L, Li S, Hu E. Experiment for the performance of a thin membrane inclined automatic wicking dew-point evaporative cooling device based on simulation results. *Energy Build* 2024;308:114021. <https://doi.org/10.1016/j.enbuild.2024.114021>.

[57]Shi W, Yang H, Ma X, Liu X. A novel indirect evaporative cooler with porous media under dual spraying modes: A comparative analysis from energy, exergy, and environmental perspectives. *J Build Eng* 2023;76:106874. <https://doi.org/10.1016/j.job.2023.106874>.

[58]Wang F, Sun T, Huang X, Chen Y, Yang H. Experimental research on a novel porous ceramic tube type indirect evaporative cooler. *Appl Therm Eng* 2017;125:1191–9. <https://doi.org/10.1016/j.applthermaleng.2017.07.111>.

[59]Sun T, Huang X, Qu Y, Wang F, Chen Y. Theoretical and experimental study on heat and mass transfer of a porous ceramic tube type indirect evaporative cooler. *Appl Therm Eng* 2020;173:115211. <https://doi.org/10.1016/j.applthermaleng.2020.115211>.

- [60]Sun T, Sun H, Tang T, Yan Y, Li P. Experimental Study on the Thermal Performances of a Tube-Type Indirect Evaporative Cooler. *Fluid Dyn Mater Process* 2023;19:2519–31. <https://doi.org/10.32604/fdmp.2023.027118>.
- [61]Guo C, Liu Q, Zheng B, You Y, Li Y. Development of model based on condensation area ratio and effect on heat transfer capacity of indirect evaporative cooling. *Appl Therm Eng* 2020;164:114557. <https://doi.org/10.1016/j.applthermaleng.2019.114557>.
- [62]Riangvilaikul B, Kumar S. Numerical study of a novel dew point evaporative cooling system. *Energy Build* 2010;42:2241–50. <https://doi.org/10.1016/j.enbuild.2010.07.020>.
- [63]Alkhedhair A, Gurgenci H, Jahn I, Guan Z, He S. Numerical simulation of water spray for pre-cooling of inlet air in natural draft dry cooling towers. *Appl Therm Eng* 2013;61:416–24. <https://doi.org/10.1016/j.applthermaleng.2013.08.012>.
- [64]Cho H, Cha B, Kim S, Ryu J, Kim J, Moon I. Numerical analysis for particle deposit formation in reactor cyclone of residue fluidized catalytic cracking. *Ind Eng Chem Res* 2013;52:7252–8. <https://doi.org/10.1021/ie302509q>.
- [65]Park H, Roh J, Oh K cheol, Cho H, Kim J. Modeling and optimization of water mist system for effective air-cooled heat exchangers. *Int J Heat Mass Transf* 2022;184:122297. <https://doi.org/10.1016/j.ijheatmasstransfer.2021.122297>.
- [66]Haghshenas Fard M, Zivdar M, Rahimi R, Esfahany MN, Afacan A, Nandakumar K, et al. CFD simulation of mass transfer efficiency and pressure drop in a structured packed distillation column. *Chem Eng Technol* 2007;30:854–61. <https://doi.org/10.1002/ceat.200700011>.
- [67]Tao W, Yimo L, Lin L. A novel 3D simulation model for investigating liquid desiccant dehumidification performance based on CFD technology. *Appl Energy* 2019;240:486–98. <https://doi.org/10.1016/j.apenergy.2019.02.068>.
- [68]Gu F, Liu CJ, Yuan XG, Yu GC. CFD simulation of liquid film flow on inclined plates. *Chem Eng Technol* 2004;27:1099–104. <https://doi.org/10.1002/ceat.200402018>.
- [69]Adam A, Han D, He W, Shi Q, Chen J, Zhong H. The influences of the plate shape on the performance of the indirect evaporative cooler based on the CFD approach. *J Brazilian Soc Mech Sci Eng* 2023;45:1–14. <https://doi.org/10.1007/s40430-023-04044-w>.
- [70]Wan Y, Ren C, Xing L. An approach to the analysis of heat and mass transfer characteristics in indirect evaporative cooling with counter flow configurations. *Int J Heat Mass Transf* 2017;108:1750–63. <https://doi.org/10.1016/j.ijheatmasstransfer.2017.01.019>.
- [71]You Y, Jiang H, Lv J. Analysis of influence of IEC heat exchanger based on CFD method. *Energy Procedia* 2019;158:5759–64. <https://doi.org/10.1016/j.egypro.2019.01.555>.

- [72] Pacak A, Baran B, Sierpowski K, Malecha Z, Pandelidis D. Application of computational fluid dynamics (CFD) methods to analyze energy efficiency of indirect evaporative coolers. *Int Commun Heat Mass Transf* 2023;143. <https://doi.org/10.1016/j.icheatmasstransfer.2023.106727>.
- [73] Zhao X, Li JM, Riffat SB. Numerical study of a novel counter-flow heat and mass exchanger for dew point evaporative cooling. *Appl Therm Eng* 2008;28:1942–51. <https://doi.org/10.1016/j.applthermaleng.2007.12.006>.
- [74] Cui X, Chua KJ, Yang WM. Numerical simulation of a novel energy-efficient dew-point evaporative air cooler. *Appl Energy* 2014;136:979–88. <https://doi.org/10.1016/j.apenergy.2014.04.040>.
- [75] Zhan C, Zhao X, Smith S, Riffat SB. Numerical study of a M-cycle cross-flow heat exchanger for indirect evaporative cooling. *Build Environ* 2011;46:657–68. <https://doi.org/10.1016/j.buildenv.2010.09.011>.
- [76] Wan Y, Soh A, Shao Y, Cui X, Tang Y, Chua KJ. Numerical study and correlations for heat and mass transfer coefficients in indirect evaporative coolers with condensation based on orthogonal test and CFD approach. *Int J Heat Mass Transf* 2020;153:119580. <https://doi.org/10.1016/j.ijheatmasstransfer.2020.119580>.
- [77] Pandelidis D, Cichoń A, Pacak A, Drąg P, Drąg M, Worek W, et al. Performance study of the cross-flow Maisots[1] D. Pandelidis et al., “Performance study of the cross-flow Maisotsenko cycle in humid climate conditions,” *Int. Commun. Heat Mass Transf.*, vol. 115, no. May, p. 104581, 2020, doi: 10.1016/j.icheatmasstransfer. *Int Commun Heat Mass Transf* 2020;115:104581. <https://doi.org/10.1016/j.icheatmasstransfer.2020.104581>.
- [78] Anisimov S, Pandelidis D, Danielewicz J. Numerical analysis of selected evaporative exchangers with the Maisotsenko cycle. *Energy Convers Manag* 2014;88:426–41. <https://doi.org/10.1016/j.enconman.2014.08.055>.
- [79] Lin J, Bui DT, Wang R, Chua KJ. On the fundamental heat and mass transfer analysis of the counter-flow dew point evaporative cooler. *Appl Energy* 2018;217:126–42. <https://doi.org/10.1016/j.apenergy.2018.02.120>.
- [80] Comino F, Romero-Lara MJ, Ruiz de Adana M. Experimental and numerical study of dew-point indirect evaporative coolers to optimize performance and design. *Int J Refrig* 2022;142:92–102. <https://doi.org/10.1016/j.ijrefrig.2022.06.006>.
- [81] Zhu G, Chen W, Zhang D, Wen T. Performance evaluation of counter flow dew-point evaporative cooler with a three-dimensional numerical model. *Appl Therm Eng* 2023;219:119483. <https://doi.org/10.1016/j.applthermaleng.2022.119483>.

- [82]Zheng B, Guo C, Chen T, Shi Q, Lv J, You Y. Development of an experimental validated model of cross-flow indirect evaporative cooler with condensation. *Appl Energy* 2019;252:113438. <https://doi.org/10.1016/j.apenergy.2019.113438>.
- [83]Somasundar KG, Soorej S, Karthikeyan S, Jayan N, Bhatlu MLD. Review on cooling tower nozzle types. *Mater Today Proc* 2020;37:3016–8. <https://doi.org/10.1016/j.matpr.2020.08.723>.
- [84]Hwang JK. Effects of nozzle shape and arrangement on the cooling performance of steel wire rod in the Stelmor cooling process. *Appl Therm Eng* 2020;164:114461. <https://doi.org/10.1016/j.applthermaleng.2019.114461>.
- [85]Zhang Z, He S, Yan M, Gao M, Shi Y, Lu Y, et al. Numerical study on the performance of a two-nozzle spray cooling system under different conditions. *Int J Therm Sci* 2020;152:106291. <https://doi.org/10.1016/j.ijthermalsci.2020.106291>.
- [86]Ham SW, Lee SJ, Jeong JW. Operating energy savings in a liquid desiccant and dew point evaporative cooling-assisted 100% outdoor air system. *Energy Build* 2016;116:535–52. <https://doi.org/10.1016/j.enbuild.2016.02.011>.
- [87]Kim MH, Dong HW, Park JY, Jeong JW. Primary energy savings in desiccant and evaporative cooling-assisted 100% outdoor air system combined with a fuel cell. *Appl Energy* 2016;180:446–56. <https://doi.org/10.1016/j.apenergy.2016.08.004>.
- [88]Zhao Y, Sun F, Long G, Huang X, Huang W, Lyv D. Comparative study on the cooling characteristics of high level water collecting natural draft wet cooling tower and the usual cooling tower. *Energy Convers Manag* 2016;116:150–64. <https://doi.org/10.1016/j.enconman.2016.02.071>.
- [89]Jain M, John B, Iyer KN, Prabhu S V. Characterization of the full cone pressure swirl spray nozzles for the nuclear reactor containment spray system. *Nucl Eng Des* 2014;273:131–42. <https://doi.org/10.1016/j.nucengdes.2014.02.025>.
- [90]Lan Z, Zhu D, Tian W, Su G, Qiu S. Experimental study on spray characteristics of pressure-swirl nozzles in pressurizer. *Ann Nucl Energy* 2014;63:215–27. <https://doi.org/10.1016/j.anucene.2013.07.048>.
- [91]Meng X, Meng L, Gao Y, Li H. A comprehensive review on the spray cooling system employed to improve the summer thermal environment: Application efficiency, impact factors, and performance improvement. *Build Environ* 2022;217:109065. <https://doi.org/10.1016/j.buildenv.2022.109065>.
- [92]Wang C, Zhang X, Xin Y, Bai J. Astrometric results of the mutual events between the Galilean satellites during 2014–15. *Planet Space Sci* 2019;175:21–4. <https://doi.org/10.1016/j.pss.2019.05.011>.

- [93] Han H, Wang P, Li Y, Liu R, Tian C. Effect of water supply pressure on atomization characteristics and dust-reduction efficiency of internal mixing air atomizing nozzle. *Adv Powder Technol* 2020;31:252–68. <https://doi.org/10.1016/j.ap.2019.10.017>.
- [94] Sun Y, Guan Z, Hooman K. A review on the performance evaluation of natural draft dry cooling towers and possible improvements via inlet air spray cooling. *Renew Sustain Energy Rev* 2017;79:618–37. <https://doi.org/10.1016/j.rser.2017.05.151>.
- [95] Sun Y, Guan Z, Gurgenci H, Wang J, Dong P, Hooman K. Spray cooling system design and optimization for cooling performance enhancement of natural draft dry cooling tower in concentrated solar power plants. *Energy* 2019;168:273–84. <https://doi.org/10.1016/j.energy.2018.11.111>.
- [96] Grant G, Brenton J, Drysdale D. Fire suppression by water sprays. *Prog Energy Combust Sci* 2000;26:79–130. [https://doi.org/10.1016/S0360-1285\(99\)00012-X](https://doi.org/10.1016/S0360-1285(99)00012-X).
- [97] Kashdan JT, Shrimpton JS, Whybrew A. A digital image analysis technique for quantitative characterisation of high-speed sprays. *Opt Lasers Eng* 2007;45:106–15. <https://doi.org/10.1016/j.optlaseng.2006.03.006>.
- [98] Sun Y, Alkhedhair AM, Guan Z, Hooman K. Numerical and experimental study on the spray characteristics of full-cone pressure swirl atomizers. *Energy* 2018;160:678–92. <https://doi.org/10.1016/j.energy.2018.07.060>.
- [99] Montazeri H, Blocken B, Hensen JLM. Evaporative cooling by water spray systems: CFD simulation, experimental validation and sensitivity analysis. *Build Environ* 2015;83:129–41. <https://doi.org/10.1016/j.buildenv.2014.03.022>.
- [100] Shi W, Ma X, Gu Y, Min Y, Yang H. Indirect evaporative cooling maps of China: Optimal and quick performance identification based on a data-driven model. *Energy Convers Manag* 2022;268. <https://doi.org/10.1016/j.enconman.2022.116047>.
- [101] Camargo JR, Ebinuma CD, Silveira JL. Thermoeconomic analysis of an evaporative desiccant air conditioning system. *Appl Therm Eng* 2003;23:1537–49. [https://doi.org/10.1016/S1359-4311\(03\)00105-4](https://doi.org/10.1016/S1359-4311(03)00105-4).
- [102] He S, Gurgenci H, Guan Z, Huang X, Lucas M. A review of wetted media with potential application in the pre-cooling of natural draft dry cooling towers. *Renew Sustain Energy Rev* 2015;44:407–22. <https://doi.org/10.1016/j.rser.2014.12.037>.
- [103] Cui X, Yang C, Yan W, Zhang L, Wan Y, Chua KJ. Experimental study on a moisture-conducting fiber-assisted tubular indirect evaporative cooler. *Energy* 2023;278:128014. <https://doi.org/10.1016/j.energy.2023.128014>.
- [104] Xuan YM, Xiao F, Niu XF, Huang X, Wang SW. Research and application of evaporative

cooling in China: A review (I) - Research. *Renew Sustain Energy Rev* 2012;16:3535–46. <https://doi.org/10.1016/j.rser.2012.01.052>.

[105] Bolotin S, Vager B, Vasilijev V. Comparative analysis of the cross-flow indirect evaporative air coolers. *Int J Heat Mass Transf* 2015;88:224–35. <https://doi.org/10.1016/j.ijheatmasstransfer.2015.04.072>.

[106] Ma X, Shi W, Yang H. Improving the performance of indirect evaporative cooler for energy recovery from the perspective of nozzle configuration: A CFD model analysis. *J Build Eng* 2023;76:107195. <https://doi.org/10.1016/j.jobe.2023.107195>.

[107] Shi W, Ma X, Min Y, Yang H. Feasibility Analysis of Indirect Evaporative Cooling System Assisted by Liquid Desiccant for Data Centers in Hot-Humid Regions. *Sustain* 2024;16. <https://doi.org/10.3390/su16052011>.

[108] Wu T, Cao B, Zhu Y. A field study on thermal comfort and air-conditioning energy use in an office building in Guangzhou. *Energy Build* 2018;168:428–37. <https://doi.org/10.1016/j.enbuild.2018.03.030>.

[109] Min Y, Chen Y, Yang H, Guo C. Characteristics of primary air condensation in indirect evaporative cooler: Theoretical analysis and visualized validation. *Build Environ* 2020;174:106783. <https://doi.org/10.1016/j.buildenv.2020.106783>.

[110] Spandagos C, Ng TL. Equivalent full-load hours for assessing climate change impact on building cooling and heating energy consumption in large Asian cities. *Appl Energy* 2017;189:352–68. <https://doi.org/10.1016/j.apenergy.2016.12.039>.

[111] Ebrahimi K, Jones GF, Fleischer AS. A review of data center cooling technology, operating conditions and the corresponding low-grade waste heat recovery opportunities. *Renew Sustain Energy Rev* 2014;31:622–38. <https://doi.org/10.1016/j.rser.2013.12.007>.

[112] Chua KJ, Chou SK, Yang WM, Yan J. Achieving better energy-efficient air conditioning - A review of technologies and strategies. *Appl Energy* 2013;104:87–104. <https://doi.org/10.1016/j.apenergy.2012.10.037>.

[113] Yang H, Shi W, Chen Y, Min Y. Research development of indirect evaporative cooling technology: An updated review. *Renew Sustain Energy Rev* 2021;145:111082. <https://doi.org/10.1016/j.rser.2021.111082>.

[114] Moshari S, Heidarinejad G, Fathipour A. Numerical investigation of wet-bulb effectiveness and water consumption in one-and two-stage indirect evaporative coolers. *Energy Convers Manag* 2016;108:309–21. <https://doi.org/10.1016/j.enconman.2015.11.022>.

[115] AS D. Future ready modular data centre solutions for DigiPlex 2020:1–2.

- [116] Will your IT withstand a sustainability review ? n.d.
- [117] Zhichao G, Xiang H, Jianli S, Junjie C. Indirect evaporative cooling air conditioning systems in domestic and international data centres 2017:1–6.
- [118] Chenyu J, Xiang H, Zhenwu T, Zhenyu L YJ. Study on the application of indirect evaporative cooling technology in domestic and international data centres. *Refrigeration and Air-Conditioning* 2020;1:61–7.
- [119] Chu J, Huang X. Research status and development trends of evaporative cooling air-conditioning technology in data centers. *Energy Built Environ* 2023;4:86–110. <https://doi.org/10.1016/j.enbenv.2021.08.004>.
- [120] Cui X, Mohan B, Islam MR, Chua KJ. Investigating the energy performance of an air treatment incorporated cooling system for hot and humid climate. *Energy Build* 2017;151:217–27. <https://doi.org/10.1016/j.enbuild.2017.06.059>.
- [121] Chen Y, Yang H, Luo Y. Indirect evaporative cooler considering condensation from primary air: Model development and parameter analysis. *Build Environ* 2016;95:330–45. <https://doi.org/10.1016/j.buildenv.2015.09.030>.
- [122] Lv J, Xu H, Zhu M, Dai Y, Liu H, Li Z. The performance and model of porous materials in the indirect evaporative cooling system: A review. *J Build Eng* 2021;41:102741. <https://doi.org/10.1016/j.jobbe.2021.102741>.
- [123] Rashidi S, Kashefi MH, Kim KC, Samimi-Abianeh O. Potentials of porous materials for energy management in heat exchangers – A comprehensive review. *Appl Energy* 2019;243:206–32. <https://doi.org/10.1016/j.apenergy.2019.03.200>.
- [124] Mudawar I, Deiters TA. A universal approach to predicting temperature response of metallic parts to spray quenching. *Int J Heat Mass Transf* 1994;37:347–62. [https://doi.org/10.1016/0017-9310\(94\)90070-1](https://doi.org/10.1016/0017-9310(94)90070-1).
- [125] Mudawar I, Estes KA. Optimizing and predicting CHF in spray cooling of a square surface. *J Heat Transfer* 1996;118:672–9. <https://doi.org/10.1115/1.2822685>.
- [126] Dong C, Lu L, Wen T. Experimental study on dehumidification performance enhancement by TiO₂ superhydrophilic coating for liquid desiccant plate dehumidifiers. *Build Environ* 2017;124:219–31. <https://doi.org/10.1016/j.buildenv.2017.08.010>.
- [127] Dong C, Lu L, Wang X. Experimental investigation on non-boiling heat transfer of two-component air-oil and air-water slug flow in horizontal pipes. *Int J Multiphase Flow* 2019;119:28–41. <https://doi.org/10.1016/j.ijmultiphaseflow.2019.07.004>.
- [128] Industries P. Analysis of Laminar Liquid Film Flowing Down 2005:1–5.

- [129] Yu J, Jin S, Xia Y. Experimental and CFD investigation of the counter-flow spray concentration tower in solar energy air evaporating separation saline wastewater treatment system. *Int J Heat Mass Transf* 2019;144:118621. <https://doi.org/10.1016/j.ijheatmasstransfer.2019.118621>.
- [130] Chen Y, Yan H, Min Y. Visualized study of wetting enhancement and thermal performance of fiber-coated indirect evaporative cooler. *Appl Therm Eng* 2023;221:119904. <https://doi.org/10.1016/j.applthermaleng.2022.119904>.
- [131] Shi W, Min Y, Ma X, Chen Y, Yang H. Dynamic performance evaluation of porous indirect evaporative cooling system with intermittent spraying strategies. *Appl Energy* 2022;311:118598. <https://doi.org/10.1016/j.apenergy.2022.118598>.
- [132] Sun K, Luo N, Luo X, Hong T. Prototype energy models for data centers. *Energy Build* 2021;231:110603. <https://doi.org/10.1016/j.enbuild.2020.110603>.
- [133] Ma X, Shi W, Yang H. Study on water spraying distribution to improve the energy recovery performance of indirect evaporative coolers with nozzle arrangement optimization. *Appl Energy* 2022;318:1–6. <https://doi.org/10.1016/j.apenergy.2022.119212>.
- [134] Zhang Y, Zhang H, Yang H, Chen Y, Leung CW. Response surface modeling and optimization scheme of an internally cooled liquid desiccant air conditioning system. *J Build Eng* 2023;76:107371. <https://doi.org/10.1016/j.jobbe.2023.107371>.
- [135] Min Y, Chen Y, Shi W, Yang H. Applicability of indirect evaporative cooler for energy recovery in hot and humid areas: Comparison with heat recovery wheel. *Appl Energy* 2021;287:116607. <https://doi.org/10.1016/j.apenergy.2021.116607>.
- [136] Sadighi Dizaji H, Hu EJ, Chen L, Pourhedayat S. Analytical/experimental sensitivity study of key design and operational parameters of perforated Maisotsenko cooler based on novel wet-surface theory. *Appl Energy* 2020;262:114557. <https://doi.org/10.1016/j.apenergy.2020.114557>.
- [137] Shi W, Yang H, Ma X, Liu X. Techno-economic evaluation and environmental benefit of hybrid evaporative cooling system in hot-humid regions. *Sustain Cities Soc* 2023;97:104735. <https://doi.org/10.1016/j.scs.2023.104735>.
- [138] Kong XQ, Wang RZ, Huang XH. Energy efficiency and economic feasibility of CCHP driven by stirling engine. *Energy Convers Manag* 2004;45:1433–42. <https://doi.org/10.1016/j.enconman.2003.09.009>.
- [139] Shi W, Ma X, Gu Y, Min Y, Yang H. Indirect evaporative cooling maps of China: Optimal and quick performance identification based on a data-driven model. *Energy Convers Manag* 2022;268. <https://doi.org/10.1016/j.enconman.2022.116047>.

- [140] Sotelo-Salas C, Pozo CE del, Esparza-López CJ. Thermal assessment of spray evaporative cooling in opaque double skin facade for cooling load reduction in hot arid climate. *J Build Eng* 2021;38. <https://doi.org/10.1016/j.jobbe.2021.102156>.
- [141] Meng C, Huang X, Qu Y. Study on performance prediction of dew point indirect evaporative cooling air conditioning unit based on BP neural network optimized by PSO. *Refrigeration* 2022;36:337–45.
- [142] Elarbi M, Bechikh S, Gupta A, Ben Said L, Ong YS. A New Decomposition-Based NSGA-II for Many-Objective Optimization. *IEEE Trans Syst Man, Cybern Syst* 2018;48:1191–210. <https://doi.org/10.1109/TSMC.2017.2654301>.
- [143] Yang X. Appendix A: Test Problems in Optimization. *Eng Optim* 2010:261–6. <https://doi.org/10.1002/9780470640425.app1>.
- [144] Berning T, Sørensen H, Nielsen MP. A COMPUTATIONAL FLUID DYNAMICS ANALYSIS OF AN INDIRECT EVAPORATIVE COOLER EMPLOYING THE PARTICLE TRANSPORT METHOD 2019:2–6.
- [145] Wang L, Zhan C, Zhang J, Zhao X. The energy and exergy analysis on the performance of counter-flow heat and mass exchanger for M-Cycle indirect evaporative cooling. *Therm Sci* 2019;23:613–23. <https://doi.org/10.2298/TSCI171221153W>.
- [146] Yang Y, Ren C, Yang C, Tu M, Luo B, Fu J. Energy and exergy performance comparison of conventional, dew point and new external-cooling indirect evaporative coolers. *Energy Convers Manag* 2021;230:113824. <https://doi.org/10.1016/j.enconman.2021.113824>.
- [147] Kashyap S, Sarkar J, Kumar A. Experimental exergy, economic and sustainability analyses of the dual-mode evaporative cooler. *Int J Refrig* 2022;135:121–30. <https://doi.org/10.1016/j.ijrefrig.2021.12.005>.
- [148] Dong C, Qi R, Zhang L, Lu L. Performance enhancement of solar-assisted liquid desiccant dehumidifiers using super-hydrophilic surface. *Energy Build* 2019;199:461–71. <https://doi.org/10.1016/j.enbuild.2019.07.027>.